REGULATION OF *DE NOVO* TELOMERE ADDITION IN *S. CEREVISIAE*: A RAD51 PERSPECTIVE

BY

Esther Akunna Epum

Dissertation

Submitted to the Faculty of the

Graduate School of Vanderbilt University

in partial fulfillment of the requirements

for the degree of

DOCTOR OF PHILOSOPHY

In

Biological Sciences

September 30th, 2019

Nashville, Tennessee

Approved:

Katherine Friedman, Ph.D.

Brandt Eichman, Ph.D.

Todd Graham Ph.D.

Antonis Rokas, Ph.D.

David Cortez, Ph.D.

DEDICATION

To my first son Brian Nwakauso Epum,

who taught me how to live and love,

and lives on forever in our hearts.

To my father-in-law Ambrose Epum,

who passed away during the writing of this thesis,

who taught us a lot about virtue and patience.

To my mother-in-law Lilian Epum,

who passed away during the writing of this thesis,

who taught us love and strength.

This work is dedicated to all three of you.

Until we meet again to declare:

O death, where is your sting?

O grave, where is your victory?

ACKNOWLEDGEMENT

It has been a long, sometimes hard road to get to this point and I am so thankful. Coming to America and excited about all the opportunities awaiting me in my future. Maybe if I knew exactly what awaited me, I would have reconsidered. But I dared believe in a dream. I dared believe it was possible. Even when I didn't understand how and when, I put one foot in front of the other in blind faith in the impossible. There are many people that have contributed to my Ph.D. journey and, in many cases, more than they will ever know.

I want to thank Dr. Ike and his family for accepting me and giving me an opportunity. They have been instrumental to my stay in the US. I want to thank the Fisk-Vanderbilt Masters to PhD Bridge program. This program was invaluable to me during my Master's program and certainly helped chart the course towards my Ph.D. I am very grateful for the tuition and stipend award during my Master's program and for funding my trip to New York for Cold Spring Harbor Meeting in 2017. And to Dina Stroud, for all she does. I will always take pride in my membership of this incredible program.

My gratitude goes to the Biological Sciences Department at Vanderbilt University for giving me an opportunity and for the tuition and stipend support all these years. The Gisela Mosig fund helped tremendously for conference attendances which have contributed to my growth as a scientist. My deep gratitude goes to my thesis mentor, Dr. Katherine Friedman, for her support and guidance over these years. I started in her lab as a Master's student with very little skills and not a lot of scientific confidence. I emerge confident and fulfilled. My future

achievements will be definitely defined by my graduate school training in the Friedman lab. I want to thank my committee members for all their time, advice, patience and support all these years. They helped shape my ideas and perspectives on experiments and were always willing to help in whatever way. To all members of the Friedman lab past and present: Laura, Charlene, Udo, Kerri-Ann, Katrina, Zachary, Nick, Clara, Ahmed, Lucy, Angie, Gabby, Elise, Sarah, Clayton, Carlos, Ty, Stephen, Natalie, Dmitriy and Michael. Thanks for inspiring and teaching me. Thanks to Laura and Charlene for their friendship. Thanks to Lauren Salay for her wonderful collaboration and vivacious attitude.

I want to deeply extend my gratitude to my Pastors Ben and Toro who have been a strong support system for my family and to my other Pastors Oyebade and Quartey and to all ministers, workers and members of the Agape house Church for their love, care and fellowship. I couldn't have made it this far without you guys.

I am deeply thankful to my brothers and sisters. I want to thank my sister Chioma for showing me the true value of selflessness. I never would have gone this far without you. To Emeka and Aham for your true and genuine love and support. To my sister Chidera, for showing me the true beauty of knowledge in girls. To my sisters Chimezie, Uloma and Emmanuella for reminding me the true value of childhood love and innocence.

To my father for his incredible courage and attitude. He believed in me even when I didn't think it possible. Thank you for you priceless sacrifice for me. For believing in the value of education and especially the value of education in the girl child. I never would have made it without you. You are a true gem.

To my husband Stephen, words cannot describe how much I have valued your love, support and encouragement over all these years. You are priceless and my most incredible gift. Thank you for been by my side even when you didn't fully understand it. You have been my biggest fan and supporter. You have told me: if I can conceive it, then I can achieve it. I am excited for the many more years we get to spend and share together.

To Eathan Chizaram Epum. You are my greatest blessing. You bring me joy every single day. You are the guide to the sunlight, thank you for lighting my way. I love you more every day. You are the best thing that happened to me during these PhD years.

To my Father and God in heaven. Thank you for being my God, Savior, Father, Comforter, Protector, Provider, Counsellor, biggest Advocate, Strengthener and Helper. I live, move and have my being in You. Thank you Father for an incredible journey so far. You are the only One who knows the future and Your Hand guides my path and destiny.

TABLE OF CONTENTS

Page

LIST OF TABLES

LIST OF FIGURES

LIST OF ABBREVIATIONS

5-FOA	5-Fluorootic acid
AAA	Acquired aplastic anemia
BIR	Break-induced replication
ChIP	Chromatin immunoprecipitation
DBD	DNA-binding domain
dHJ	Double Holliday junction
DKC	Dyskeratosis congenita
D-loop	Displacement loop
DSB	Double-strand break
EMS	Ethyl methanosulfonate
EST	Ever shorter telomere
G1	Gap phase 1
G2	Gap phase 2
GCR	Gross chromosomal rearrangement
H1	Histone
H2A	Histone 2A
H3	Histone 3
H4	Histone 4
HHS	Hoyeraal Hreidersson syndrome

HO	Homothallic switching endonuclease
HR	Homologous recombination
IPF	Idiopathic pulmonary fibrosis
IR	Ionizing radiation
M	Mitosis Phase
MMEJ	Microhomology-mediated end joining
MMS	Methyl methanosulfonate
MRX	Mre11, Rad50, Rrs2
RAP	Repeat addition processivity
RPA	Replication protein A
ROS	Reactive oxygen species
S phase	Synthesis phase
SDSA	Synthesis-dependent strand annealing
SiRTA	Site of repair-associated telomere addition
TEN	Telomerase essential N-terminal domain
T-loop	Telomere loop

CHAPTER 1

INTRODUCTION TO TELOMERES, TELOMERASE AND DNA DOUBLE-STRAND BREAK REPAIR

1.1 Overview

Telomeres, the protein-DNA structures at the ends of chromosomes are important for maintaining genome stability and cell viability. Telomeres distinguish normal chromosome ends from DNA double-stranded breaks, preventing degradation and fusion of these ends. Telomeres also facilitate the complete replication of the ends of the chromosomes. Due to the inability of DNA polymerases to initiate DNA synthesis *de novo*, terminal sequences are lost during each cell division, an issue termed the end replication problem. Telomerase, a ribonucleoprotein enzyme, counteracts the end replication problem by adding TG repeats to telomeric DNA using an intrinsic RNA template. These functions make telomeres and telomerase critical for maintaining genome integrity. Telomerase can also act on DNA termini produced by double-strand breaks (DSBs), in a process called *de novo* telomere addition. *De novo* telomere addition is associated with terminal deletions and may occur at the expense of normal DNA repair processes. Not surprisingly, cells have evolved mechanisms to regulate the activity of telomerase at these broken ends.

This thesis describes *de novo* telomere addition occurring at two different endogenous hotspots of telomere addition called SiRTAs (site of repair-associated telomere addition) on the left arms of chromosome V and IX in *Saccharomyces cerevisiae*. These SiRTAs undergo telomere addition at frequencies ~200-fold higher than neighboring regions and show a high degree of

mechanistic conservation. In chapter 2 of this thesis, I explore the requirements for the high frequencies of *de novo* telomere addition at SiRTAs. I present evidence to show that SiRTAs are composed of a bipartite structure consisting of TG-rich 'Stim' and 'Core' sequences. The more upstream Stim sequence is infrequently targeted for telomere addition, but is important for the high levels of telomere addition that occur at the Core sequence. This activity of the Stim sequence directly correlates with its ability to bind the single-stranded telomere binding protein, Cdc13. In chapter 3, I present evidence to show that Cdc13 activity at these SiRTAs is regulated by the action of the homologous recombination repair proteins Rad51 and Rad52, with some contribution from Replication Protein A complex (RPA).

This introductory chapter is divided into two main sections: **Telomeres/telomerase** (1.2) and **DNA double-strand breaks** (DSBs) (1.3). In the first section, I begin with a historical overview of the curiosity-driven research from the 1930's through to the turn of the millennium that led to the discovery of the enzyme telomerase, with special focus on model organisms such as *Tetrahymena thermophila* and the budding yeast *S. cerevisiae*. Then I delve into our current understanding of the mechanisms underlying telomere replication and regulation of telomerase activity at telomeres with an emphasis on *S. cerevisiae*. Telomere and telomerase biology have important consequences for human health. Telomere dysfunction is linked to a myriad of human diseases and is briefly addressed in section (1.2.8).

DNA DSBs are highly toxic lesions that result from endogenous sources (such as reactive oxygen species) or exogenous sources (such as ionizing radiation). Failed or inaccurate repair of DSBs can cause deletions, translocations and other forms of genome rearrangements. Therefore, appropriate detection and repair of DSBs is important for maintaining genome

integrity. There are two major, mechanistically distinct pathways of DSB repair in eukaryotes: Homologous recombination (HR) and non-homologous end-joining (NHEJ). HR requires a homologous template to initiate repair while NHEJ involves direct ligation of the broken ends with very little or no homology necessary. Other forms of less accurate repair such as break-induced replication (BIR), single-strand annealing (SSA), micro-homology mediated end joining (MMEJ) and *de novo* telomere addition are also utilized. These different repair pathways are briefly described in section 1.3. Also in this section, I discuss the assays used to study *de novo* telomere addition in *S. cerevisiae* and the information derived from these assays. I conclude section 1.3 with our current understanding of the regulation of *de novo* addition in *S. cerevisiae*.

1.2 Telomeres and telomerase

1.2.1 History of telomeres: The beginnings of the ends of chromosomes

The ends of most linear chromosomes are organized into special nucleoprotein structures called telomeres. Telomeres were discovered independently by Herman Muller and Barbara McClintock in the 1930's. Both investigators observed that the ends of the natural chromosomes were different from those of broken chromosomes and speculated that normal ends must possess special structures that confer this apparent uniqueness. In the 1930s, as the chromosome theory of inheritance gained increasing acceptance, scientists were becoming interested in understanding the effects of mutagens such as X-rays on chromosome structure and behavior. Unable to generate chromosomes lacking the endogenous termini following treatment with X-rays in fruit flies, Muller deduced that the ends of the chromosomes must be

important for maintaining the stability of chromosomes and called them telomeres [1]. He hypothesized that the ends of the chromosomes must have the special function of 'sealing' the ends and that chromosomes cannot persist indefinitely without sealed ends [1]. Independently, McClintock was analyzing the consequences of breakage-fusion-breakage events in maize strains with the goal of identifying the frequency with which dicentric chromosomes could be produced [2]. Dicentric chromosomes break when the two centromeres are pulled apart to opposite poles of the mitotic spindle during cell division. She observed that the broken chromosome ends generated from mitosis in endosperm cells were very unstable and that these ends regularly fused with other broken chromosome ends [2]. McClintock noticed however, that broken ends were never fused to the natural ends of the chromosomes (telomeres) and therefore hypothesized that normal chromosome ends must have the distinct capacity of protecting the chromosomes from fusion [2]. In essence, unlike broken chromosome ends, telomeres do not engage in fusion and recombination either with other telomeres or broken chromosome ends.

In 1941, McClintock observed that when she applied X-rays to embryonic maize cells, this cycle of breakage and fusion did not persist as it did in the endosperm, suggesting that the broken ends were somehow 'healed' [3]. We now know that these broken ends were healed by the addition of telomeres by the enzyme called telomerase. Telomerase is present and functional in embryonic cells and germ cells but not in endosperm cells that McClintock initially analyzed [4]. However, at this time, before the discovery of the double-helix structure of DNA, it was impossible to establish the mechanisms underlying telomere function. In 1953, the work of James Watson and Francis Crick uncovered the double helical structure of DNA and the

pairing rule for its nucleotides. This structure of DNA also predicted that, when separated, both strands served as template to guide synthesis of their complementary strands [5]. This semi-conservative mechanism of replication in which each replicated helix consists of a parental template strand and a newly replicated daughter strand was later proven by the work of Matthew Messelson and Frank Stahl [6]. Therefore, the DNA molecule serves as a template for the production of exact copies of itself and also carries genetic information. However, it would take some time to understand the mechanism(s) of the enzymes responsible for DNA replication.

With the discovery of DNA polymerases (enzymes responsible for catalyzing DNA replication in the 5' to 3' direction, primed from a short stretch of RNA molecule), it was suggested that this mechanism of replication could be problematic for the complete replication of chromosome ends. Alexey Olovinkov, in his paper '*Principles of marginotomy in template synthesis of polynucleotides'* postulated that the ends of the chromosomes could not be completely replicated because DNA polymerases cannot initiate DNA synthesis *de novo* at the ends of the chromosomes [7]. One year later, in 1972, this end replication problem was also proposed independently by Watson [8] who proposed that removal of the last RNA primer on the lagging strand would generate a gap of unreplicated sequence, creating the end-replication problem (Figure 1-1A).

We now understand that the original description of the end-replication problem must be revised. At the time Watson conceived of this problem, the chromosome termini were assumed to be blunt ended [7,8] (Figure 1-1A). In that case, removal of the terminal RNA primer on the lagging strand leaves a gap on the newly replicated strand, resulting in loss of terminal

sequences (Figure 1-1A). However, subsequent work has established that eukaryotic chromosomes termini are not blunt ended but rather carry a 3' overhang [9,10]. In this scenario, the template strand for leading-strand synthesis starts out shorter than the template strand for lagging-strand synthesis (Figure 1-1B). While leading-strand synthesis proceeds all the way to the end of the template [10,11], this creates a blunt ended molecule that must be processed by resection to recreate the 3' overhang (Figure 1-1B). The consequence is still telomere shortening with every cell division, but due to chromosome end processing and not DNA replication.

In 1961, Leonard Hayflick and Paul Moorhead showed that human cells derived from embryonic tissues could only divide finitely (~50 cell doublings) in culture before ceasing to divide, a phenomenon that came to be known as the 'Hayflick limit' [12]. This decrease in replicative potential is called senescence. Although, incompletely understood at this time, senescence was later shown to result from the progressive erosion of telomeric DNA during cell division and acts as a tumor suppressor mechanism (see section 1.2.3) (reviewed in [13]).

1.2.2 Telomere research in 1980's

Prompted by a desire to understand the molecular basis of telomere function, Elizabeth Blackburn ushered in the modern era of telomere biology in the 1980s. Before the advent of current DNA cloning methods, one of the biggest challenges to telomere research at this time was isolating the small amount of telomeric DNA from the rest of the chromosome. Blackburn reasoned that an organism with very short chromosomes would provide a much higher ratio of

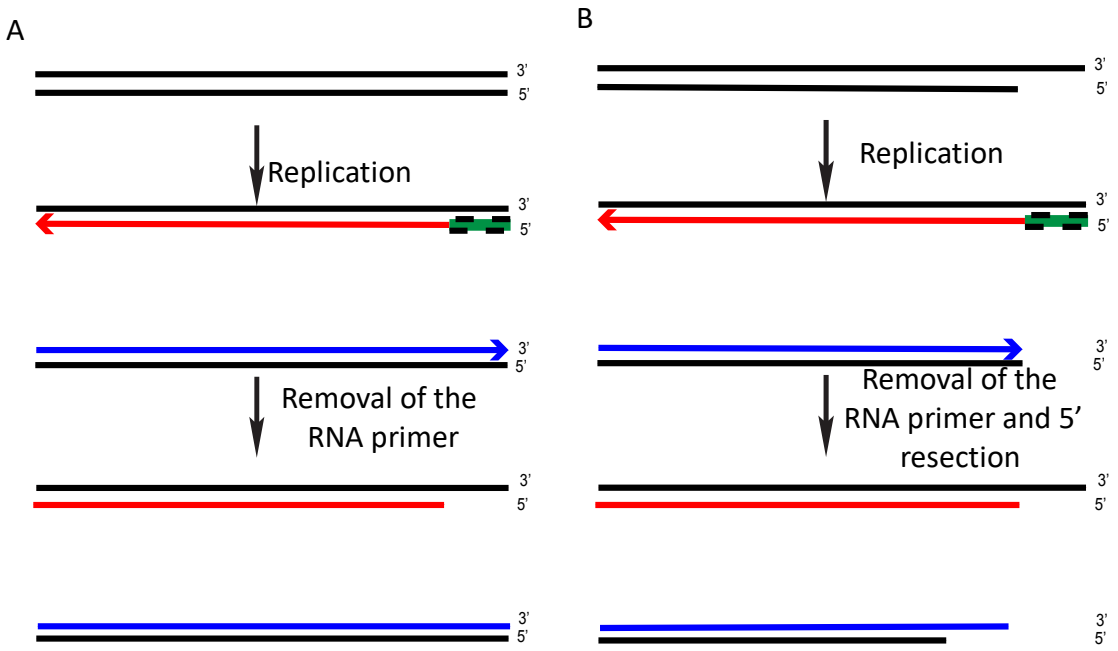

Figure 1-1.The end-replication problem. (A) The end-replication problem with blunt-ended molecules as proposed by Olovnikov and Watson. Replication of the lagging strand requires an RNA primer (black/green) and generates a 5' unreplicated gap (red) while replication of the leading strand replication regenerates a blunt ended molecule (blue). (B) Updated understanding of the end replication problem. Chromosome ends terminate in 3' overhangs. Replication of the lagging strand requires an RNA primer that when removed, recreates the 3' overhang. However, leading strand generates a blunt ended molecule that must be further processed to create a 3' overhang.

telomeric to non-telomeric DNA. Ciliated protozoans contain both a macronucleus and a micronucleus. During differentiation of the macronucleus, the chromosomes are fragmented by site-specific breakage into mini-chromosomes ranging from about 21 to 1, 500 kb in size [14]. These mini-chromosomes provided the perfect system for telomere research. Working in the laboratory of Joe Gall, Blackburn set out to determine the telomere sequences of the highly abundant rDNA mini-chromosomes. Surprisingly, she found they were made up of a 6-

nucleotide tandem repeat (5'-TTGGGG-3') that varied in number from 20 to 90 [15]. These repeats were oriented such that the TG-rich strand represented the 3' end of the mini-chromosome. The sequence of telomeres in another class of ciliates was also analyzed and found to be made up of tandem repeats of TTTTGGG, slightly different from *Tetrahymena* [16]. However, it was unclear whether other eukaryotes utilize a similar mechanism for telomere maintenance and chromosome end capping.

To address this question, Elizabeth Blackburn and Jack Szostak collaborated in 1982 to understand the relationship between telomere-maintenance mechanisms in *S. cerevisiae* and *T. thermophila*. While circular DNAs containing an origin of replication and selectable marker can be successfully transformed and maintained in *S. cerevisiae*, linear DNA molecules are usually integrated into chromosomes or degraded. They reasoned that addition of telomeres to the ends of linear DNAs might stabilize them and allow them to be maintained extra-chromosomally. They constructed a linearized yeast plasmid terminating in *Tetrahymena* telomeric repeats and observed that, when transformed into yeast strains, this plasmid was stably maintained [17]. Their results suggested that the structural features necessary for telomere replication may be conserved across species. They further demonstrated that if the *Tetrahymena* repeats were removed from one end of the plasmid, then it was no longer maintained in yeast cells. A successful search for functional yeast telomeres was carried out by joining random pieces of yeast genomic DNA onto this linear fragment to identify sequences that stabilized the plasmid [17]. Consistent with Muller's observation, this work showed that telomeres were important for stable maintenance of chromosomes.

Together with Janis Shampay in 1984, Blackburn and Szostak cloned and sequenced yeast chromosomes and found them to consist of tandem irregular repeats of the form TG_{1-3}. Unexpectedly, they found that the *Tetrahymena* repeats of the stable linearized plasmid (from their first experiment) had been extended by the addition of the yeast TG_{1-3} repeats rather than the Tetrahymena T_2G_4 repeat [18]. Altogether, these data suggested that the maintenance of telomeres was an evolutionarily conserved process. They further speculated that a terminal transferase-like enzyme may be involved in the synthesis of *de novo* telomere to ends of the chromosome [18]. The activity of this enzyme would potentially counteract the erosion of telomeric DNA caused by the end replication problem (Figure 1-1B). In 1988, the sequence of the highly repetitive tandem TTAGGG repeats at human telomeres was established [19] and remarkably, this same sequence was found to be conserved across many eukaryotes including all mammals [20]. Consistent with previous observations, the conserved structure of telomeres across species suggested a conserved function for telomeres as well.

1.2.3 Discovery of telomerase

These experiments and others prompted Elizabeth Blackburn and Carol Greider (a graduate student in Blackburn's lab) to search for non-templated telomere replication properties in *Tetrahymena*. They reasoned that telomere terminal transferase would be abundant in *Tetrahymena* since this organism contains thousands of telomeres. They developed an assay in which cell-free *Tetrahymena* extracts were incubated with labeled nucleotides and single-stranded primer consisting of four copies of the *Tetrahymena* telomere repeat. A terminal transferase-like enzymatic activity capable of extending the primer with a 6-

base periodicity was detected on sequencing gels [21]. Using dideoxynucleotides, they determined that this activity added TTGGGG repeats to the primer, corresponding to the *Tetrahymena* telomere sequence. They further showed that the elongation activity is template-independent and susceptible to heat and proteinase-K treatments, suggesting that this was an enzyme-catalyzed reaction [21].

In 1987, they purified this terminal transferase-like enzyme from *Tetrahymena* extracts and renamed it telomerase, a telomere-specific reverse transcriptase that utilizes an integral and essential RNA component as template for synthesis of *de novo* telomeric repeats [22]. They showed that telomerase is capable of adding TTGGGG repeats to telomeric sequences derived from several different organisms [22], congruent with the earlier observation that yeast $TG_{1\text{-}3}$ repeats were added onto *Tetrahymena* telomeres *in vivo* [17]. Cloning of the telomerase RNA component in *Tetrahymena* revealed that it contained the sequence CAACCCCAA which could provide the template for synthesis of the TTGGGG repeats [23]. Indeed, a templating function for telomerase RNA was conclusively demonstrated by target-specific mutagenesis. Mutations in the telomere complementary sequences of the telomerase RNA of *Tetrahymena* resulted in altered telomere sequences both *in vitro* and *in vivo* [24]. This experiment showed definitively that telomerase uses the CAACCCCAA template sequence to specify the addition of telomeric repeats and established the reverse transcriptase model of telomere extension both *in vivo* and *in vitro*. This model was further supported when the Blackburn group cloned and sequenced the RNA subunit from another ciliate, *Euplotes crassus* and identified the template sequence CAAAACCCCAAAACC which corresponds to the *Euplotes* telomere repeat TTTTGGGG [25].

1.2.4 Telomere research: Identification and characterization of telomerase components

At the same time the biochemical experiments were ongoing in the Blackburn lab, Vicki Lundblad, a graduate student in the Szostak lab, took a genetic approach to identify genes in yeast responsible for telomere replication. This genetic approach is unbiased and therefore required no prior assumption about the exact nature of telomerase enzymatic activities. We now know that this genetic screen was wildly successful, identifying three components of yeast telomerase and a fourth protein that binds telomeres to facilitate telomerase recruitment.

EST1 was the first telomerase gene to be identified using this genetic screen in 1989 [26]. The authors devised a clever method to identify mutants with defects in telomere replication. In this screen, a circular plasmid containing inverted *Tetrahymena* telomeric repeats separated by the *URA3* gene was transformed into yeast cells and monitored for spontaneous linearization. Stable maintenance of this plasmid as a linear molecule requires addition of yeast telomeric sequences onto the *Tetrahymena* telomeric repeats, thereby resulting in loss of the *URA3* gene. Following growth of mutagenized cells on 5-FOA (5-fluoroorotic acid), a drug toxic to *URA3* expressing cells, mutants with altered ability to convert the circular plasmid to a stable linear mini-chromosome were identified. 32 mutants out of 7,000 colonies screened displayed either increased or reduced resistance to 5-FOA when compared to wild type. In addition to being defective in the plasmid-linearization assay, one mutant strain showed shorter telomere length, increased frequency of chromosome loss and senescence, phenotypes predicted for mutants defective in telomere replication [26]. The mutated gene was cloned, sequenced and called *EST1*. Yeast cells carrying a complete deletion of the *EST1* gene displayed shorter telomere length, senescence and an increased frequency of

chromosome loss, collectively termed the '*est*' (ever shorter telomere) phenotype [26]. At this time, it wasn't clear yet whether Est1 was a part of the telomerase complex or simply had some other role in telomere maintenance, although a *Tetrahymena* telomerase RNA mutant that inhibited the addition of telomeres onto telomeric ends also displayed progressively shortened telomeres and underwent senescence [24]. Taken together, these results showed strongly suggested that telomere replication in yeast was dependent on telomerase.

Five years later, in 1994, the telomerase RNA Tlc1 was fortuitously identified in a screen designed to identify suppressors of telomeric silencing by gene overexpression [27]. The authors hypothesized that telomeric factors responsible for telomeric silencing (a phenomenon in which transcription is suppressed when a gene is integrated in close proximity to a telomere, presumably through heterochromatin formation) might be a part of a multimeric complex that may in turn be sensitive to stoichiometric imbalance of its components. This screen utilized a yeast strain in which the *ADE2* gene was integrated adjacent to the telomere on the right arm of chromosome V and the *URA3* gene was integrated on the left arm of chromosome VII [27]. Cells expressing *ADE2* are white, while those lacking *ADE2* expression are red. Strains with defects in telomeric silencing are *URA3*$^{+}$ and white. This strain was transformed with a library of yeast cDNAs expressed under control of a galactose-inducible promoter. Library plasmids resulting in a galactose-dependent decrease in telomeric silencing were then identified. *TLC1* was identified and demonstrated to be a telomere-specific suppressor of silencing when overexpressed. The *TLC1* gene was sequenced and shown to lack an open reading frame and to contain the sequence CACCACACCCACACAC, which includes the predicted template sequence for yeast telomeres, suggesting that *TLC1* encodes the yeast telomerase RNA [27]. Cells carrying

a deletion of *TLC1* displayed progressively shortened telomeres and mutation of the template region resulted in altered sequence *in vivo*, demonstrating conclusively that *TLC1* encodes the yeast telomerase RNA [27].

In the following year, the Lundblad group expanded the initial genetic screen [26] to identify additional genes required for telomere replication, incorporating all phenotypes displayed by the initial *est1* mutants [28]. Here, the plasmid linearization assay was preceded by a screen for colonies with increased frequency of chromosome loss. Candidates that displayed this phenotype were then screened for defects in the plasmid linearization assay and alterations in telomere length. *EST2*, *EST3* and *EST4* genes were identified [28]. The *est4* mutation was later shown to be an allele of *CDC13*, which encodes a single-stranded telomere binding protein also required for chromosome end protection [29]. In 1997, the gene encoding the p123 subunit of the *Euplotes aediculatus* telomerase was cloned and sequenced by the Cech group using reverse genetics. In a BLAST search to identify homologs, they discovered that the p123 subunit is homologous to the previously identified yeast Est2 [30]. Following alignment of the sequences, it was possible to recognize that both proteins contain homology to motifs characteristic of reverse transcriptases, including three invariant aspartate residues, suggesting that both proteins are the catalytic subunits of their respective telomerase complexes. Mutation of any of the three conserved aspartates in *EST2* resulted in *est* phenotypes similar to *est2*Δ and abolished telomerase activity *in vitro*, showing conclusively that Est2 is the yeast telomerase reverse transcriptase [30].

These experiments in model organisms paved the way for the identification of human telomerase. Using an *in vitro* primer extension assay similar to that of the Blackburn group

(section 1.2.3), Gregg Morin detected telomerase activity in crude Hela cell extracts capable of adding a 6 nucleotide repeating pattern to single-stranded oligonucleotide primers containing human or nonhuman telomeric sequences [31]. In 1994, telomerase activity was found in ~90% of immortal cell lines and primary tissues but not in actively proliferating normal somatic cell cultures, a distinction that was proposed to explain the limited the replicative potential of the latter [32].

The human telomerase reverse transcriptase, hTERT, was identified by the Cech group in 1997 and shown to contain all reverse transcriptase motifs [33]. This discovery allowed the role of telomere shortening in senescence to be directly addressed. As mentioned briefly earlier (section 1.2.1), in 1961, Drs. Hayflick and Moorehead showed that normal primary cells derived from fetal tissues have a replicative limit and stop dividing (senescence) in culture after 50 generations [12]. Harley *et al.* showed that the telomeres of cultured human fibroblasts progressively shortened with serial passaging during ageing of the cells in culture [34] and suggested that senescence was due to a lack of telomerase activity and inability to maintain chromosome ends in these cells. Introduction of telomerase into these fibroblasts allowed telomere maintenance and an improved proliferative capacity compared to control fibroblasts lacking telomerase [35]. Germ line cells have longer telomeres than telomeres of somatic cells [36]. Importantly, these studies showed that telomere length can be used as an indicator of the number of cell divisions undertaken by a particular tissue and reinforced the molecular mechanism for the Hayflick limit.

1.2.5 Role of telomerase components in telomere maintenance

With the realization that the *EST2* gene encodes the catalytic subunit of the yeast telomerase, attention focused on understanding the composition of the telomerase complex and how these components interact and function. Currently, *TLC1*, *EST1*, *EST2*, *EST3* and *CDC13* are the only genes known to exhibit the *est* phenotype when mutated. Tlc1 and Est2 make up the catalytic core of the telomerase complex and are indispensable for telomerase activity *in vivo* and *in vitro,* while Est1 and Est3 are accessory components dispensable for *in vitro* telomerase activity. The functions of each component are discussed in the following paragraphs.

As described above, normal telomere maintenance in *S. cerevisiae* requires the *EST1* gene and disruption of *EST1* causes telomere shortening [26]. However, *in vitro* telomerase activity is detected from extracts prepared from cells lacking the *EST1* gene, suggesting that *EST1* is dispensable for enzymatic activity [37]. Nevertheless, Est1 immunoprecipitates with Tlc1 RNA and telomerase activity, suggesting that Est1 is a telomerase component [38,39]. Fusion of the DNA binding domain of Cdc13 to Est2 (the catalytic subunit) bypasses the need for Est1 *in vivo*, suggesting that Est1 mediates the interaction between telomerase and telomeres [40]. Physical interaction between Est1 and Cdc13 was shown by the Zakian group using two-hybrid and co-immunoprecipitation experiments [41]. Charge swap alleles of *EST1* (K444E; *est1-60*) and *CDC13* (E252K; *cdc13-2*) independently confer a telomerase null phenotype [42]. However, cells carrying both mutations have short but stable telomeres and do not exhibit senescence [42]. These experiments further support the conclusion that Est1 interacts directly with Cdc13 and that this interaction is required for telomerase activity. Consistent with this interpretation,

cells carrying the *cdc13-2* mutation have low levels of telomere-associated Est1 and Est2 proteins [43]. Cells carrying the Cdc13-Est2 fusion construct have over-elongated telomeres in WT cells but not in cells lacking Est1, suggesting that Est1 may also be involved in activating an already telomere-bound telomerase [40]. Est1 binds directly to a stem-bulge region in Tlc1 [44] and this interaction is important for recruiting Est1 and Est2 to telomeres in late S/G2 phase [43]. Est1 interacts directly with Est3 and this interaction is required for Est3 telomere binding [45]. Est1 activation function might be explained by its role in recruiting Est3 (discussed below). The Est1 protein lacks a basic structural motif but binds RNA and telomeric DNA containing a 3' OH end *in vitro* [46,47]. The abundance of Est1 is cell cycle regulated, low in G1 phase and much higher in late S/G2 phase when telomerase is active [48,49]. This is due primarily to proteasome-dependent cell cycle regulated proteolysis [48–51] (see section 1.2.8 for more discussion).

Est2 is the catalytic reverse transcriptase subunit of yeast telomerase (reviewed in [52]) and, as discussed above, contains motifs found in other reverse transcriptases including three invariant aspartate residues. Similar to other telomerase reverse transcriptases, Est2 contains a basic N-terminal domain (TEN) required for its activity both *in vivo* and *in vitro* [53]. The TEN domain supports interaction with Tlc1 and Est3 [53,54]. Est2 is a low abundance protein and its levels are Tlc1-dependent [45].

Like Est1, Est3 is required for *in vivo* but not *in vitro* telomerase activity [28] (reviewed in [52]). Nevertheless, Est3 co-immunoprecipitates with telomerase [55]. The association of Est3 with telomerase is Est1 dependent [50] and purified Est1 and Est3 interact *in vitro* [45]. As mentioned earlier, Est3 interacts with the TEN domain of Est2, consistent with the observation

that the association of Est3 with telomeres requires Est2 [45,54,56]. Forced recruitment of Est3 to the telomeres through a fusion of Est3 to the DNA binding domain of Cdc13 facilitates telomere maintenance in *est3Δ* but not in *est1Δ* cells [55], suggesting that Est1 and Est3 have different functions at telomeres. Interestingly, Est3 contains structural similarities to the mammalian telomere structural protein TPP1 which may provide a clue to its precise role in telomere maintenance [57]. However, TPP1 is not a telomerase subunit but is part of the shelterin complex that protects mammalian telomeric repeat and is involved in increasing telomerase processivity (reviewed in [52], see section 1.2.9). Est3 has been shown to stimulate telomerase activity *in vitro* in a manner dependent on the interaction with the TEN domain of Est2 [54].

At more than a kilobase, the Tlc1 RNA is much larger than its ciliate and mammalian counterparts. A short 384 nt region is nevertheless sufficient for stable maintenance of yeast telomeres *in vivo* and for catalysis *in vitro*, suggesting that most of Tlc1 RNA is not required for telomerase activity [58]. A conserved pseudoknot domain of Tlc1 contains the templating region and an Est2 interaction region [59–62]. The Tlc1 RNA also forms three duplex arms that act as scaffolds for the assembly of Tlc1-interacting proteins. The interaction between Tlc1 and Ku80 occurs on one arm. This interaction recruits Est2 to telomeres in G1 phase and is also involved in trafficking of Tlc1 to the nucleus [63–66]. Another arm of Tlc1 interacts with Est1 and this interaction is required for telomerase activity *in vivo* [44]. The third arm acts as a scaffold for the assembly of the seven-member Sm protein ring, an interaction dispensable for telomerase activity but important for Tlc1 stability [67].

1.2.6 Telomere function, structure and organization

Thus far, I have established that telomeres facilitate the complete replication of chromosome ends by serving as substrates for telomerase. I have also established the roles for telomerase components in *S. cerevisiae*. However, telomerase expression (including the roles of its subunits) does not account for the other role of telomeres in preventing chromosome ends from being recognized as DNA DSBs. In this section, I discuss the functional organization of telomeres. How this organization contributes to the role of telomeres in chromosome end capping in addressed in section 1.2.7.

The repetitive sequences of telomeres described above are characteristic of most eukaryotic telomeres but are not sufficient to provide the protective functions first described by Muller and McClintock. Rather, functional telomeres are bound by a large number of proteins that protect these chromosome ends from the activities of the DNA repair machinery, thereby preventing nucleolytic degradation and chromosome fusions (reviewed in [68]). On the other hand, chromosome internal double-strand breaks (DSBs) lacking telomeres are recognized and rapidly repaired in cells. If telomere function is disrupted, either by loss of the DNA sequence or telomere-binding proteins, normal chromosome ends are no longer distinguished from DNA double-stranded breaks. Such uncapped ends trigger checkpoint arrest and undergo end-to-end fusions, which can be detrimental to cells during mitosis (reviewed in [52,68]).

As described above, the structure of telomeres is highly conserved among eukaryotes, consisting of an array of short tandem repeats. The Human telomeres comprise ~ 10-15 kb of hexameric (5'-TTAGGG-3') repeats while yeast telomeres comprise about 250-350 bp of

irregular TG_{1-3} repeats. The directionality of telomeres is conserved across species such that the 3' end of the chromosome is always the G-rich strand. The G-rich strand protrudes to form a 3' overhang usually present at both ends of the chromosome called the G-tails (Figure 1-2). In budding yeast, these G-tails are only about 12-15 nucleotides but can get much longer (>30-100 nucleotides) in late S/G2 phase of the cell cycle [69,70]. G-tails are generated by cell-cycle regulated C-strand degradation (reviewed in [52]). Human telomeres possess relatively long 3' single stranded G-tails, consisting of about 50-200 nucleotides throughout the cell cycle [71] which invade and displace G-strands in the double-stranded portion of the telomere, forming a telomere loop (t-loop) that is thought to provide a protective cap [72]. In addition to t-loops, G-rich telomeric DNA from most organisms forms stable G-quadruplex (G_4) structures arising from multiple guanine-guanine base pairing *in vitro* (reviewed in [73]). These structures may also contribute to telomere capping [74] and can either inhibit or promote telomerase activity *in vitro* depending on their exact nature [75–77].

The ends of the chromosome in yeast contain subtelomeric repeat elements. The X and Y' elements occur exclusively at subtelomeric regions, adjacent to the telomeric repeats (Figure 1-2) [78]. The X element is found at all chromosome ends at slightly varying sizes while the Y' is present at only about half of all yeast telomeres in 1-4 tandem repeats (reviewed in [52]). TG repeats are sometimes found between X and Y' elements [79]. Linear chromosomes lacking the terminal TG repeats are unstable and eventually lost from the cells [80]. However, cells lacking either X or Y' elements or both are very stable (reviewed in [52]). Amplification of the Y' elements by recombination is sometimes used to maintain telomeres in telomerase-deficient cells [81].

1.2.7 Telomere binding proteins in yeasts

Telomere-binding proteins can be divided into those that bind single-stranded or double-stranded DNA. Telomere function is carried out by the different proteins assembled on the ends of the chromosome. In this section, I briefly discuss the major telomere binding proteins in yeast and their implications for chromosome capping and genome stability.

The 3' overhang is bound by the **CST complex**, consisting of Cdc13, Stn1 and Ten1 (reviewed in [52,68]) (Figure 1-2). The CST complex binds single-stranded telomeric repeats through the OB-fold (oligonucleotide/oligosaccharide) domain of Cdc13 [42]. There are structural similarities between the three member CST and Replication Protein A (RPA) complexes. One model proposes that the CST complex out-competes RPA at telomeres for binding telomeric DNA [82,83]. However, RPA is telomere-associated and active at least during DNA replication [84,85]. The CST complex protects the C-strand from degradation and is also involved in telomere length regulation (reviewed in [52,68]). Cells carrying the temperature-sensitive *cdc13-1* allele exhibit extensive C-strand telomere degradation when exposed to high temperature and arrest at the G2/M phase [29], indicating that Cdc13 plays a critical role in chromosome capping. The capping function of Cdc13 also requires Stn1 and Ten1 [82,86–88]. However, the capping functions of the CST complex are only essential during late S and G2/M phases of the cell cycle [89–91].

The DNA binding domain of Cdc13 is located between amino acids 497-694 and this domain is able to fully reproduce the DNA binding activities *in vitro* [55]. The N-terminal domain of Cdc13 contains two OB fold domains and an Est1 interaction domain (recruitment domain, RD) involved in telomerase recruitment [42,92]. The first OB fold domain is important for Cdc13

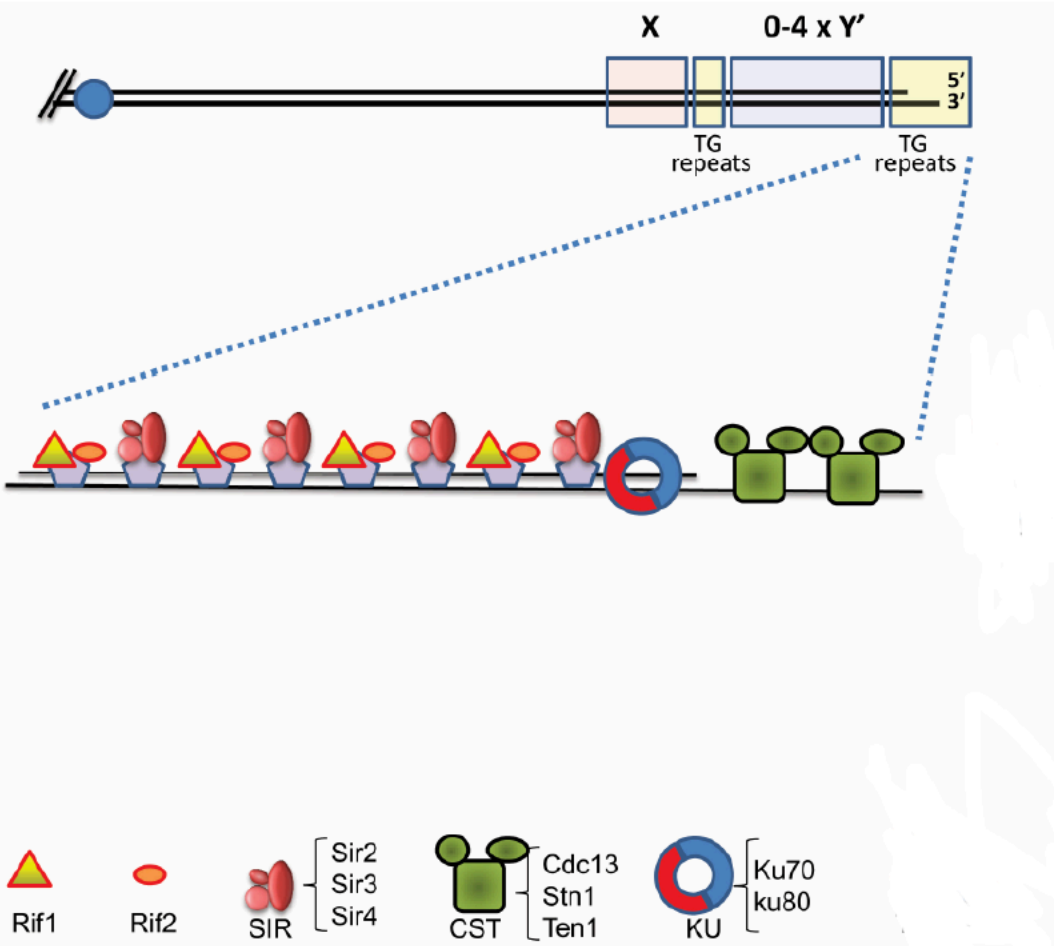

Figure 1-2: Structure of the yeast telomere. Yeast telomeres are made up of TG_{1-3} repeats. Yeast chromosomes contain subtelomeric X elements and 0-4 copies of the Y' element sometimes separated by TG repeats. The 3' strand protrudes to form a 3' overhang that is bound by the CST complex. The junction between the single-stranded and double-stranded portions of the telomere is bound by the Ku70/80 complex. The duplex DNA is bound by Rap1 bound to either Rif1/Rif2 or Sir proteins. Figure modified from [68].

dimerization and interaction with the DNA polymerase component Pol1 required to initiate both leading and lagging strand DNA synthesis (reviewed in [52]). Mutations in *STN1* or overexpression of both Stn1 and Ten1 can suppress the lethality of the *cdc13-1* mutants

[93,94]. The N-terminal domain of Stn1 is required for its interaction with Ten1 [87,95] while the C-terminal domain interacts with Cdc13 and Pol12 [96].

The double-stranded telomeric repeat DNA is bound with high affinity by **Rap1** (Figure 1-2) using a highly conserved MYB domain (reviewed in [52]). Given its abundance, not all Rap1 molecules in a given cell are telomere-associated (reviewed in [52]) and indeed, Rap1 was first discovered due to its ability to either repress or activate gene expression [97]. It is estimated that about 20 Rap1 molecules bind each individual telomere and this association plays a central role in determining telomere length [98]. The C-terminal domain of Rap1 recruits Rif1 and Rif2 proteins, which limit telomerase elongation in *cis* by affecting telomerase function. In fact, the amount of telomere-bound Rap1, in conjunction with Rif1 and Rif2, establishes the length of individual telomeres [99,100]. Rap1 also recruits Sir3 and Sir4 proteins which in turn recruit the Sir2 histone deacetylase involved in transcriptional silencing of adjacent genes [101]. Rap1 is important for chromosome capping in G1 phase of the cell cycle [91], perhaps largely due to its recruitment of Rif1 to telomeres. Rif1 is required to maintain viability in cells carrying a deletion of *STN1* and lack of Rif1 further reduces viability of *cdc13-1* cells [91]. *cdc13-1Δ rif1Δ* cells display very high amounts of telomeric single-stranded DNA and checkpoint activation, again consistent with a role of Rif1 in telomere capping [91]. Rap1 also prevents telomere to telomere fusions and determines the localization of telomeres to the nuclear periphery (reviewed in [102]).

The **Ku complex** is composed of two proteins (Yku70 and Yku80 in yeast). This complex is conserved in eukaryotes and plays central roles in double-strand break (DSB) repair by non-homologous end joining (NHEJ) (reviewed in [68]), a repair pathway in which the broken ends

are directly ligated together in a sequence-independent manner (section 1.3.4.1). Given this role in DSB repair, it is surprising that the Ku complex is a natural component of telomeres and plays an important role in telomere maintenance (reviewed in [68]). The Ku complex interacts with the telomerase RNA (Tlc1) and disruption of that interaction results in telomere shortening, but not senescence [63,64]. The Ku complex is also involved in chromosome capping as cells lacking Ku undergo modest telomeric C-strand degradation in G1 phase [90,91,103]. In that regard, it is interesting to note that Ku limits exonucleolytic activity both at broken DNA ends and telomeres [103,104].

1.2.8 Regulation of yeast telomerase activity

Telomerase isolated from yeast at any point in the cell cycle is capable of extending naked single-stranded DNA substrates *in vitro*. However, despite the presence of single-stranded overhangs at yeast telomeres throughout the cell cycle, experiments from several groups have established that telomerase elongation is regulated both as a function of cell cycle stage and telomere length. In this section, I highlight our current understanding of the mechanisms regulating telomerase activity *in vivo* in yeast.

1.2.8.1 Cell cycle regulation of telomerase

To identify mechanisms regulating telomere replication, the Gottschling group designed an assay in which a recognition site for the HO-endonuclease is placed immediately adjacent an 81 bp telomeric seed sequence on the left arm of chromosome VII (Figure 1-8B) [105]. HO endonuclease expression is induced by exposing cells to galactose, resulting in a double-strand break and exposure of the telomeric seed sequence. This telomeric seed sequence is efficiently

elongated within 4 hours following HO cleavage and ~ 90% of cells acquire a new telomere in a telomerase-dependent manner [105]. To address whether telomerase activity is cell cycle regulated, they performed this assay in cells arrested at the different stages of the cell cycle. New telomere formation is confined to S and late G2/M phases and does not occur in G1 phase [105]. However, telomerase purified from G1-arrested cells was active in an *in vitro* assay using synthetic telomeric primers [105]. These observations suggested that even though telomerase (at least the catalytic core) is present in G1 cells, it is not active at telomeres. Marcand *et al.* designed an assay in which the left end of chromosome VII was replaced with a short TG tract and a *URA3* marker flanked by two Flp1 recognition sites under control of a regulated promoter [106]. Following Flp1 induction, this short telomeric sequence serves as a seed for telomerase-mediated telomere extension. Consistent with the results of the Gottschling group, this short telomere was preferentially extended by telomerase only in late S/G2 phase and not in G1 phase [106]. One possible explanation for these results is that telomerase fails to associate productively with telomeres outside of late S/G2 phase of the cell cycle.

To address this possibility, the Zakian group used chromatin immunoprecipitation to examine the association of telomerase components with the telomeres. They arrested cells in G1, released them into the cell cycle, and monitored the subsequent association of telomerase components and the telomere-binding proteins Cdc13 and Ku80 with telomeres. They made several important discoveries. First, Cdc13 associates with the telomeres throughout the cell cycle, but its binding increases in S-phase, coincident with an increase in the single-stranded 3' overhang [48]. Second, Est2 and Tlc1 associate with telomeres in G1 phase in a manner that requires the 48 bp stem loop structure in Tlc1 RNA that interacts with yKu80 [64]. However,

mutations that disrupt this interaction cause only minor telomere shortening and no senescence phenotype [107], suggesting that the ability of telomerase to associate with telomeres in G1 phase contributes to, but is not required for, telomere-length maintenance.

As cells progress into S-phase, the association of both Est2 and Tlc1 with the telomeres initially decreases but then peaks again in late S-phase, the time of telomere replication [48]. This late S/G2 phase telomere association of Est2 is accompanied by increased association of Est1 and Est3 with telomeres, both of which are present at very low or undetectable levels at the telomere in G1 phase [43]. Indeed, the late S/G2 phase association of Est2 with telomeres requires the binding of Est1 to the stem-bulge region of Tlc1 and the Est1-Cdc13 interaction [48,64]. Est1 protein levels are low in G1 phase due to proteasome-dependent degradation, but peak as cells enter into late S-phase [48,50], providing an explanation for its cell-cycle restricted association with telomeres and suggesting that association of all telomerase components occurs in late S-phase when Est1 levels become sufficiently elevated to allow for the assembly of the fully functional telomerase complex [45,48,64]. Stabilization of Est1 in G1 phase through inhibition of the proteasome, although sufficient to restore the Est2-Est1 interaction, is not sufficient to promote telomerase activity, suggesting that at least one additional mechanism restricts telomerase activity in G1 phase (see below) [50].

Using fluorescence microscopy to monitor the movement and association of Tlc1 RNA with telomeres in real time, Gallardo *et al.* observed similar dynamics of telomerase in the cell cycle. In G1 and G2 cells, GFP-tagged telomerase RNA is much more mobile and its interactions with telomeres are more transient compared to late S phase when its movement slows and it displays stable telomere associations [108]. This stable association of Tlc1 in late S phase most

likely reflects telomerase actively engaging with telomeres as this association is reduced in genetic backgrounds with impaired telomerase recruitment [108]. Gallardo *et al.* find that Rif1 and Rif2 contribute to the restriction of telomerase activity in G1 phase. Short telomeres can be extended in G1 phase, but only in the absence of both Rif proteins [108]. Taken together, these results show that while telomerase is telomere-associated throughout most of the cell cycle, only late S-phase association of telomerase with telomeres is critical for telomere replication.

1.2.8.2 Telomere length regulation of telomerase

The identification of mutants in yeast that maintain longer or shorter than average telomere length over many generations implied the existence of specific mechanism(s) to regulate telomere length. The idea that such regulation might occur at individual telomeres *in cis* arose from assays similar to the one briefly described above (section 1.2.8.1) in which a short artificial telomere sequence is exposed following HO-induced cleavage. Conversion of this short telomeric seed to steady state WT length took about 50 generations, but the rate of elongation progressively decreased as the telomeric seed increased in length [106], suggesting that shorter telomeres may be preferentially extended in any given cell cycle.

To address this possibility, the single-telomere extension assay (STEX) was developed by *Teixeira et al*. to measure telomere elongation events at nucleotide resolution [109]. In this system, a *tlc1Δ* strain carrying a genetically marked telomere (recipient) is cultured for ~30 generations causing progressive loss of telomeric DNA, and then mated to a WT strain (donor). Telomeres that had shortened during growth of the *tlc1Δ* strain can be extended in the resulting zygote due to the presence of telomerase. After allowing just a single S phase to occur in the zygotes, the marked telomere is cloned and sequenced. Since the yeast telomeric

sequence is heterogenous (*i.e* each time telomerase acts, it generates a slightly different pattern of $TG_{1\text{-}3}$ repeats), repeats synthesized in the zygotic S phase can be easily identified [109]. The authors showed that the frequency of telomere extension decreases as a function of telomere length. About 6%-8% of WT length telomeres (250-350 bp) were extended in one cell cycle, while 42%-46% of telomeres $\leq$ 100 in length were extended [109]. These results show that not all short telomeres are lengthened in any given cell cycle, but that shorter telomeres are more frequently elongated compared to telomeres of average length.

Another layer of regulation is imposed by the checkpoint kinase Tel1 and the Mre11-Rad50-Xrs2 (MRX) complex. Very little Tel1 is detected at telomeres of normal length, while association is increased 10-fold at shorter telomeres [110]. Tel1 binding to short telomeres occurs in early S phase, increases as the cell cycle progresses, and persists for at least two cell cycle divisions [111]. Similar to the association of Tel1 with double-strand breaks, this binding depends on an interaction between Tel1 and the C-terminus of Xrs2 [110,111]. The binding profile of the MRX complex closely follows that of Tel1 [112] and occurs mostly on telomeres that have been replicated by the leading strand DNA replication [113]. These results suggest that MRX binds preferentially to short telomeres following leading strand DNA synthesis and that this binding recruits Tel1. The kinase activity of Tel1 is required for telomere maintenance [114] but the substrates of Tel1 phosphorylation at telomeres are currently unknown. Tel1 may phosphorylate one or more proteins involved in telomerase recruitment allowing for increased telomerase recruitment and/or activity at these short ends.

1.2.9 Mammalian telomere structure, function and organization

Much of our early understanding of the biology of telomeres and telomerase came from studies conducted in lower organisms such as *Saccharomyces cerevisiae* and *Tetrahymena thermophila*. Nevertheless, the structure and function of telomeres are conserved across eukaryotes. In the following sections, I briefly discuss the structure and function of mammalian telomeres and diseases associated with telomere dysfunction (section 1.2.10).

Human telomeres consist of 10-15 kb of double-stranded 5'-TTAGGG-3' repeats and terminate in 50-200 TG-rich 3' overhang [13]. These telomeres are coated by a six-member protein complex called shelterin consisting of TRF1, TRF2, TIN2, TPP1, RAP1 and POT1 that prevents the activation of the DNA damage double-strand break response at chromosomal ends (reviewed in [115]) (Figure 1-3). TRF1 and TRF2 proteins are bound to the double-stranded portion of the telomeres through their MYB domain and recruit the rest of the complex by interacting with TIN2. TIN2 interacts with TPP1 and TPP1 in turn interacts with POT1, a single-stranded DNA binding protein that associates with the 3' overhang [116]. The sixth protein, RAP1, is recruited to the complex through an interaction with TRF2 and is dependent on TRF2 for its telomeric localization (reviewed in [115]) (Figure 1-3).

Mammalian Rap1 has three domains: a MYB domain required for protein-protein interaction, an N-terminal BRCT motif and a C-terminal domain that mediates the interaction with TRF2 (reviewed in [117,118]). Unlike *S. cerevisiae* Rap1 (ScRap1) that contains a second MYB domain for binding telomeric DNA directly, mammalian Rap1 lacks a MYB DNA binding domain and so has low affinity for DNA and depends on TRF2 for DNA binding. As discussed above, yeast Rif1 and Rif2 are important binding partners of ScRap1. In contrast, mammalian

Rif1 is not constitutively associated with telomeric DNA and plays a role in the DNA damage response. No homolog of Rif2 has been identified in mammals (reviewed in [118]).

TRF1 and TRF2 are structurally similar; each contains a TRF homology (TRFH) domain and a C-terminal MYB domain connected through a flexible hinge domain. High affinity DNA binding by TRF1 and TRF2 depends on the formation of homodimers (reviewed in [117]) through interactions in the TRFH domain (reviewed in [118]). However, TRF1 and TRF2 do not form heterodimers (reviewed in [118]). The TRFH domain of TRF1 and TRF2 contains a peptide docking site for recruiting other proteins to telomeres (reviewed in [118]), but interestingly, the assembly of the shelterin complex does not require association with telomeric DNA (reviewed in [115,117]). TRF1 and TRF2 overexpression causes telomere shortening, suggesting that both proteins are negative regulators of telomere elongation [125,126]. TRF2 also stimulates the formation of telomere loops (t-loops), protective structures formed when the 3' overhang invades the duplex telomeric sequence (reviewed in [115]).

TIN2 provides a bridge between the shelterin components that bind to double-stranded DNA and Pot1, associated with single-stranded telomeric DNA (Figure 1-3). The FxLxP domain in TIN2 and the TRFH domain in TRF1 mediate the TIN2-TRF1 interaction. Two different regions in the N-terminal domain of TIN2 interact with TRF2 and TPP1 separately since a TRF2/TIN2/TPP1 tripartite complex can be formed (reviewed in [118]). The TIN2-TRF1 and TIN2-TRF2 interaction can also occur simultaneously. TIN2 plays a pivotal role in shelterin assembly and composition. Consistent with this observation, depletion of TIN2 destabilizes the shelterin complex (reviewed in [117,118]). However, it is not known whether TIN2 is constitutively bound to all three components.

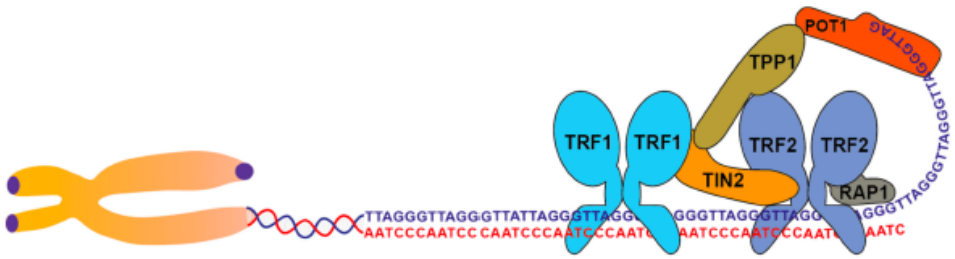

Figure 1-3: Structure of mammalian telomeres in association with the shelterin complex. TRF1 and TRF2 are shown as dimers. Although many complexes are loaded onto the telomeric repeats, only one shelterin complex is shown here for simplicity. Figure modified from [121].

Although POT1 binds single-stranded telomeric DNA with two N-terminal OB-fold domains, this interaction is not sufficient (reviewed in [118]). TPP1 mediates the interaction between POT1 and TIN2 through its POT1 interaction domain and C-terminal TIN2 interaction domain. This interaction is hypothesized to be the primary way POT1 is recruited to the telomeres. Consistent with this hypothesis, depletion of TPP1 leads to a depletion of POT1 from telomeres as well (reviewed in [117,118]). TPP1 mutants also display telomere deprotection and short telomere length phenotypes, phenotypes similar to those exhibited by POT1 mutants (reviewed in [118]).

POT1 and TPP1 promote telomerase recruitment to telomeres and stimulate telomerase repeat addition processivity (RAP), which defines the number of telomeric repeats that can be synthesized by telomerase before dissociating from the telomere. These activities require a cluster of acidic residues on the surface of TPP1 called the TEL patch [122]. The corresponding residues in human telomerase reverse transcriptase (hTERT) that mediate the interaction with

TPP1 have been characterized. Mutation of two residues in the TEN domain of hTERT reduces the TPP1-POT1 stimulation of telomerase RAP and causes a telomere maintenance defect [123]. Furthermore, a charge-swap mutation in the TPP1 TEL patch, rescues these defects, further suggesting that a direct interaction between the TEN domain of hTERT and the TEL patch of TPP1 is required both for telomerase recruitment and stimulation of telomerase RAP [123]. These observations are consistent with those from *S. cerevisiae* showing that Est3 (a potential structural homolog of TPP1) interacts with the TEN domain of Est2 [54]. Est3 stimulates *in vitro* telomerase activity in a manner dependent on its interaction with the TEN domain of Est2. Mutation of residues predicted to lie on the surface of Est3 disrupts the interaction with the TEN domain, causing telomere shortening and senescence [54]. Taken together, these results suggest that the Est3-Est2 TEN and TPP1-hTERT TEN interactions are important for *in vivo* telomerase assembly and telomerase activity.

1.2.10 Telomere dysfunction and human diseases

As discussed in section 1.2.4, one of the earliest connections between telomeres and cancer was inferred from the studies of the growth of human fibroblasts in cell culture. Whereas primary human cells exhibited limited replicative capacity [12], cancer cell lines divided indefinitely with passage in culture [34]. Later, it was observed that telomeres progressively shorten with cell passage in primary cells, but are stable in most cancer cell lines. Identification of the telomerase catalytic subunit, hTERT, led to the observation that most somatic cells have undetectable levels of hTERT, but hTERT is expressed in tumor cell lines (reviewed in [13]).

We now understand that critically short telomeres trigger senescence, a cellular state characterized by limited proliferation that is thought to serve as a DNA damage signaling mechanism to protect genome integrity and prevent further proliferation of cells that may contain mutations. Very short telomeres trigger a cell cycle checkpoint growth arrest signal (reviewed in [13]). Cells that are able to bypass this checkpoint enter another phase called 'crisis' characterized by loss of telomere capping functions, leading to chromosomal instability, spontaneous mitotic catastrophe and apoptosis (reviewed in [124]). Senescence and crisis can be completely overcome by overexpression of hTERT [35,125]. A rare somatic cell may be able to activate telomere maintenance mechanism (either through telomerase expression or telomere recombination) and undergo indefinite cell divisions (reviewed in [13]). Telomerase activity has been detected in ~90% of cancers, and this activity is required to maintain immortality (reviewed in [126]). In fact, telomerase-mediated telomere lengthening is one of the few essential steps that a normal mammalian fibroblast must undertake to become cancerous [127]. Telomerase expression in cancer cells maintains telomeres at a short but stable length. In the other ~10% of cancer cells, telomeres are maintained by an alternative recombination-based mechanism (reviewed in [126]). Somatic mutations in the hTERT promoter are prevalent in many cancer cell types (reviewed in [13]).

Dyskeratosis Congenita (DKC), Acquired Aplastic Anemia (AAA) and Idiopathic Pulmonary Fibrosis (IPF) are telomeropathies (telomere disorders) caused by germline mutations in telomerase components or telomere capping genes, leading to shorter than average telomeres in patients carrying these mutations (reviewed in [128]). DKC was the first disorder identified with a direct link to impaired telomere maintenance. Population studies of

DKC patients have identified mutations in *DKC1* (which encodes dyskerin), *TIN2*, *TR* (telomerase RNA), *TERT*, *NOP10* and several other genes involved in telomere maintenance [128]. DKC is characterized by leukoplakia, nail dystrophy, hyperpigmentation and bone marrow failure (reviewed in [13]). Hoyeraal-Hreidersson Syndrome (HHS) is a severe form of DKC associated with intrauterine growth retardation, cerebellar hypoplasia and microcephaly [129]. Revesz syndrome is a rare disease linked to mutations in *TINF2* which encodes TIN2 and characterized by similar symptoms of HHS [130]. IPF also can occur due to germline mutations in either *TR* or *TERT* and is the most common manifestation of a telomeropathy characterized by liver fibrosis and inflammation. Werner's syndrome is a premature-aging disease that affects telomere length through an unknown mechanism. Studies have demonstrated a correlation between telomere length and cardiovascular complications in this disease [131].

1.3 DNA double-stranded breaks (DSBs)

In the previous sections, I discussed telomere functions and telomerase activity at telomeres. However, telomerase activity is not restricted to telomeres but can be directed at DNA double-strand breaks (DSBs) to form new, or *de novo* telomeres. In this section, I review the mechanisms of DSB generation and repair with particular emphasis on the yeast model system, *S. cerevisiae*. I begin with a discussion of the sources and types of DNA DSB lesions and then follow with a review of some of the major pathways available to a cell for repair of DSBs. I end this section and chapter with a discussion of our current understanding of the mechanisms that regulate *de novo* telomere addition in *S. cerevisiae* as an introduction to my thesis studies of this phenomenon presented in Chapters 2 and 3.

1.3.1 Introduction

The structure of double-stranded DNA is easily imagined as that of a naked double helix molecule. However, DNA rarely exists in its naked linear form, but rather in association with core histone proteins to form nucleosome core particles, a structural unit of chromatin. Each nucleosome consists of about 147 bp of DNA wrapped around a histone octamer (two copies each of core histones H2A, H2B, H3 and H4) in a helical manner. Individual nucleosomes are connected by linker histones and further compacted into higher order chromatin structures by non-histone components and eventually form a chromosome (reviewed in [132]).

Chromosomes are constantly subjected to both endogenous and exogenous agents that threaten their integrity. By some estimates, a eukaryotic cell must repair up to 10,000 lesions (mostly single-strand breaks) per cell cycle to counteract the damaging effects of endogenous sources of DNA damage (reviewed in [133]). In normal human cells, it is estimated that ~1 % percent of single-strand lesions are converted to form ~ 50 double-strand breaks (DSBs) per cell in any given cell cycle [134]. DSBs occur when the two complementary strands are broken simultaneously and are the most toxic forms of DNA lesions. Cells have evolved two major pathways to repair DSBs: homologous recombination (HR) and non-homologous end joining (NHEJ). Although endogenous DSBs are typically repaired with high fidelity, failure to repair such breaks or errors during the repair process can lead to large-scale chromosomal changes including deletions, translocations and chromosome fusions that contribute to genome instability and cell death.

1.3.2 Sources and types of DSB lesions

The major endogenous source of DSBs stems from the collapse of replication forks that occur when such forks encounter unrepaired DNA or collide with the transcription machinery [135]. DSBs can arise from exposure to external agents such as ionizing radiation (IR), ultraviolet rays (UV), crosslinking agents and chemotherapeutic drugs such as methyl methane sulphonate (MMS), bleomycin, phleomycin and topoisomerase inhibitors [136]. IR creates DSBs directly or indirectly via production of reactive oxygen species (ROS) while UV light creates replication blocking lesions such as alkyl adducts, pyrimidine dimers and crosslinks (reviewed in [137]).

It is difficult to ascertain how often DSBs are triggered in a normal cell in the absence of exogenous agents, but studies in yeast reveal that just one persistent DNA DSB is sufficient to lead to cell death [80]. Defective repair of DSBs can create mutations, deletions and other forms of genome rearrangements that contribute to genome instability. For example, a growing body of evidence suggests that chromosomal translocations arise from the generation of two or more DSBs that were subsequently ligated together incorrectly [138]. Inaccurate repair of DSBs is associated with various neurological and immunological disorders and is a major driver in cancer cell progression [139]. Activation of proto-oncogenes or inactivation of tumor suppressors in cancer cells often results from loss and/or amplification of chromosomal regions due to inappropriate DSB repair [138]. Furthermore, mutations in factors responsible for DSB signaling and repair can also lead to mutations, deletions and other chromosomal rearrangements and are frequent initiating events in carcinogenesis [140,141].

1.3.3 Programmed DSBs

Despite posing serious threats to genome stability, DNA DSBs are precisely and intentionally employed in several biological processes. A well characterized example in higher eukaryotes is V(D)J recombination in which DNA DSBs are generated by the site-specific nuclease composed of RAG1 and RAG2 proteins at defined sites in developing B- and T-lymphocytes to allow for antigen-based diversity of immunoglobulin and T-cell receptor proteins (reviewed in [140,142]). Some lymphoid cancers bear oncogenic chromosomal rearrangements that result from defective repair of V(D)J recombination intermediates [143,144]. Class switch recombination (CSR) is another example of a recombination event involving the generation of DSBs in mature B cells. B cells undergo CSR to alter their immunoglobulin (Ig) constant heavy chain in response to antigen stimuli while retaining the same antigen specificity. Recombination occurs through cleavage and excision of constant heavy chains via DSB generation, followed by ligation of the remaining segments (extensively reviewed in [145]).

Beyond roles in lymphoid cells, DSB-induced recombination occurs in meiosis to promote efficient homologous recombination between chromatids of the maternal and paternal homologues in germ line cells. Meiotic recombination contributes to the fidelity of chromosome segregation and acts to achieve genetic variability. In *S. cerevisiae*, DSBs are created by the Spo11 endonuclease in prophase of meiosis I (reviewed in [135]). In budding and fission yeasts, *MAT* switching on chromosome III begins with the induction of a DSB in the mating-type locus that is repaired by ectopic recombination with donor sequences located on the same chromosome. *MAT* switching in *S. cerevisiae* uses the HO endonuclease, which

cleaves a 24-bp sequence to generate a DSB with 4-bp overhang [146]. In *Schizosaccharomyces pombe*, *mat1* switching initiates during replication from a single-strand nick which is then converted to a DSB. In *Kluyveromyces lactis*, *MAT* switching does not utilize the HO endonuclease but rather a transposon-like sequence excises from the MAT locus initiating switching [147].

Although not a programmed event *per se*, excision of transposable elements creates DSBs that are typically repaired by gene conversion with an unbroken homologous chromosome. In some ciliates such as *Tetrahymena* and *Paramecium*, programmed DSBs occur during development of the macronucleus leading to formation of many mini-chromosomes containing *de novo* telomeres [148]. In summary, programmed DSBs have proved useful to organisms as part of their normal cellular development. However, mis-regulation or aberrant repair of these programmed DSBs can result in extensive genome rearrangements.

1.3.4 DSB repair pathways

Homologous recombination (HR) and non-homologous end joining (NHEJ) represent two mechanistically distinct sets of pathways that have evolved to repair DSBs and the choice between these pathways is partly regulated by cell cycle stage. The HR pathway utilizes homologous sequences such as the sister chromatid or homologous chromosome as a template to effect repair, while NHEJ typically involves direct ligation of broken ends. Other forms of homology-dependent pathways such as single-strand annealing (SSA) and microhomology-mediated end joining (MMEJ) are also utilized in repair. These pathways have been studied extensively especially in the budding yeast *S. cerevisiae*. A large number of mutants in many

DNA repair pathways have been identified and extensively characterized using both genetic and biochemical analyses. These mutants have aided in the classification of these repair pathways. In the following sections, I review our current understanding of these repair pathways with an emphasis on *S. cerevisiae* and the proteins involved in each pathway.

1.3.4.1 Non-homologous end joining (NHEJ)

NHEJ involves ligation of the broken ends of a double-strand break with minimal processing, often resulting in small mutations or deletions at the break site. NHEJ is frequently observed in yeast strains without functional HR repair due to deletion of HR factors, or in situations where the DSB occurs in a sequence without a homologous partner (*i.e* G1 phase in haploid cells). NHEJ can occur at any phase of the cell cycle but especially in the G1 phase when 5' to 3' resection of the DNA break, a commitment to HR, is restricted.

The proteins involved in NHEJ and required for efficient DNA end joining can be classified into three different groups: Yku70/80, DNA ligase IV/Lif1 and Mre11/Rad50/Xrs2 (Figure 1-4). Most components of NHEJ are conserved between yeast and mammalian cells (reviewed in [149]). The Ku heterodimer is central to NHEJ from yeasts to humans and there is a high degree of conservation between the yeast and human Ku proteins [150]. In yeast, the Ku proteins are constitutively associated with telomeres, but are relocalized to sites of DSBs [151]. The Ku heterodimer is abundant and binds various DNA ends such as blunt ends or overhangs with very high affinity in a sequence-independent manner [152]. Ku binding tethers the broken ends and is necessary for the recruitment of other proteins involved in the repair process [153].

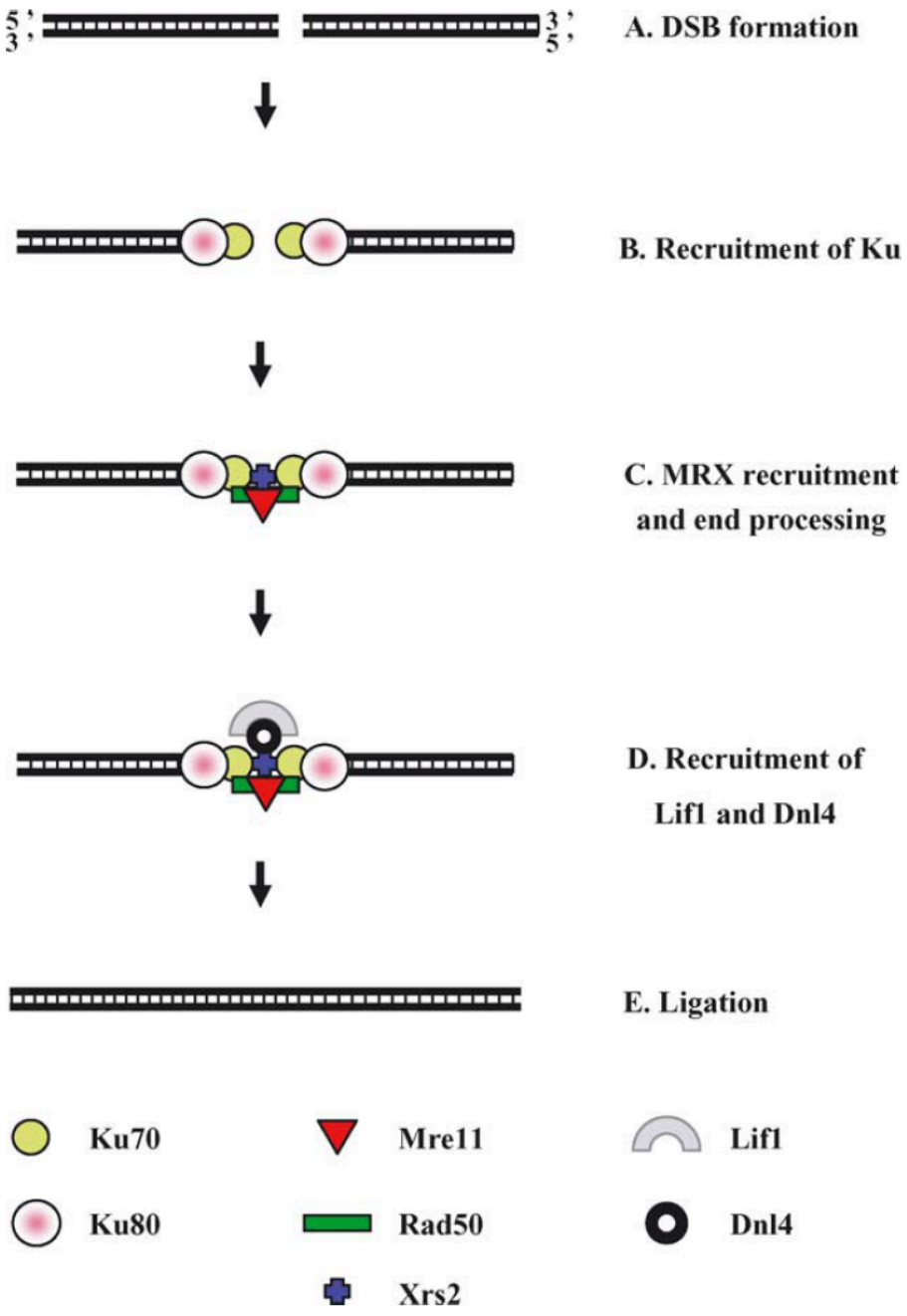

Figure 1-4: Repair of a DSB by non-homologous end joining (NHEJ). Following DSB creation (A), the Ku and MRX complexes are the first factors to arrive at the broken end. Both complexes are involved in tethering the broken ends. (B-C) The MRX complex further engages in DNA end processing (C). The Lif1/Dnl4 complex is recruited (D). The MRX and Lif1/Dnl4 complexes promote the activity of Lif1/Dnl4 complex, resulting in (E) ligation of the broken ends. Figure adapted from [149].

NHEJ requires rejoining of the DNA ends through ligation. Ku recruits DNA ligase IV/Lif1 complex to the broken DNA ends, in a process that is necessary for accurate and efficient end-joining both *in vitro* and *in vivo* [154] (Figure 1-4). Lif1 acts an adaptor between Ku and DNA ligase IV [154] (Figure 1-4). A haploid-specific gene *NEJ1* also regulates NHEJ in budding yeast. Cells lacking *NEJ1* exhibit an 8-fold reduction in NHEJ efficiency compared to wild type. Moreover, cells lacking both *DNL4* (which encodes for DNA ligase IV) and *NEJ1* exhibit the same level of NHEJ efficiency as either single mutant, suggesting that both genes are involved in the same epistasis group [155].

When presented with broken ends with perfect complementarity, NHEJ is usually very precise resulting in perfect ligation. However, DSBs often contain incompatible ends that cannot be effectively ligated. In these cases, DNA end processing is required to facilitate ligation, resulting in deletions and insertions that extend in both directions (reviewed in [156]). End processing is dependent on the MRX (Mre11, Rad50 and Xrs2) complex required also for homologous recombination in mitotic and meiotic cells [157]. Xrs2 recruits the MRX complex to the DSB and is also believed to enhance the helicase and exonuclease activity of the complex [158,159]. The MRX complex is thought to bridge and tether the broken DNA ends [160] and may also stimulate Ku and DNA ligase IV activity (reviewed in [161]). Loss of *RAD50*, *MRE11* or *XRS2* disrupts NHEJ to the same degree as loss of *YKU70*, *YKU80* or *DNL4*, suggesting that the MRX complex is intricately involved in NHEJ processes in the budding yeast (reviewed in [156]).

1.3.4.2 Homologous recombination (HR)

DSB repair by HR can occur through a number of different homology-dependent mechanisms. Repair by gene conversion and break induced replication (BIR) involve the annealing of the broken ends with homologous sequences present on a sister chromatid, homologous chromosome or a homologous sequence located elsewhere in the genome. Gene conversion is further divided into two different pathways: double Holliday Junction (dHJ; often leads to crossovers) and synthesis-dependent strand annealing (SDSA; usually no crossovers) pathways. While gene conversion typically restores the original DNA sequence, BIR occurs in situations where homology is only present on one side of the DSB and results in non-reciprocal translocations or deletions. Single-strand annealing (SSA) occurs through the annealing of homologous sequences flanking a break-site, resulting in deletion of the intervening sequences. The error-prone pathways of homology-dependent repair including BIR (section 1.2.3.3) and SSA (section 1.2.3.4) are addressed in detail below.

To different extents, these homology-dependent repair pathways require genes belonging to the *RAD52* epistasis group including *RAD50*, *RAD51*, *RAD52*, *RAD54*, *RAD55*, *RAD57*, *XRS2* and *MRE11*. Proteins belonging to this group interact in yeast two-hybrid experiments [162,163] and cluster as foci with DSBs [164,165]. The detailed temporal order of association with DSBs has been defined by genetic, biochemical and chromatin immunoprecipitation experiments, the conclusions of which are described below.

For HR to occur, the 5’ strands exposed at both sides of the break must undergo considerable resection to generate 3’ended single-stranded DNA that is used in the search for homologous template sequences (Figure 1-5). Initial processing of the DSB begins with the

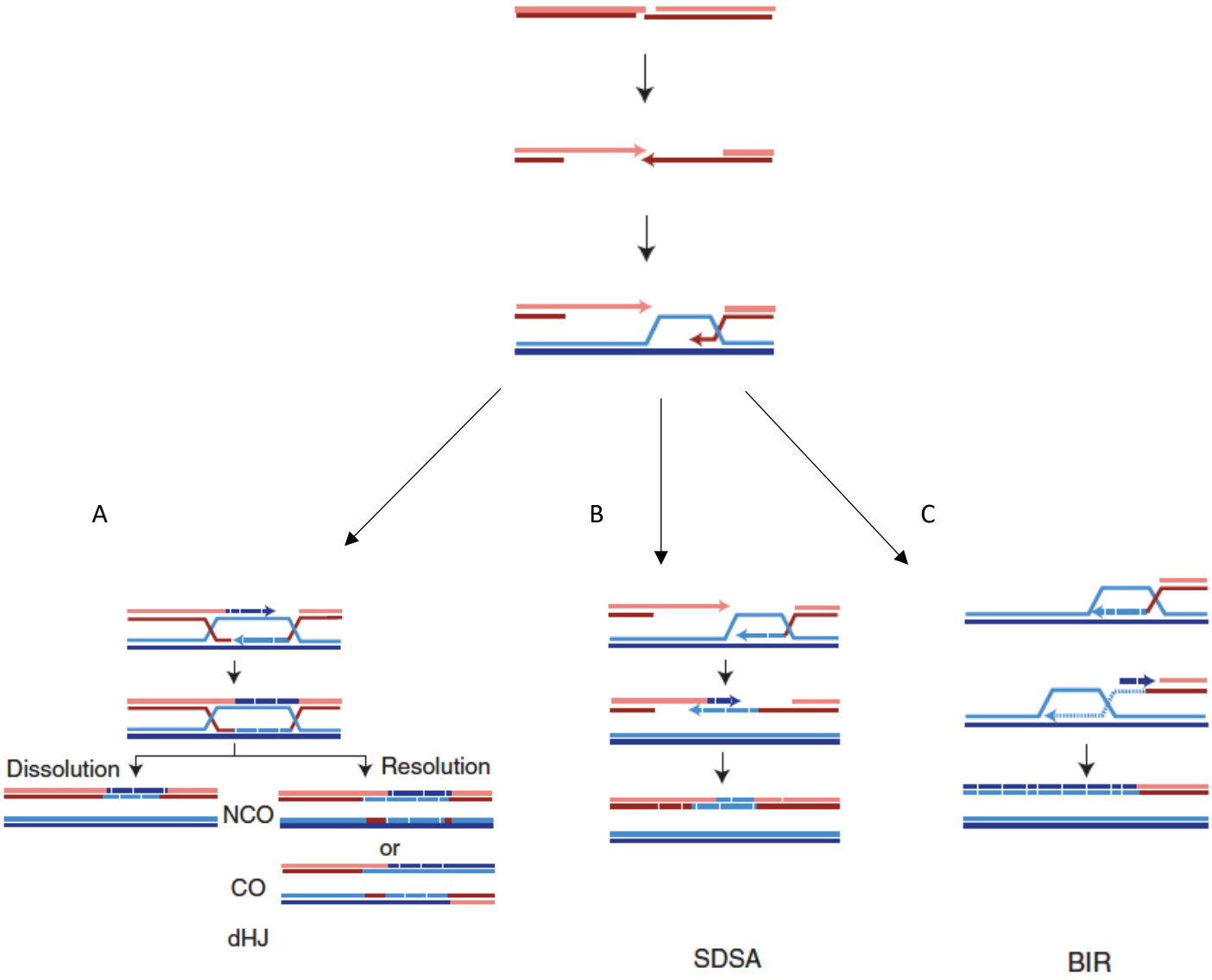

Figure 1-5: Repair of a DSB by homologous recombination (HR). Following DSB creation, resection of the broken ends occurs, generating 3' single stranded DNA. The 3' strand invades a homologous template duplex and anneals with the complementary strand. (A)The double Holliday Junction pathway involves the action of HJ resolvases which mediate the dissolution of the Junctions to produce either crossover or non-crossover outcomes (B) In synthesis-dependent strand annealing (SDSA), the newly synthesized strand is displaced from the loop and anneals to the ssDNA on the opposite side of the break to form a non-crossover outcome. (C) DNA replication in break induced replication (BIR) typically proceeds to the end of the duplex template and results in a non-reciprocal translocation. Newly synthesized DNA is shown as dashed lines. Figure modified from [166].

Mre11-Rad50-Xrs2 complex [167,168] and Sae2 followed by more extensive resection by Exo1/Sgs1 (reviewed in [166]). Resection of a DSB is limited in G1 phase of the cell cycle when cyclin-dependent kinase Cdck1 activity is low and increases in G2/M phase when Cdck1 activity is high (reviewed in [166]). As a result, HR is favored over NHEJ outside of G1 phase. The single-stranded DNA produced by resection is bound by RPA to prevent formation of secondary structures and to stabilize the single-stranded DNA [169,170].

As resection proceeds, RPA is replaced with the Rad51 recombinase to form the pre-synaptic filament on the single-stranded DNA. Replacement of RPA by Rad51 requires the aid of recombination mediators such as Rad52 [171] (reviewed in [166]. The Rad51 nucleofilament catalyzes homology search and strand invasion, processes facilitated by the Rad51 paralogs such as Rad55/Rad57. Rad54, a homolog of the Swi2/Snf2 family of ATP-dependent translocases, is required for strand invasion reactions and post-synaptic recombination (reviewed in [149]). The invading 3' strand can anneal with the complementary homologous template while displacing the non-complementary strand, forming a displacement loop (D-loop) (Figure 1-5A), consisting of a heteroduplex region and the displaced ssDNA. When both ends of the DSBs contain homologous sequences to the donor template, repair proceeds by gene conversion involving either dHJ or SDSA pathways. If homology is present on only one end of the DSB, repair proceeds by the break-induced replication (BIR) pathway (Figure 1-5C) (section 1.3.4.3).

The invading 3' end serves as primer for new DNA synthesis using DNA polymerase Polδ or Polε (reviewed in[166]). If homology is extensive, this D-loop can be extended by DNA synthesis allowing for more extensive base-pairing such that the ssDNA of the opposite side of

the DSB also invades the template, a process known as second-end capture, allowing the formation of a dHJ following ligation (Figure 1-5A). These dHJs are resolved by HJ resolvases to yield non-crossovers or crossovers depending on which pair of strands is cut (Figure 1-5A) (reviewed in [166]). This HR pathway is a type of gene conversion referred to as the double Holliday Junction repair pathway.

Alternatively, as new DNA synthesis proceeds, the newly synthesized strand can be displaced by branch migration and reanneal with the opposite resected 3' ssDNA on the opposite side of the DSB without the formation of a Holliday Junction (HJ) and no crossovers are formed (Figure 1-5B). This pathway does not involve second-end capture. This mechanism of HR not involving crossovers is a type of gene conversion called synthesis-dependent strand annealing (SDSA) (reviewed in [149]).

1.3.4.3 Break-induced replication (BIR)

One-ended DSBs created when replication forks collapse can be repaired using the BIR pathway in which DNA synthesis from the invading 3' strand usually proceeds all the way to the end of the template donor (Figure 1-5C). BIR has been studied extensively in *S. cerevisiae*, predominantly by using HO endonuclease to create a single, defined DSB that contains homology only to one side of the cleavage site. As described in the section 1.3.4.2, canonical BIR requires resection, Rad52-dependent formation of the Rad51 nucleofilament, and D-loop formation. Following extension of the original replication fork to the end of the template, the invading strand is extruded from the donor template and used as template for synthesis of its complementary strand (Figure 1-5C). Pif1 helicase is important for long-range DNA synthesis involved in BIR, though its specific role is largely unknown [172]. The Pol32 subunit of Polδ is

also required for BIR, possibly by enabling strand displacement during migration [173]. BIR is associated with increased mutagenesis, non-reciprocal translocation, loss of heterozygosity in diploids and other forms of chromosomal rearrangements (reviewed in [173]), but has also been shown to provide a mechanism to maintain telomeres in telomerase-deficient cells (reviewed in [174]). Rad51-independent BIR has also been observed and requires Rad59, Rdh54 (also known as Tid1) and the MRX complex (reviewed in [173]).

1.3.4.4 Single-strand annealing (SSA)

SSA is a DSB repair pathway that utilizes direct repeat sequences (typically >30 bp) flanking a break site to mediate repair of the broken ends, causing a deletion between the repeats (reviewed in [166]). SSA has been observed in many organisms, including *S. cerevisiae, D. melanogaster* and in mammalian cells. Following 5' to 3' resection by the MRX complex through the repeated regions, the single-stranded repeats anneal and the resulting non-homologous flaps are removed by the Rad1-Rad10 flap endonuclease (Figure 1-6). Because such repair removes all DNA sequences between the repeats (Figure 1-6), it is invariably mutagenic (reviewed in [175]). In one study, SSA occurred efficiently with 200bp of flanking homology, but 3% mismatches in the homologies greatly reduced repair efficiency (reviewed in [166]). The strand annealing activity of Rad52 is required for SSA with the aid of Rad59, a homolog of Rad52 [166]. However, as the length of homology increases, Rad52 becomes less important, likely reflecting the ability of longer sequences to spontaneously anneal and form stable duplexes [176]. Since strand invasion is not involved in SSA, Rad51 is typically not required for SSA [177].

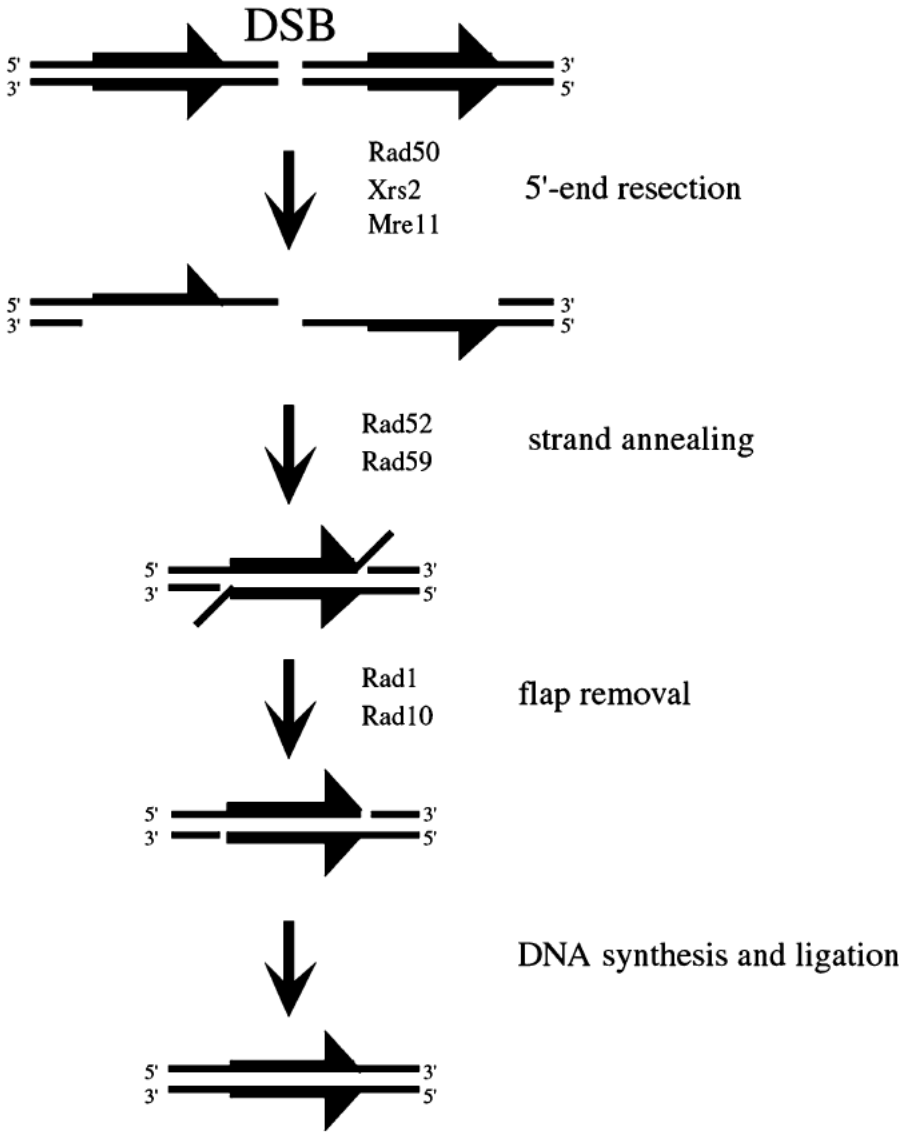

Figure 1-6: DSB repair by single-strand annealing (SSA). A DSB flanked by direct repeats undergoes 5’ to 3’ end resection, exposing the region of homologies. Strand annealing followed by removal of the 3’ non-homologous tails leads to the deletion of both the intervening sequence and one of the repeats. Each line represents a single-strand DNA molecule. Adapted from [178].

1.3.4.5 Micro-homology mediated end joining (MMEJ)

MMEJ describes an error-prone mechanism of repair that utilizes 5-25 bp microhomologies flanking the break site to facilitate annealing of the broken ends before end joining. In *S. cerevisiae*, the probability of MMEJ increases when a DSB is blunt-ended or contains incompatible overhangs, substrates that are not ideal for NHEJ [152,179]. Mre11 nuclease activity is essential for MMEJ and deletion of both *MRE11* and *EXO1* further reduces the efficiency of MMEJ [180]. Presumably, MMEJ requires the MRX complex to expose proper microhomologies that mediate annealing (Figure 1-7).

Following annealing, the non-complementary 3' flaps are cleaved from the annealed intermediate by the Rad1-Rad10 endonuclease (Figure 1-7). Ligation of the annealed DNAs is achieved by both DNA Ligase I and IV. Deletion of *DNL4* which encodes for DNA ligase IV, reduces but does not completely eliminate MMEJ, implicating a role for DNA ligase I in MMEJ [180]. Since resection is mostly restricted to S/G2 phase of the cell cycle, MMEJ might predominate in non-G1 cells [181]. MMEJ in *S. cerevisiae* occurs independently of the Ku complex. Moreover, the frequency of MMEJ increases significantly in the absence of Ku, with all survivors repairing DSBs by MMEJ [182]. Whether MMEJ requires Rad52 and is a subclass of SSA (section 1.3.4.4) discussed above is still controversial (reviewed in [181]). The length of the microhomology appears to be a contributing factor in whether Rad52 is required for MMEJ. Rad52 is required for MMEJ events that utilize $\geq$ 15 bp of microhomology but inhibits events utilizing < 15 bp of microhomology [183]. These findings show that the role of Rad52 in MMEJ is complex, depending on the length of microhomology at the DSB site. MMEJ is associated with chromosomal rearrangements and in cancers. Non reciprocal translocations arising from human

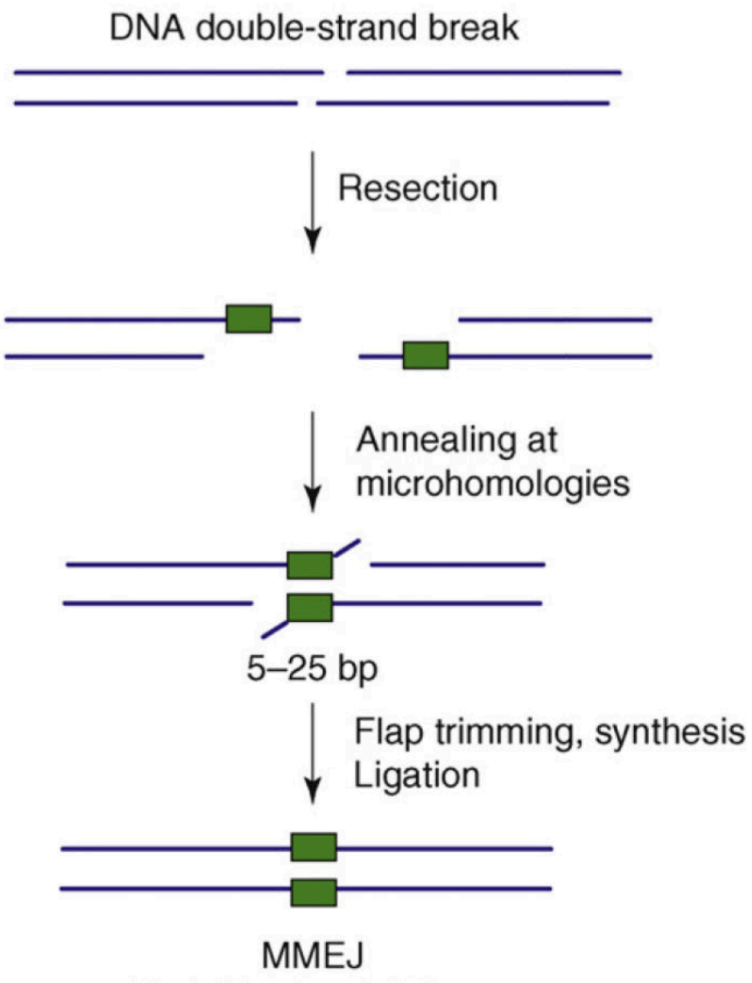

Figure 1-7 DSB repair by microhomology mediated end joining (MMEJ). MMEJ requires end resection to reveal homologous sequences. These microhomologies then anneal to each other. Once a stable intermediate is formed, repair is completed by flap trimming, fill-in DNA synthesis and ligation, resulting in a deletion relative to the original sequence. The end result is a deletion plus insertion event. Figure modified from [181].

cancers, including bladder cancers and leukemias, contain extensive microhomologies at the break site [184,185].

1.3.5 Chromosome healing by *de novo* telomere addition

De novo telomere addition with associated terminal deletion was observed in the early 1930's in experiments conducted with maize by McClintock [2] as described in section 1.2. Interestingly, in this case, addition of a new telomere to a broken chromosome allowed the cell to exit a lethal bridge-breakage-fusion cycle, thereby earning the name 'chromosome healing'. This may be the first reported *de novo* telomere addition event. Such *de novo* telomere addition events result in deletion of all DNA distal to the site of the break and are therefore considered a type of gross chromosomal rearrangement (GCR).

Several human genetic diseases are the result of terminal deletions resulting from telomere addition. The most characterized of these diseases involve telomere healing of a break on chromosome XVI adjacent to the α-globin locus, resulting in α-thalassemia [186]. Terminal deletion of chromosome XXII is observed in some patients with mental retardation (reviewed in [187]). These observations suggest that, although *de novo* telomere addition has the ability to prevent further resection of an unrepaired break, the action of telomerase at a DSB is likely to be regulated and coordinated with other repair pathways.

Despite the clearly deleterious nature of *de novo* telomere addition in the human diseases described above, such events have been reported in many organisms. *De novo* telomere addition also occurs as a part of the developmentally programmed chromosome fragmentation in ciliated protozoa. *Euplotes aeudiculatus* contains approximately 10 million telomeres, most of which are formed *de novo* during sexual conjugation. During this process, the micronucleus from its germline undergoes developmentally controlled chromosome fragmentation, DNA replication and *de novo* telomere formation to generate a new somatic

macronucleus. This newly formed macronucleus is made up of thousands to millions of linear DNA molecules capped by *de novo* telomeres [188]. Developmentally programmed chromosome breakage and *de novo* telomere addition also occurs in nematodes, crustaceans and some insects (reviewed in [189]). Taken together, these observations suggest that *de novo* telomere addition has significant consequences for cell development, genome integrity and cell viability.

1.3.5.1 Assays used to monitor *de novo* telomere addition in *S. cerevisiae*

The majority of assays used to monitor *de novo* telomere addition and other forms of GCRs in yeast have been conducted using modified substrates on the non-essential regions of chromosomes. Here, I review the current *de novo* telomere addition assays utilized in yeast studies and the information gleaned from these assays.

The Kolodner lab constructed an assay to detect spontaneous GCR events (Figure 1-8A) [190]. In this assay, the left arm of chromosome V is modified to contain the *URA3* gene adjacent to the *CAN1* gene in the non-essential region of chromosome V. Cells experiencing large-scale chromosome rearrangements that result in the loss of the chromosome terminus can be selected on media containing canavanine and 5-FOA, drugs toxic to cells expressing *CAN1* and *URA3* (Figure 1-8A) [190]. In wild-type cells, spontaneous GCR events occur at a very low rate of 3.5×10^{-10} [190]. The GCR events recovered include *de novo* telomere additions, translocations, deletions, duplications and inversions (reviewed in [191]). This assay has been used extensively to identify mechanisms underlying GCR suppression pathways in *S. cerevisiae* [187,189,190,192–194]. However, there are two major limitations to this assay. First, the events are very rare and require fluctuation analysis to determine the frequency of events.

Treatment of cells with DNA damaging agents can increase the frequency of GCR events but adds additional variables. Second, the site of the initiating lesion is unknown, so it can be difficult to ascertain whether a region that is prone to GCR formation represents a hotspot of DNA breakage or DNA repair or both. To address some of these concerns, assays have been developed in which the DSB is intentionally generated through nuclease action.

One such assay was constructed by Kramer and Haber in 1993. In cells lacking *RAD52* (therefore incapable of using HR), 13 copies of T_2G_4 repeats were integrated on chromosome III, internal to an HO cleavage site [195]. Induction of cleavage resulted in the recovery of cells bearing terminal deletions and further analysis verified that these cells had undergone *de novo* telomere addition near the T_2G_4 repeats [195]. Remarkably, such events occurred following extensive resection since the HO site was located 10 kb distal to the site of telomere addition. Moving the T_2G_4 sequence closer to the HO site (1.6 kb) increased *de novo* telomere addition 10-fold, consistent with a role for resection. *De novo* telomere addition was strongly dependent on these nearby T_2G_4 repeats in *cis* to the cleavage site as no terminal deletions occurred in the absence of these repeats. Importantly (and surprisingly), telomere healing did not occur within the T_2G_4 repeats but rather these repeats acted as a type of 'enhancer' of these telomere healing events, occurring in the flanking non-telomeric sequences [195].

The Gottschling group designed a *de novo* telomere addition assay, a variant of the Kramer and Haber assay, that has been used widely in the field to monitor the frequency of telomere healing on the left arm of chromosome VII (Figure 1-8B) [105]. Here, a haploid yeast strain carries the *ADE2* gene and 81 bp of TG-rich telomeric sequence placed immediately

A

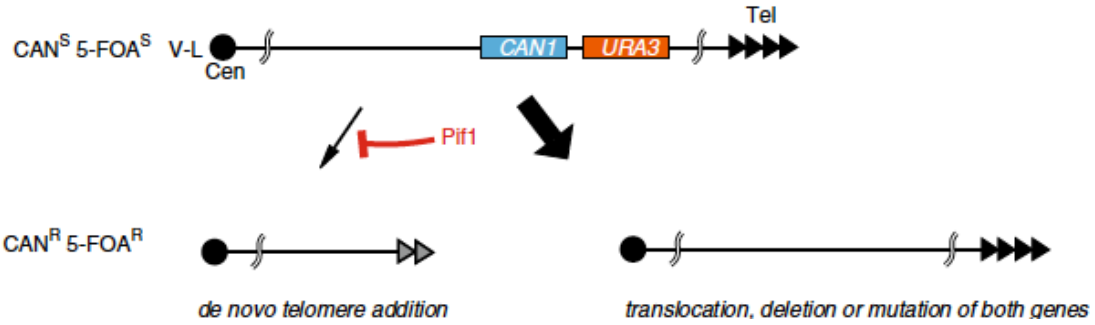

B

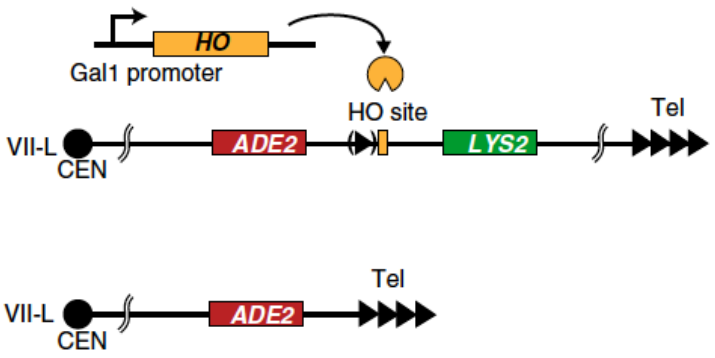

Figure 1-8: *De novo* telomere addition assays used in *S. cerevisiae*. (A) This assay was developed by the Kolodner group to isolate GCR events including *de novo* telomere additions. The *URA3* gene is inserted approximately 7.5 kb distal to the CAN1 gene. The region distal to the *URA3* gene contains non-essential sequences and can be lost. Following exposure to canavanine and 5-FOA, CAN^R 5-FOA^R cells are isolated and can involve *de novo* telomere addition (left) or translocation/deletion/mutation (right). Pif1 action negatively regulates *de novo* telomere addition (see text for more details). (B) This assay was developed by the Gottschling group (see text for detailed explanation). HO endonuclease is under control of a galactose-inducible promoter. HO induction leads to exposure of the telomeric seed that can be acted upon by telomerase to initiate DNA synthesis very efficiently. Figure modified from [191].

adjacent to a HO recognition site on the left arm of chromosome VII (Figure 1-8B) [105]. All genes distal to this integration site are non-essential. Following induction of HO endonuclease expression, cleavage exposes a 4 nucleotide TGTT 3' overhang that can be used by telomerase to initiate DNA synthesis. The *LYS2* gene is inserted distal to the HO recognition site to monitor loss of the terminal sequences (Figure 1-8B). *RAD52* is deleted to eliminate repair by homologous recombination. Healing by *de novo* telomere addition is efficient in this modified strain. Approximately 90% of all cells that incur a DSB undergo *de novo* telomere addition at this telomeric seed within 4 hours following HO endonuclease expression [105]. Because they rely on artificial sequences to stimulate *de novo* telomere addition, the assays described above may not accurately mimic repair at endogenous sequences.

To partly address this concern, Mangahas *et al*. constructed a haploid strain containing two copies of chromosome VII and a galactose-inducible allele of the HO endonuclease gene [196]. One copy of chromosome VII (the test chromosome) was modified to contain a HO recognition site immediately internal to the telomere, with *URA3* integrated internal to the HO site. Following induction of HO expression to remove the endogenous telomere from the test chromosome, surviving cells were recovered. In wild-type strains, about 70% of cells had retained the test chromosome, while this frequency was reduced to 0.3% in the absence of the *RAD52* gene [196]. This result suggests that in WT cells, the cleaved chromosome is frequently repaired by homologous recombination, likely using the intact chromosome VII [196]. In the absence of *RAD52*, terminally deleted test chromosomes arising as a result of *de novo* telomere additions were recovered in the absence of *RAD52* [196]. These *de novo* telomere addition breakpoints almost always occurred close to, but not within, naturally occurring TG-tracts and

these results provided the first evidence that a naturally occurring telomere-like tract could act as an enhancer to promote chromosome healing by *de novo* telomere addition [196]. The results from Kramer and Haber [195] and Mangahas *et al.* [196] argue that tracts of telomere-like sequence (artificial or natural) act as enhancers to increase the propensity for telomerase-mediated telomere addition. Significantly, these enhancer telomere-like sequences are not the site of actual *de novo* telomere addition but rather act as stimulatory sequences for *de novo* telomere addition.

Stellwagen *et al.* analyzed GCR events occurring in the 12 kb non-essential region on chromosome V using the Kolodner GCR assay (Figure 1-8A) [63]. Consistent with previous reports [189,190,192], these authors discovered that the vast majority of resulting GCR events were due to *de novo* telomere addition [63]. The frequency of GCR events was higher within a 23 bp TG-rich sequence within the *NPR2* gene compared to neighboring regions. All GCR events within this *NPR2* hotspot were *de novo* telomere additions [63]. However, the sequence requirements for this phenomenon was not explored. In work described in Chapter 2, I present detailed analysis of this hotspot of *de novo* telomere addition on chromosome V, which we called a SiRTA (Site of repair-associated telomere addition). Both this SiRTA on chromosome V and a second site that I subsequently identified on chromosome IX contain 'enhancer' sequences that stimulate *de novo* telomere addition [197]. Furthermore, mutation of these nearby enhancing sequences (which we call SiRTA-Stim sequences) reduces the frequency of *de novo* telomere additions following HO-induced double-strand break [197]. The basis of this enhancing function is described in Chapter 2.

1.3.5.2 Pathways that negatively regulate chromosome healing by *de novo* telomere addition

Given that *de novo* telomere addition following a DSB results in loss of all distal sequences, it is perhaps not surprising that the cell has evolved mechanisms to inhibit the action of telomerase at DSBs. Most strikingly, the Pif1 helicase is a potent suppressor of *de novo* telomere healing at double-stranded breaks (Figure 1-8A) [198,199]. In the absence of Pif1 helicase, the frequency of telomere healing events increases in both spontaneous and targeted assays (over 200-1000 fold) and these events tend to occur much closer to the break site at smaller TG tracts when no telomere seed is present [198]. Loss of Pif1 also affects normal telomeres, resulting in an ~50% increase in the steady-state telomere length [198,199]. The Pif1 helicase has functions in the nucleus and mitochondrion. Not surprisingly, an allele of Pif1 (*pif1-m2*) that eliminates its nuclear localization results in telomere over-elongation and increased *de novo* telomere addition, while an allele that eliminates its mitochondrial localization (*pif1-m1*) does not display these phenotypes [192]. The helicase activity of Pif1 is required to inhibit telomerase action and it has been proposed that Pif1 unwinds the telomerase RNA-telomere hybrid that is formed prior to telomere extension, thereby suppressing both *de novo* telomere addition at double-stranded breaks and excessive native telomere elongation [196]. While Pif1 does exhibit this capacity *in vitro*, it is unclear whether this is the primary mechanism through which it affects telomere addition *in vivo*.

Interestingly, the action of Pif1 at endogenous telomeres and DSBs maybe mechanistically distinct (or at least differentially regulated). Makovets and Blackburn showed that, in response to DNA damage, nuclear Pif1 is phosphorylated on residues T763 and S766 in a Mec1- and Rad53-dependent manner [200]. A *pif1* allele, *pif1-4A*, that cannot be

phosphorylated at these residues is unable to inhibit telomere addition at DSBs but is nevertheless competent for activity at telomeres. A phosphomimetic allele, *pif1-4D*, restores the repression of *de novo* telomere addition at DSBs [200].

Using the assay designed by the Gottschling group [105] (Figure 1-8B), the Durocher lab noticed that long TG-tracts (for example, the 81 bp tract originally used by the Gottschling lab; Figure 1-8B) exhibited the same efficiency of *de novo* telomere addition in the presence or absence of Pif1. In contrast, a very short TG-tract was extended by telomerase much more efficiently when Pif1 was deleted. To examine this phenomenon in more detail, the group placed different number TG-rich repeats adjacent to the HO cut site in an attempt to identify the minimum number of TG nucleotides required to render Pif1 inactive at such ends [201]. They found that Pif1 suppresses *de novo* telomere addition when the TG-tract is less than 34 nucleotides [201,202], suggesting that TG-tracts longer than 34 bp might be interpreted by the cell as critically short telomeres, rather than DSBs. The N-terminus of Cdc13 contains an OB-fold domain that forms dimers and binds ssDNA containing 37 but not 18 TG repeats *in vitro* [203,204]. The authors proposed that Cdc13 binding to sequences containing at least 36 repeats might allow these ends to bypass Pif1 inhibitory activity. Indeed, mutations that disrupt Cdc13 function allowed Pif1 inhibition of telomere addition at TG-tracts longer than 34 bp. Their results implicate a role for Cdc13 in blocking Pif1 inhibition at these longer repeats, although the exact mechanism is unclear. Altogether, these results suggest that Pif1 is able to distinguish DNA DSBs from telomeres and that phosphorylation of nuclear Pif1 is restricted to situations where telomerase might interfere with the normal DNA repair machinery.

Another layer of regulation is provided by the phosphorylation of Cdc13 by Mec1. The Durocher group (in a different work from that described above) utilized a variation of the GCR assay developed by the Kolodner group [190] to identify mutants required to sustain the high frequency of GCR events obtained in the *pif1Δ* background [202]. The *RRD1* gene, which encodes for an activator of protein phosphatase 2A (PP2A), was one of the genes identified. Further characterization was conducted by monitoring *de novo* telomere addition at TG-rich tracts of different lengths adjacent to an inducible HO cleavage site. In the absence of *RRD1*, *de novo* telomere addition was impaired at TG-repeat tracts of less than 11 bp, but was unaffected at longer tracts [202]. This activity of Rrd1 reflects activation of the PP2A-type phosphatase Pph3 since deletion of *PPH3* also impaired *de novo* telomere addition and the double mutant (*rrd1Δ pph3Δ)* was indistinguishable from either single mutant [202]. The authors further showed that phosphorylation of Cdc13 on S306 by Mec1 kinase counteracts the accumulation of Cdc13 at double-strand breaks containing <11 TG nucleotides. In summary, Pph3 phosphatase (positively regulated by Rrd1) counteracts Mec1 phosphorylation to facilitate Cdc13 association at DSBs containing very short telomere-like sequences, thereby modulating the frequency of *de novo* telomere formation [202]. It is not clear from this work why Mec1 phosphorylation of Cdc13 is required to restrict telomerase activity only at DSBs containing very minimal TG sequences and not at longer TG sequences. Taken together, these observations suggest that phosphorylation of Cdc13 and Pif1 cooperate to prevent aberrant activity of telomerase at double-strand breaks, allowing repair to occur by more accurate repair pathways.

1.3.5.3 Role of Cdc13 in promoting *de novo* telomere addition at double-strand breaks

The work presented in this thesis explores the role of Cdc13 in promoting *de novo* telomere addition at two endogenous TG-rich sites (SiRTAs). In this section, I discuss our current understanding of the role of Cdc13 in promoting *de novo* telomere addition at modified DSBs containing artificial seed sequences.

As discussed in section 1.2.5, Cdc13 is a single-strand telomere binding protein required both for chromosome end protection and for providing telomerase access to the telomere [28,92]. Its role in telomere replication was uncovered in the Lundblad screen designed to identify additional components of the telomerase machinery (section 1.2.4) [28]. Upon cloning, the *est4* mutation was discovered to be a separation-of-function allele of *CDC13* that retains the end protection function, but fails to recruit telomerase. This allele was subsequently renamed *cdc13-2* [26]. Cdc13 recruits telomerase to the telomeres through a direct interaction with Est1 [42]. In contrast, strains carrying the *cdc13-1* allele (a temperature-sensitive allele identified by Hartwell that results in uniform G2/M arrest at the restrictive temperature) undergo extensive resection of the 5' terminating strand at telomeres and accumulate long sub-telomeric tracts of single-stranded DNA [29].

In the *de novo* telomere addition assay designed by the Gottschling group (Figure 1-8B), Cdc13 was shown to be required for protecting the newly exposed TG_{1-3} end from extensive 5' to 3' nucleolytic degradation as *cdc13-1* cells displayed considerable degradation of the cleaved ends compared to WT cells [105]. Furthermore, *de novo* telomere addition was eliminated in cells carrying the *cdc13-2* mutation. Therefore, the 81 bp TG-tract utilized in this assay most likely allows Cdc13 association, with subsequent recruitment of telomerase to the DSB.

In a similar system employed by the Shore group, the *ADE2* gene and four copies of the Gal4 DNA binding site were integrated centromere-proximal to a HO recognition site on chromosome VII [205]. The *URA3* or *LYS2* genes were integrated on the distal side of the HO site to monitor for loss of the chromosome end [205]. Cdc13 was then expressed as a fusion to the Gal4 DNA binding domain. The Shore group showed that cells containing the GBD-Cdc13 construct survived the induction of cleavage at a higher rate compared to GBD-only controls. Furthermore, over 90% of these survivors generated red colonies due to telomeric silencing imposed on the *ADE2* gene and all candidates analyzed by Southern blot had a *de novo* telomere added [206]. These results further implicate a role for Cdc13 in promoting *de novo* telomere addition events at DSBs.

Piazza *et al*. also reported a role for Cdc13 in stimulating GCR formation on the left arm of chromosome V [207]. These authors employed the GCR assay developed by the Kolodner group that measures the rate of GCR formation resulting in terminal deletions (Figure 1-8A) [190]. Three different GC-rich mini-satellites (HRAS1, CEB1 and CEB25) derived from subtelomeric regions in the human genome were integrated centromere-proximal to the *CAN1* gene. When compared to a control strain lacking the mini-satellites, the presence of these motifs strongly increased GCR rates: 20-fold for HRAS1, 1,620-fold for CEB1 and 276,000-fold for CEB25 [207]. The GCR events induced by these mini-satellites were shown to be *de novo* telomere addition by Southern blot analysis. GCR formation in the of the presence the CEB25 mini-satellite was strongly dependent on orientation such that when the C-rich strand was on the same strand as the G-rich 3' overhang, GCR formation rate of CEB25 was reduced over 500-fold [207]. The CEB25 mini-satellite contains a GT/GG/TG dinucleotide bias and several

consensus binding sites for Cdc13. *In vitro*, Cdc13 binds the CEB25 mini-satellite with very high affinity and mutation of the Cdc13 binding sites resulted in lower Cdc13 affinity [207]. When this mutant motif was introduced into the chromosome, GCR formation was reduced 380-fold [207]. These results suggest that the recruitment of Cdc13 to CEB25 very strongly stimulates GCR formation. Altogether, these observations show that Cdc13 plays an important role in stimulating *de novo* telomere addition at DSBs containing artificial telomeric seed sequences.

1.3.5.4 The role of Ku in *de novo* telomere addition at double-strand breaks

As described in section 1.1.4, the Ku complex, consisting of Ku70/80 proteins, associates with both telomeres and DSBs and has also been implicated in the recruitment of Est2 to telomeres in the G1 phase of the cell cycle, independently of the Cdc13-Est1 telomerase recruitment pathway [64]. Ku also contributes to spontaneous *de novo* telomere addition at DSBs [192]. In the Kolodner spontaneous assay [197], a Ku mutant unable to interact directly with *TLC1* RNA strongly reduced *de novo* telomere addition induced in response to treatment to MMS in regions lacking extensive TG repeats [63]. Since telomere elongation still occurs in the absence of Ku [206], Ku and Cdc13 work cooperatively to recruit telomerase to telomeres and double-strand breaks [64].

1.4 Significance

As described in section 1.3, much of our knowledge of *de novo* telomere addition in *S. cerevisiae* has been derived from studies done using artificial sequences. In many of these cases, these artificial sequences were integrated immediately adjacent to the HO recognition

site. However, telomere healing occurring within these sequences may not fully recapitulate *de novo* telomere addition occurring within endogenous sequences. Moreover, telomere addition occurring near the break site maybe differentially regulated from that occurring several kb distal to the break site. My thesis has focused on exploring the requirements for *de novo* telomere addition at two different endogenous sequences (SiRTAs) on chromosomes V and IX.

Results described in Chapters 2 and 3 are the first to show that Cdc13 binding to these endogenous SiRTAs promotes high levels of telomere addition at these sequences following a DSB. Chapter 2 provides evidence that SiRTAs contain a bipartite structure in which Cdc13 binds to an upstream stimulatory sequence (enhancer sequence) to promote telomere addition occurring at an adjacent, TG-rich 'core' sequence. In Chapter 3, I present evidence that Cdc13 binding at these sequences is further regulated by the action of the homologous recombination proteins RPA, Rad51 and Rad52.

CHAPTER 2

ENDOGENOUS HOTSPOTS OF *DE NOVO* TELOMERE ADDITION CONTAIN PROXIMAL ENHANCERS THAT BIND CDC13[1]

2.1 Introduction

Chromosomes in all eukaryotes including the budding yeast *Saccharomyces cerevisiae* terminate in specialized nucleoprotein structures called telomeres. Telomeres in *S. cerevisiae* consists of ~250bp to 350bp of TG_{1-3} repeats and a short (~10bp) terminal G-rich overhang [208]. Because the conventional DNA replication machinery cannot fully replicate the ends of the chromosome, telomeres shorten with each cell cycle division. Telomerase is a ribonucleoprotein complex that utilizes an intrinsic RNA subunit as template for telomere synthesis, counteracting telomere shortening. Telomeres exist in association with telomere-binding proteins that protect chromosomes from nucleolytic degradation and prevent chromosome end-to-end fusions by distinguishing natural chromosome ends from DNA double-strand breaks (DSBs) [209]. These protective functions make telomeres essential for the maintenance of genome integrity and cell viability.

Optimal telomere length in *S. cerevisiae* requires a balance between positive and negative regulatory mechanisms mediated by telomere-binding proteins, including Cdc13 and Rap1. Cdc13 is a telomere sequence-specific single-stranded DNA (ssDNA) binding protein

[1] This chapter is published [197] *Obodo, U.C., *Epum, E.A., Platts, M.H., Seloff, J., Dahlson, N., Velkovsky, S.M., Paul, S.R., Friedman, K.L. *Endogenous hotspots of de novo telomere addition contain proximal enhancers that bind Cdc13.* Mol.Cell.Biol.,vol. 36, no.12, pp.1750-1763, 2016. *authors contributed equally to this work. Each author contribution is noted in each figure legend.

involved in recruiting telomerase to the telomeres during the S/G2 phase of the cell cycle through an interaction with Est1, a subunit of the telomerase holoenzyme (reviewed in [52]). Rap1 binds to the double-stranded telomeric repeat, forming a telomere length-regulatory complex through interactions of its C-terminal domain with Rif1 and Rif2 [210,211]. Regulation occurs through a counting mechanism in which telomere length is inversely proportional to the number of Rif1 and Rif2 molecules present at a telomere [99,100]

Cells experience insults to their genome from endogenous and exogenous sources, including reactive oxygen species, radiation, and chemical mutagens [212]. DSBs resulting from these sources pose an enormous threat to genome stability and cell viability, since failure to repair DSBs can cause chromosome rearrangements and/or chromosome loss. Eukaryotic cells utilize two main pathways for DSB repair: a homologous recombination (HR) pathway, which utilizes a sister chromatid or homologous chromosome as the template for repair, and a nonhomologous end joining (NHEJ) pathway, in which broken chromosome ends are directly ligated [161]. Inappropriate repair of DSBs can give rise to gross chromosomal rearrangements (GCRs), large internal deletions, translocations and chromosome end-to-end fusions [193]. Direct action of telomerase at DSBs results in yet another type of GCR, *de novo* telomere addition, in which all genetic information distal to the DSB is lost [187].

In yeast, either Cdc13 or Rap1 can stimulate *de novo* telomere addition. Cdc13 appears to facilitate telomerase recruitment to DSBs in a manner similar to its role at endogenous telomerase [206]. Following DSB induction by homothallic switching (HO) endonuclease, Cdc13 and Est1 are both recruited to an artificial telomere seed (~80bp TG tract) inserted adjacent to the HO site, and artificial tethering of Cdc13 adjacent to the break is sufficient to stimulate *de*

novo telomere addition [206]. Est1 recruitment depends on its interaction with Cdc13, although the converse is not true [206]. In contrast to its negative regulatory role at endogenous telomeres, Rap1 stimulates *de novo* telomere addition at artificial chromosomal [213,214] or extrachromosomal termini containing short telomere-like sequences [215]. While informative about mechanisms of telomerase recruitment, the vast majority of these studies utilize artificial sequences to facilitate the formation of *de novo* telomeres. Cdc13 and/or Rap1 could stimulate *de novo* telomere addition at endogenous intrachromosomal TG-rich sequences with the potential to bind one or both proteins. However, a potential role for Cdc13 or Rap1 at such sequences has not been directly addressed.

Given that *de novo* telomere addition at intrachromosomal TG-rich sequences has the potential to influence genome stability, we sought to identify the *cis*- and *trans*-acting factors required for *de novo* telomere addition at endogenous sequences. In this chapter, we investigate the requirement for *de novo* telomere addition at an 84-bp site of repair-associated telomere addition, located 35kb from the left telomere of chromosome V (SiRTA 5L-35). As previously described [216], the vast majority of telomere additions at SiRTA 5L-35 occur within a 23-bp TG-rich sequence, which we refer to as the Core. A separate TG-rich sequence located centromere proximal to the Core, and which itself is infrequently targeted for telomere addition, is required for high levels of telomere addition at the Core (referred to as the "Stim" sequence). We showed that it is likely the ability of Cdc13 to bind the Stim sequence that promotes telomere addition at SiRTA 5L-35. SiRTA 5L-35 therefore has a bipartite structure in which Cdc13 binding to an upstream sequence stimulates telomere addition at a neighboring target site. Finally, we report the identification of a new SiRTA located 44 kb from the left

telomere of chromosome IX and show that SiRTA 9L-44 has a bipartite structure similar to that of SiRTA 5L-35.

2.2 Results

2.2.1 An internal telomere-like sequence on chromosome V in *S. cerevisiae* is a target of *de novo* telomere addition

In *S. cerevisiae*, a short sequence within the NPR2 gene on the left arm of chromosome V (ChrV-L) incurs a high frequency of *de novo* telomere addition relative to that observed in flanking sequences [63]. To determine the magnitude of this effect in our strain, we utilized an assay [190] in which *CAN1* and *URA3* are utilized to select GCR events within a 12-kb region on chrV-L between *CAN1* and the first essential gene (Figure 2-1A). Independent liquid cultures were plated on medium containing canavanine (Can) and 5-fluoroorotic acid (5-FOA), drugs toxic to cells expressing *CAN1* and *URA3*, respectively. A single surviving colony was isolated from each culture for analysis. As previously shown [63,190], nearly all cells resistant to both drugs lost DNA sequences distal to *CAN1*. The approximate location of each rearrangement was determined by multiplex PCR using primer pairs spanning the 12 kb region (Figure 2-2), and each chromosome rearrangement was subsequently classified as “telomere addition” or “other” using Southern blot analysis to detect the characteristic “smear” generated by heterogenous telomeric repeats.

Three PCR primers were designed to detect GCR formation within an 84 bp TG-rich sequence encompassing the telomere addition hotspot within *NPR2* (Figure 2-2; PCR products 4

and 5). To reflect the propensity for *de novo* telomere addition, we refer to this sequence as the Site of Repair-associated Telomere Addition 35 kb from the left telomere of chromosome V (SiRTA 5L-35). Similar to previous report [63], 48.3% (14 of 29) of GCR events occurred in SiRTA 5L-35. The remaining events were split evenly between the regions centromere- and telomere-proximal to SiRTA 5L-35 (Figure 2-1B). In every case, GCR events within SiRTA 5L-35 involved *de novo* telomere addition, whereas GCRs in the flanking regions consisted of both telomere additions and other chromosome rearrangements (Figure 2-1B). Given that the 84-bp SiRTA 5L-35 comprises less than 1% of the total region analyzed, this sequence incurs a remarkably high frequency of *de novo* telomere addition.

To eliminate concern that telomere addition arises from a propensity for DNA breakage within or near this region, we utilized a second approach in which a site-specific DNA break is introduced ~3 kb distal to SiRTA 5L-35. The strain utilized [217] contains a single recognition site for the yeast homothallic switching endonuclease (HO endonuclease) within the *CAN1* gene (Figure 2-1C). Homologous sequences on chromosome III are deleted to eliminate repair by gene conversion. The HO endonuclease gene is expressed from a galactose-inducible promoter such that growth on media containing galactose results in a DSB ~3 kb distal to SiRTA 5L-35 (Figure 2-1C). Most cells accurately repair the DSB, resulting in a cleavage-repair cycle that culminates in cell death. However, approximately 0.1% of cells survive as a result of mutations at the HO site that prevent further cleavage. These cells have incurred small insertions or deletions or have lost all DNA distal to the HO site. The latter are identified by selection on 5-FOA for cells lacking the distal *URA3* marker (Figure 2-1C). We refer to cells that survive on

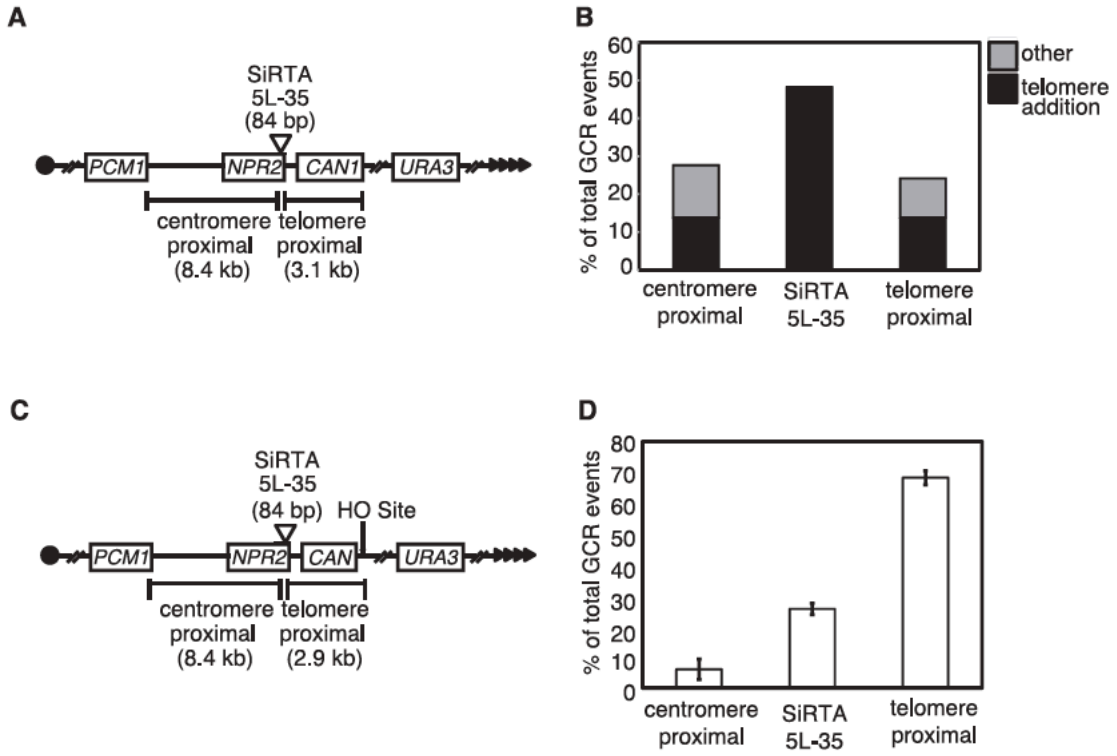

Figure 2-1: SiRTA 5L-35 incurs a high frequency of *de novo* telomere addition relative to flanking sequences. (A) Schematic of chromosome V GCR assay system. Filled triangles represent the terminal telomeric repeats. Throughout the figures, chromosome arms are diagrammed with the telomere to the right. This convention places the 3' terminus upon which telomerase directly acts on the top strand of DNA. (B) Distribution of spontaneously occurring GCR events in the WT strain. GCR events were mapped by multiplex PCR (Figure 2-2) to one of the three regions indicated in panel A. The type of event (telomere addition or "other") was determined by Southern blotting. A total of 29 events were analyzed. The enrichment of GCR events within the 84-bp SiRTA relative to the expected frequency (assuming a random distribution of GCR events across the 11.5-kb target region) was significant by Fisher's exact test ($P < 0.001$). (C) Schematic of the chromosome V HO-inducible GCR assay system. Expression of the HO endonuclease is induced by growth on medium containing galactose, and the site of HO cleavage is indicated (arrow). (D) Distribution of HO endonuclease-induced GCR events in the WT strain. Data are from three independent experiments and ~30 to 40 GCRs per experiment. Error bars represent standard deviations. Contributing authors: UCO, MHP, SMV, SRP.

A

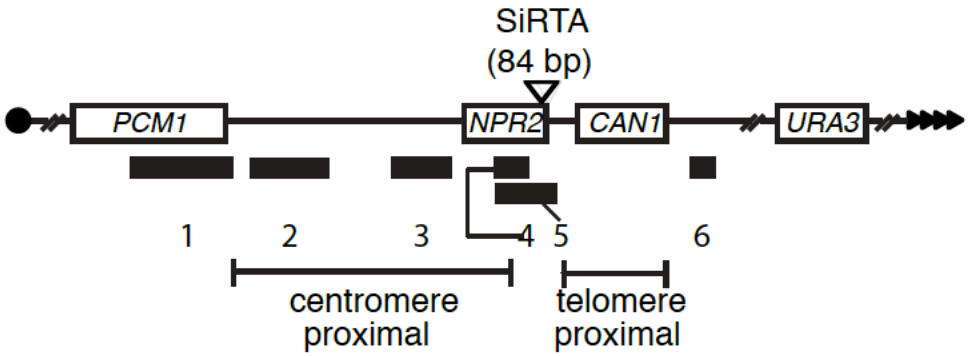

B

PCR product (size in bp)	Primer sequences
1 (620)	5'-CGATGAAGGTTGATTACGAGC-3'
	5'-GAAGGCTCCTATAAAGAACG-3'
2 (508)	5'-CGAGGTCACGGACACATATACC-3'
	5'-CGAGTGTAAATAGAGTATTTTCTAAC-3'
3 (415)	5'-GAAAATCGACATAATAAGAGTAGATTTCC-3'
	5'-GATTTGCGATAGCGTCGCTGCC-3'
4 (341)	5'-CTTAGTTTAGAAATTTTGGCAATG-3' *
	5'-GAAAAGGATACAAAGGATATGAG-3'
5 (452)	5'-CTTAGTTTAGAAATTTTGGCAATG-3' *
	5'GTTTTCTTCGATTTGAAGGTGTTGG-3'
6 (242)	5'-GAGTTTGCTAGATTCATAAAAGCC-3'
	5'-CCGATAATGTCTGAGTTAGGTGAG-3'

* Shared primer

Figure 2-2: Multiplex PCR analysis of GCR events. (A) Schematic of chromosome V in the strain utilized for HO cleavage. PCR products 1-6 are identical to those shown in Figure E1. The reverse primer for PCR product 7 is located within 60 bp of the HO cleavage site. (B) Characterization of 69 GCR events resulting from two independent HO cleavage assays. The approximate location of each event was determined by PCR as indicated in (A). Southern blot analysis was used to classify each event as "telomere addition" or "other."

galactose and have lost the *URA3* marker (Gal^R $5\text{-}FOA^R$ colonies) as GCR events. The propensity for GCR formation to occur at SiRTA 5L-35 is expressed in two ways: 1) as the overall rate at

which GCR formation occurs within SiRTA and 2) as the fraction of GCR events that occur within SiRTA. In both cases, values are the average (with standard deviation) of at least three independent experiments with 25-35 GCR events analyzed per experiment.

By PCR analysis, 25.7 ± 1.9% of GCR events following HO cleavage occurred within SiRTA 5L-35, 68.3 ± 2.3% occurred between the HO cleavage site and SiRTA 5L-35, and the remainder occurred in the centromere-proximal region between SiRTA 5L-35 and the first essential gene (Figure 2-1D). We analyzed a subset of events (69 from two independent assays) by Southern blot. 94.4% (17 of 18) events that mapped to SiRTA 5L-35 involved *de novo* telomere addition. Events that occurred distal to SiRTA 5L-35 fell into two classes. The majority of distal events (36 of 48) occurred at or immediately adjacent to the HO cleavage site (within 60 base pairs) and of those, 75.0% involved *de novo* telomere addition. In contrast, only 12 events occurred within the 3 kb separating the HO site from SiRTA 5L-35 and 58.3% of those events involved *de novo* telomere addition. *De novo* telomere addition events at SiRTA 5L-35 are mediated by telomerase since deletion of *RAD52* to eliminate recombination-mediated telomere maintenance did not reduce the fraction of GCR events occurring at SiRTA 5L-35.

2.2.2 A sequence internal to the direct target of telomere addition is required for high levels of *de novo* telomere addition at SiRTA

To identify sequences required to direct high levels of *de novo* telomere addition at SiRTA 5L-35, we cloned and sequenced 14 telomere addition events following HO cleavage. Telomere addition occurred at seven different sites, four of which were used more than once (Figure 2-3A). All 14 events were independent, as reflected in the divergent telomere

sequences added to each. Of the 14 telomere additions, 8 (57.1%) occurred within the original 23-bp TG-rich sequence defined by Stellwagen *et al.* [63]. Interestingly, very few events occurred at the centromere-proximal end of SiRTA 5L-35, despite the telomere-like nature of that sequence (Figure 2-3A). To determine which sequences contribute to the high rate of *de novo* telomere addition, we created a series of mutations, diagrammed in Figure 2-3A. Mutation of the 23-bp TG-rich sequence in which telomere addition frequently occurs (each base mutated to its complement) decreased the overall frequency of GCR events at SiRTA 5L-35 16-fold (Figure 2-3B; mutation a). In contrast, mutation of the neighboring sequence (mutation b) did not significantly change the overall rate of GCR formation (Figure 2-3B). To address a potential role for the TG-rich sequence at the centromere-proximal end of SiRTA 5L-35, we mutated this 18-bp region to adenine (mutation c). Although this sequence is rarely the direct target of telomere addition, the effect on the rate of GCR formation within SiRTA 5L-35 was nearly as pronounced as that seen when the target sequences themselves were mutated (Figure 2-3B; compare mutations a and c). Furthermore, only 3 of 5 of those events involved *de novo* telomere addition (data not shown). While this sequence enhances telomere addition at SiRTA 5L-35, it is insufficient to support high levels of *de novo* telomere addition since a strain containing only the centromere-proximal sequences (mutation d) underwent a low rate of GCR formation within SiRTA 5L-35 (Figure 2-3B).

We conclude that high levels of telomere addition at SiRTA 5L-35 require a bipartite structure in which one sequence serves as the primary, direct target of telomere addition (the SiRTA Core; defined by mutation a), while the other sequence (SiRTA Stim; defined by mutation

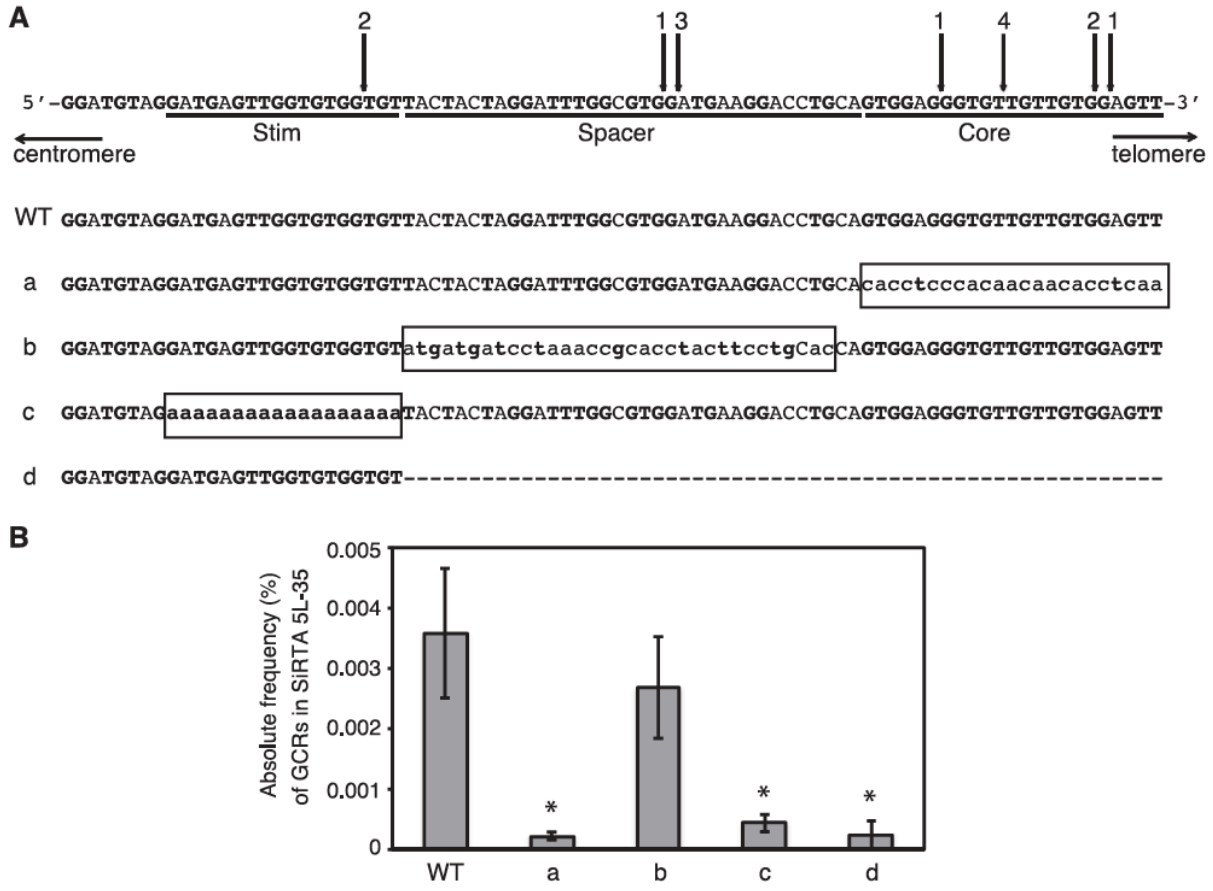

Figure 2-3: High rates of telomere addition at SiRTA 5L-35 require two separable sequences. (A) Top schematic, sequence of SiRTA 5L-35 with arrows indicating sites of *de novo* telomere addition. The most 3' chromosomal nucleotide with identity to the cloned *de novo* telomere is indicated. Numbers above arrows indicate the number of independent telomere addition events mapped to each site. Stim, Spacer, and Core are defined in the text. Bottom schematic, mutations created in SiRTA 5L-35. Uppercase letters represent unchanged nucleotides, lowercase letters enclosed in box represent mutated nucleotides, and the dashed line indicates deleted nucleotides. (B) Core and Stim sequences contribute to the formation of GCR events within SiRTA 5L-35. The frequency (%) at which GCR events occur within SiRTA 5L-35 following induction of HO endonuclease expression on medium containing galactose is shown for the WT strain and for the mutant strains as depicted in panel A. Averages from three independent replicates are shown with standard deviations. Mutants marked with an asterisk are significantly different from WT (*P* 0.05) by analysis of variance (ANOVA) with *post hoc* Tukey's honestly significant difference (HSD). Contributing authors: KLF, UCO, JS, NAD.

c) stimulates telomere addition within or near the Core sequence. The spacer between these sites makes no sequence-specific contribution to the stimulation of *de novo* telomere addition.

2.2.3 The Core and Stim sequences of SiRTA 5L-35 are sufficient to stimulate high levels of *de novo* telomere addition at an ectopic site

Given that the spacer between the SiRTA 5L-35 Core and Stim sequences could be mutated with little effect on telomere addition, we tested the effect of deleting this sequence (Figure 2-4A). Strikingly, the overall rate of GCR formation within SiRTA 5L-35 following HO cleavage increased 36-fold compared to the wild-type SiRTA 5L-35 (spacerΔ) (Figure 2-4B), and 74.2% $\pm$ 15.6% of total GCR events occurred within SiRTA 5L-35. Analysis by Southern blotting of 35 GCR events from one representative assay showed that all 28 events within SiRTA 5L-35 spacer involved *de novo* telomere addition (data not shown). In addition, 5 of the remaining 7 events, originally classified as telomere proximal by PCR, actually involved telomere addition within 100 bp of the spacerΔ variant of SiRTA 5L-35. No events of this type were observed among 69 GCR events characterized in the wild-type (WT) strain.

We took advantage of this remarkably high level of *de novo* telomere addition to ask whether the SiRTA 5L-35 Core and Stim sequences are sufficient to confer this property to an ectopic site. A 49-bp sequence containing the SiRTA 5L-35 Core and Stim sequences (SiRTA-spacerΔ) was integrated within nonessential sequences on chromosome VII-L, ~20 kb from the first essential gene (*BRR6*). The galactose-inducible HO cleavage cassette was placed 3 kb telomere proximal to the ectopic SiRTA sequence, and *URA3* was integrated to monitor the rate

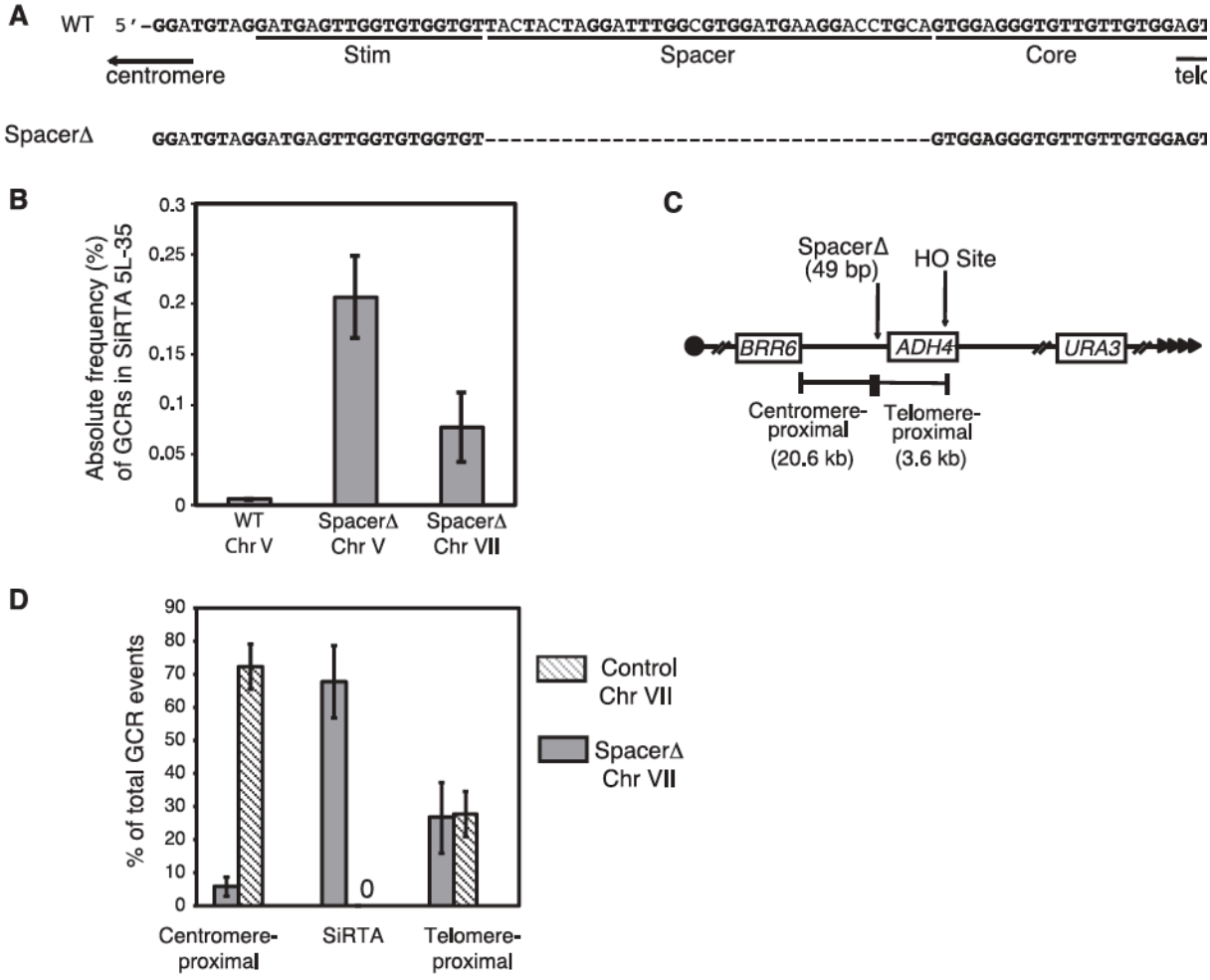

Figure 2-4: The SiRTA Stim and Core sequences are sufficient to stimulate *de novo* telomere addition at an ectopic location. (A) Top schematic, sequence of SiRTA 5L-35 as described for Figure 2-3A. Bottom schematic, spacerΔ mutation created in SiRTA 5L-35. The dashed line indicates deleted nucleotides. (B) The absolute frequency (% total cells) of GCR formation at SiRTA 5L-35 is shown for the spacerΔ variant at its endogenous location on chromosome V and at an ectopic site on chromosome VII. Data for WT SiRTA 5L-35 are shown for comparison (same as Figure 2-3B. Values are the averages from three independent experiments with standard deviations. (C) Schematic of the modified left arm of chromosome VII. Sizes of the regions between the integrated spacerΔ sequence and either the HO cleavage site (telomere proximal) or the most distal essential gene (*BRR6*; centromere proximal) are indicated. (D) The percentage of GCR events occurring in each indicated region on chromosome VII is shown for the experimental strain (SiRTA 5L-35 spacerΔ) and a control strain (no integration). In the control strain, no GCR events were observed in the 219-bp region that is replaced by the spacer variant in the experimental strain. Values are averages from three independent experiments with standard deviations. Contributing authors: EAE, NAD.

of terminal deletion (Figure 2-4C). A strain containing only the HO cleavage site and *URA3* marker served as a control. In the control strain, no GCR events were observed within a 542-bp sequence corresponding to the insertion site and 72.2% $\pm$ 6.9% of the GCR events occurred centromere-proximal to this location (Figure 2-4D). In striking contrast, 67.6% $\pm$ 10.8% of total GCR events in the experimental strain occurred within SiRTA- spacerΔ and only 5.7% $\pm$ 2.8% mapped to the centromere-proximal region (Figure 2-4D). Southern analysis was conducted on 35 events from a single experiment. Of 22 events mapped by PCR to the SiRTA-spacerΔ sequence, 20 (91%) involved telomere addition. Furthermore, of 12 events that mapped telomere proximal to the SiRTA-spacerΔ sequence, all but one involved telomere addition within 100 bp of SiRTA-spacerΔ. Therefore, in this subset of 35 GCR events, 91.4% involved *de novo* telomere addition within or immediately adjacent to the SiRTA-spacer insert. The overall rate of GCR formation within SiRTA-spacer was modestly (2.7- fold) lower on chromosome VII than at the endogenous location on chromosome V but still much higher than that observed for the endogenous SiRTA 5L-35 (Figure 2-4B). Taken together, these results indicate that the SiRTA 5L-35 Core and Stim sequences are sufficient to support *de novo* telomere addition following a distal chromosome break. Reducing the spacing between the stimulatory and core sequences dramatically increases the rate of *de novo* telomere addition. Interestingly, sequences located within approximately 100 bp of the SiRTA nucleate telomere addition when the spacer sequence is deleted, most likely because the stimulatory sequence is now closer to these sites.

2.2.4 Sequences that bind Rap1 and Cdc13 stimulate *de novo* telomere addition at SiRTA 5L-35

We reasoned that the enhancing properties of SiRTA Stim may arise from one or more proteins bound at that site. Given the TG-rich nature of this sequence, we investigated the ability of Rap1 and Cdc13 to bind the SiRTA Stim sequence *in vitro*. Rap1 is a double-stranded DNA binding protein that binds at high frequency within the endogenous telomeric repeat [218], but binds additional internal chromosomal sites as a transcription factor [97]. Cdc13 binds the single-stranded overhang at the yeast telomere [55,92,219–221] and could bind at SiRTA Stim following resection of a DSB at a distal site.

Electrophoretic mobility shift assays (EMSAs) were performed using recombinant Rap1 and the DNA binding domain of Cdc13 (Cdc13-DBD; amino acids 497 to 694) to monitor binding to double-stranded or single-stranded target DNAs, respectively. The DNA binding domain of Cdc13 alone closely mimics the binding specificity of the full-length protein [222]. Indeed, the endogenous SiRTA Stim sequence is bound by both Rap1 (Figure 2-5A and B, probe I) and by Cdc13-DBD (Figure 2-5A and C, probe III). As predicted, the poly(A) mutation that disrupts SiRTA Stim function (Figure 2-3) reduces binding by Rap1 and Cdc13-DBD (Figure2-5A-C, probes II, IV, and V), consistent with one or both of these proteins playing a role in the stimulation of *de novo* telomere addition.

To address whether binding by Rap1 and/or Cdc13 is sufficient to stimulate *de novo* telomere addition, we designed a sequence predicted to contain two tandem Rap1 binding sites and to have the ability to bind Cdc13. By EMSA, this sequence (Stim-Subst; Figure 2-5D) binds Rap1 with higher affinity than the endogenous SiRTA Stim sequence (compare binding to

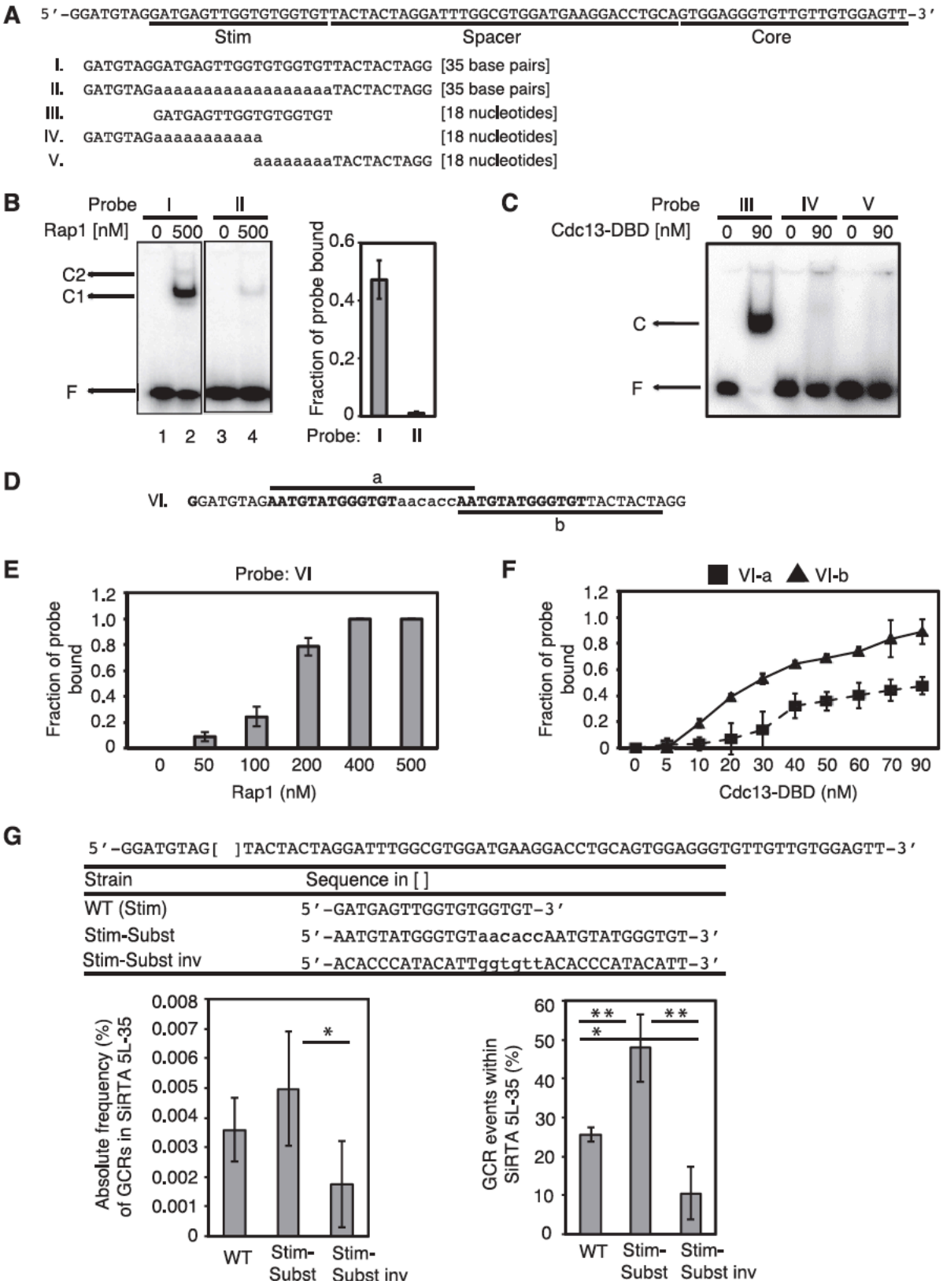
A
5′-GGATGTAGGATGAGTTGGTGTGGTGTTACTACTAGGATTTGGCGTGGATGAAGGACCTGCAGTGGAGGGTGTTGTTGTGGAGTT-3′
Stim
Spacer
Core
I. GATGTAGGATGAGTTGGTGTGGTGTTACTACTAGG [35 base pairs]
II. GATGTAGaaaaaaaaaaaaaaaaaaTACTACTAGG [35 base pairs]
III. GATGAGTTGGTGTGGTGT [18 nucleotides]
IV. GATGTAGaaaaaaaaaaa [18 nucleotides]
V. aaaaaaaaTACTACTAGG [18 nucleotides]
B
Probe I II
Rap1 [nM] 0 500 0 500
C2
C1
F
1 2 3 4
Fraction of probe bound
Probe: I II
C
Probe III IV V
Cdc13-DBD [nM] 0 90 0 90 0 90
C
F
D
a
VI. GGATGTAGAATGTATGGGTGTaacaccAATGTATGGGTGTTACTACTAGG
b
E
Probe: VI
Fraction of probe bound
Rap1 (nM)
F
VI-a VI-b
Fraction of probe bound
Cdc13-DBD (nM)
G
5′-GGATGTAG[ ]TACTACTAGGATTTGGCGTGGATGAAGGACCTGCAGTGGAGGGTGTTGTTGTGGAGTT-3′
Strain Sequence in [ ]
WT (Stim) 5′-GATGAGTTGGTGTGGTGT-3′
Stim-Subst 5′-AATGTATGGGTGTaacaccAATGTATGGGTGT-3′
Stim-Subst inv 5′-ACACCCATACATTggtgttACACCCATACATT-3′
Absolute frequency (%) of GCRs in SiRTA 5L-35
WT
Stim-Subst
Stim-Subst inv
GCR events within SiRTA 5L-35 (%)
WT
Stim-Subst
Stim-Subst inv

Figure 2-5: The Stim sequence of SiRTA 5L-35 binds Cdc13 and Rap1 *in vitro* and can be functionally replaced with a sequence that binds both proteins.
(A) Top schematic: Sequence of SiRTA 5L-35 as in Figure 2-3A. Bottom schematic: Sequences of probes utilized for Cdc13-DBD and Rap1 binding assays. Mutated bases are shown in lower case. Probes are identified with Roman numerals and this numbering is maintained throughout the manuscript. Probes I and II are double-stranded; probes III-V are single-stranded.
(B) Binding of recombinant Rap1 to probe I (WT SiRTA 5L-35) and probe II (Stim poly(A) mutation, Figure 2-3A). The mobility of free probe (F) and two bound complexes (C1 and C2) is indicated. The fraction of probe bound when utilizing 500 nM Rap1 is quantified on the right from three independent experiments. Error bars represent standard deviations.
(C) Binding of recombinant Cdc13-DBD to probes III, IV, and V, as indicated. Probe III contains the WT SiRTA 5L-35 sequence. Probes IV and V contain the Stim poly(A) mutation from Figure 2-3A. This sequence was tested in two pieces to avoid the formation of secondary structure. The mobility of free probe (F) and bound complex (C) is indicated.
(D) The sequence shown was designed to contain two predicted Rap1 binding sites (bold) separated by a linker sequence (lower case). Probe VI is double-stranded and is utilized in (E). Probes VI-a and VI-b are single- stranded sequences as indicated and are utilized in panel F.
(E) Binding of the indicated concentration of recombinant Rap1 to probe VI.
(F) Binding of the indicated concentration of recombinant Cdc13-DBD to probes VI-a or VI-b. For panels E and F, the average fraction of probe bound was determined from three independent experiments. Error bars represent standard deviations.
(G) The SiRTA 5L-35 Stim sequence (indicated by brackets) was replaced at the endogenous locus on chromo- some V with the three sequences depicted here. Stim-Subst is identical to the sequence of Probe VI. Stim-Subst inv is the reverse complement of the Stim-Subst sequence. Average results and standard deviation of three HO-cleavage assays are shown as the absolute frequency (%) of GCR formation within SiRTA 5L-35 (left graph) or the percent of total GCR events that occur within SiRTA 5L-35 (right graph). Samples with statistically different values by ANOVA with post-hoc Tukey HSD are indicated (* $p<0.05$; ** $p<0.01$). Contributing authors: UCO, EAE.

probes I and VI, Figure 2-5B and E) and also binds Cdc13-DBD (Figure 2-5F, probes VIa and VIb). The Stim-Subst sequence was integrated in place of the SiRTA Stim sequence on chromosome V and the frequency of GCR events at SiRTA 5L-35 was measured. Consistent with either Rap1 and/or Cdc13 playing a role in the stimulation of telomere addition, this artificial sequence stimulated GCR events at SiRTA 5L-35 at a rate equivalent to the endogenous sequence and increased the fraction of GCR events occurring within SiRTA 5L-35 (Figure 2-5G).

To test whether stimulation is orientation-dependent, we inverted the Stim-Subst sequence. Inversion reduced the rate of GCR formation at SiRTA 5L-35 by 2.8-fold and reduced the fraction of GCR events within SiRTA 5L-35 from 47.8±7.1% to 10.4±6.8% (Figure 2-5G). Rap1 is expected to retain binding to the Stim-Subst sequence regardless of orientation. In contrast, the ability of Cdc13 to bind requires orientation-dependent exposure of its single-stranded TG-rich binding site during resection from a distal double-strand break, suggesting that Cdc13 may be the functionally relevant protein in this context.

2.2.5 Binding of Cdc13 within SiRTA Stim is sufficient to drive *de novo* telomere addition at the neighboring Core sequence

To distinguish effects by Rap1 and Cdc13, we designed sequences to support differential binding. To create a sequence that binds Rap1, but not Cdc13, we began with the Stim-Subst sequence containing two sites predicted to bind Rap1 separated by an AC-rich spacer sequence (Figures 2-5D and 2-6A, probe VI). Since the 5' portion of this sequence binds weakly to Cdc13-DBD (Figure 2-5F, probe VIa), we mutated only the most 3' residue in this repeat, a change predicted to retain Rap1 association but disrupt Cdc13 binding. At the second Rap1 site, we mutated both that same 3' nucleotide and several nucleotides that lie adjacent to the defined Stim sequence (Figure 2-6A, probe VII). As shown in Figure 2-6B, the engineered "Rap1 only" sequence binds Rap1 with higher affinity than either the original SiRTA-Subst sequence or the endogenous SiRTA Stim. Mutations in the second Rap1 binding site essentially eliminate Cdc13-DBD binding to this sequence (compare Figure 2-5F, probe VIb, with Figure 2-6C, probe VIII).

We took a similar approach to create a sequence capable of binding Cdc13 and not Rap1. Here, the starting sequence was 11 bases shown to support strong association with Cdc13 [55] (Figure 2-6A, probe IX). The second base of this sequence [known to have little or no effect on Cdc13 binding was mutated to reduce similarity with the Rap1 binding consensus and two of these sites were placed in tandem. As shown in Figure 2-6B, this "Cdc13 only" sequence shows no detectable binding to Rap1 (probe X). Binding of this sequence to Cdc13 was measured using two probes that monitor binding to the 5' (probe XI) or 3' (probe XII) repeat. The 3' repeat shows similar affinity for Cdc13-DBD as the 11 base consensus sequence (Figure 2-6C, compare probes IX and XII), and both of these probes are bound more strongly than is the endogenous SiRTA Stim (Figure 2-6C, probe III). The 5' repeat is also bound by Cdc13-DBD, although more weakly than the 3' repeat (Figure 2-6C, probe XI). In conclusion, these *in vitro* binding analyses demonstrate that binding by Rap1 and Cdc13 can be separated, allowing us to test the specific effects of these proteins on SiRTA 5L-35 function.

The sequences defined above were integrated in place of the endogenous SiRTA Stim sequence on chromosome V (Figure 2-6D). Integration of the "Rap1 only" sequence reduced the overall frequency of GCR formation at SiRTA 5L-35 to about half that of the Stim-Subst sequence upon which it is based, a rate similar to that observed for the Stim-Subst inverted sequence (compare Figure 2-6D with Figure 2-5G). In contrast, the sequence containing only binding sites for Cdc13 resulted in a GCR rate eight fold higher than that of the endogenous sequence, 70.0 ± 9.8% of all GCR events occurred within SiRTA 5L-35 (Figure 2-6D), and all of those events were the result of *de novo* telomere addition (data not shown).

A

Purpose	Probes used in EMSA
WT	I - GATGTAGGATGAGTTGGTGTGGTGTTACTACTAGG (Rap1 EMSA)
	III - GATGAGTTGGTGTGGTGT (Cdc13 EMSA)
Stim-subst*	VI - GGATGTAG**AATGTATGGGTGT**aacacc**AATGTATGGGTGT**TACTACTAGG (Rap1 EMSA)
Rap1 only	VII - GGATGTAG**AATGTATGGGTGC**aacacc**AATGTATGGGTGC**AACACCTAGG (Rap1 EMSA)
	VIII - **AATGTATGGGTGC**AACACCTA (Cdc13 EMSA)
Cdc13 consensus**	IX - **GTGTGGGTGTG** (Cdc13 EMSA)
Cdc13 only	X - GGATGTAG**GAGTGTGTGTG**aacacc**GAGTGTGTGTG**TACTACTAGG (Rap1 EMSA)
	XI - **GAGTGTGTGTG**aacacc**GA** (Cdc13 EMSA)
	XII - **GAGTGTGTGTG**TACTACTA (Cdc13 EMSA)

* This sequence contains two predicted Rap1 binding sites (bold) and was used as the base for creating the "Rap1 only" sequence; identical to the Stim-Subst sequence utilized in Figure 4.

** This sequence conforms to a canonical Cdc13 binding site; used as the base for creating the "Cdc13 only" sequence.

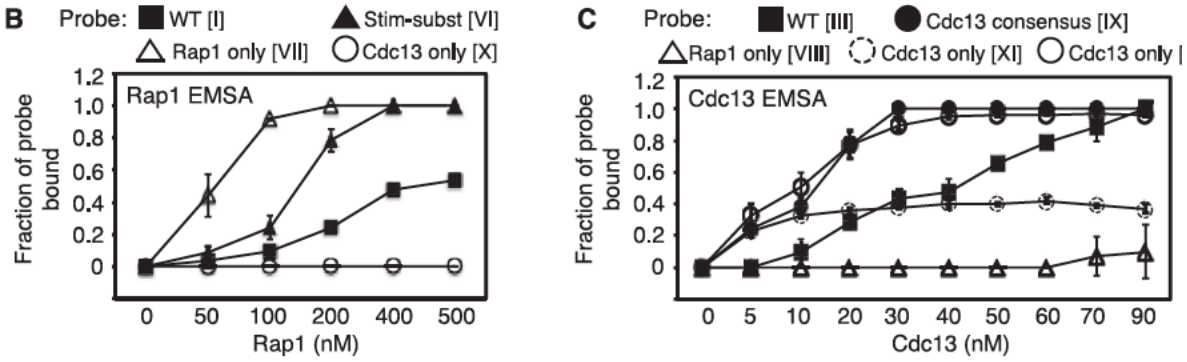

D

5′-GGATGTAG[ ]TACTACTAGGATTTGGCGTGGATGAAGGACCTGCAGTGGAGGGTGTTGTTGTGGAGTT-3′

Strain	Sequence within brackets
Rap1 only	[AATGTATGGGTGCaacaccAATGTATGGGTGC]AACAC#
Cdc13 only	GAGTGTGTGTGaacaccGAGTGTGTGTG

#Additional mutations were made beyond the bracketed sequence to prevent Cdc13 binding.

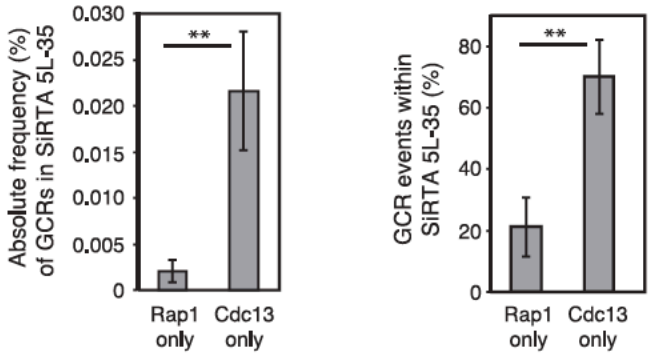

Figure 2-6: The rate of *de novo* telomere addition at SiRTA 5L-35 correlates with the ability of the SiRTA Stim sequence to bind Cdc13. (A) Probes utilized for Cdc13-DBD and Rap1 binding assays. Probes I, III, and VI are identical to those used in Figure 2-5. Probes followed by "Rap1 EMSA" are double-stranded. Those indicated with "Cdc13 EMSA" are single-stranded.(B) Binding of the indicated concentration of recombinant Rap1 to double-stranded probes shown in panel A. (C) Binding of the indicated concentration of recombinant Cdc13-DBD to single-stranded probes shown in panel A. In panels B and C, the average fraction of probe bound was determined from three independent experiments. Error bars represent standard deviations. D. The SiRTA 5L-35 Stim sequence (indicated by brackets) was replaced at the endogenous locus on chromosome V with the sequences depicted here. Average results and standard deviation of three HO-cleavage assays are shown as absolute frequency (%) of GCR formation within SiRTA 5L-35 (left graph) or percent of total GCR events within SiRTA 5L-35 (right graph). Averages indicated (**) are significantly different ($p<0.01$) by unpaired Students T test. Contributing authors: UCO.

To confirm the ability of Cdc13 to stimulate *de novo* telomere addition, we replaced the SiRTA Stim sequence with two copies of the Gal4 upstream activating sequence (stim::2XUAS), which is recognized by the Gal4 DNA binding domain (GBD; Figure 2-7A). Into this strain, we introduced either an empty vector or a plasmid expressing a fusion of GBD with full-length Cdc13 or Rap1. As expected, the strain containing stim::2XUAS and empty vector supported a rate of GCR formation at SiRTA 5L-35 indistinguishable from a strain containing the stim::poly(A) mutation (Figure 2-7B; comparable to mutation c in Figure 2-3). Expression of the GBD-Rap1 fusion protein in the stim::2XUAS strain failed to increase the rate of GCR formation at SiRTA 5L-35 (Figure 2-7B), suggesting that Rap1 plays either no role or a minor role in stimulating telomere addition following a DSB. In contrast, expression of the GBD-Cdc13 fusion protein in the stim::2XUAS strain increased the rate of GCR formation at SiRTA 5L-35 nearly 15-fold relative to the strain containing vector only (Figure 2-7B). This increase is largely attributable to the recruitment of GBD-Cdc13 to the 2XUAS sequences on chromosome V since

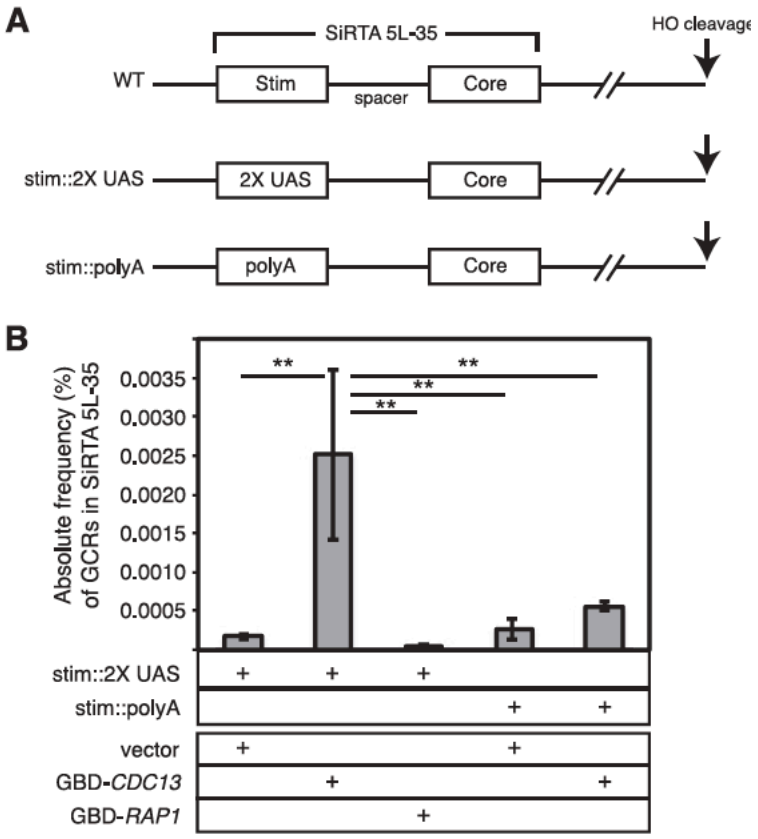

Figure 2-7. Artificial recruitment of Cdc13 to the SiRTA 5L-35 stimulatory site increases the rate of GCR formation. (A) The SiRTA 5L-35 Stim sequence was replaced with two tandem copies of the Gal4 upstream activating sequence (2X UAS) or with a string of adenines [poly(A); identical sequence to that of mutation d in Figure 2-3A. (B) The rate of GCR formation within SiRTA 5L-35 is shown for strains containing either the 2X UAS or poly(A) sequences integrated in place of SiRTA 5L-35 Stim. Cells are transformed with pRS314 (empty vector) or with pRS414 expressing either *CDC13* or *RAP1* as N-terminal fusions with the Gal4 DNA binding domain (GBD). Values for the three rightmost columns are maximum estimates (see Materials and Methods). Error bars indicate standard deviations for three independent experiments. Averages indicated with 2 asterisks are significantly different ($P < 0.01$) by ANOVA with *post hoc* Tukey's HSD. Contributing authors: EAE, UCO, KLF.

expression of the fusion protein in the stim::polyA strain had no significant effect on GCR formation at SiRTA 5L-35 compared to the same strain containing the empty vector (Figure 2-7B). Taken together, these results are consistent with a model in which resection of the 5'

strand following a DSB exposes one or more sites at which Cdc13 is able to associate with the SiRTA Stim sequence. Such binding is required to increase the rate at which the more telomere-proximal Core sequence is capable of nucleating *de novo* telomere addition and explains why the telomere-like SiRTA 5L-35 Core sequence alone is insufficient to maintain a high rate of GCR formation at that site.

2.2.6 A second SiRTA on chromosome IX also has a bipartite structure

In searching for additional sequences with the hallmarks of a SiRTA, we identified a TG-rich sequence within the *BNR1* gene. This site is located ~16 kb distal to the first essential gene, *MCM10*, on chromosome IX-L. We integrated the HO recognition site ~3 kb distal to this sequence (Figure 2-8A) in a strain that expresses the HO endonuclease under galactose regulation and placed *URA3* on the distal arm, allowing us to select GCR events as described above for SiRTA 5L-35. Our PCR strategy was designed to capture GCR events occurring in the most prominent TG-rich sequence ("Core 1," Figure 2-8B). However, Southern blotting revealed a second cluster of *de novo* telomere addition events ~130 bp distal to the original sequence ("Core 2," Figure 2-8B; Figure 2-9). These two sequences result in a combined frequency of GCR formation of 0.015 ± 0.006%, approximately three times higher than the rate observed at SiRTA 5L-35 (Figure 2-8C). We subsequently refer to this site as SiRTA 9L-44 (SiRTA, 44 kb from the left telomere of chromosome IX). Similar to SiRTA 5L-35, 33.0 ± 1.4% of the GCR events obtained on chromosome IX occurred within SiRTA 9L-44 (including both Core sequences; Figure 2-8D). Interestingly, although Core 1 lies centromere-proximal to Core 2 (and therefore will be rendered single-stranded after Core 2 in response to a distal DSB), 28.2 ± 5.2% of all GCR events

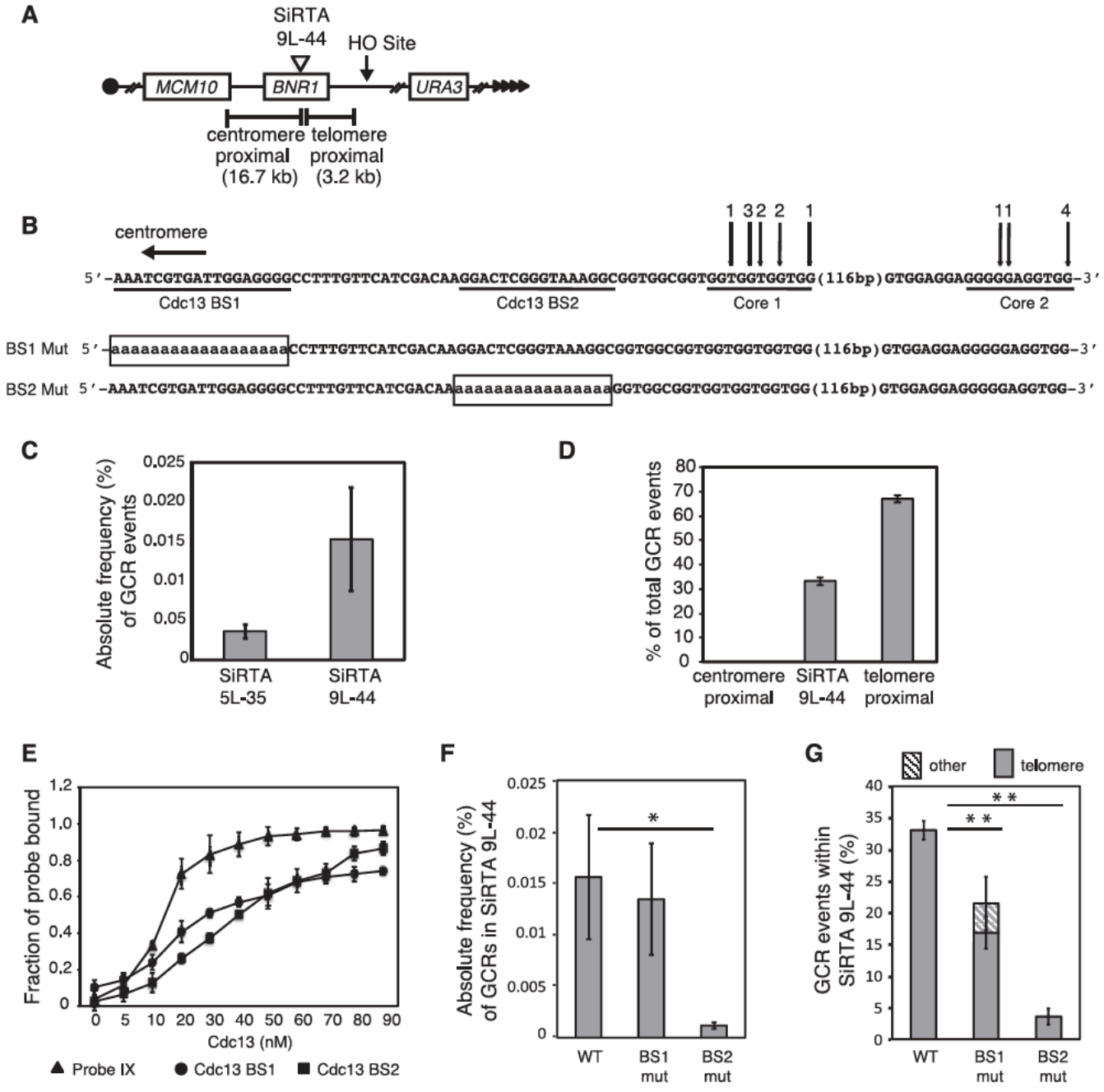
A
SiRTA
9L-44
HO Site
MCM10
BNR1
URA3
centromere
proximal
(16.7 kb)
telomere
proximal
(3.2 kb)
B
centromere
1 3 2 2 1
11 4
5′-AAATCGTGATTGGAGGGGCCTTTGTTCATCGACAAGGACTCGGGTAAAGGCGGTGGCGGTGGTGGTGGTGG(116bp)GTGGAGGAGGGGGAGGTGG-3′
Cdc13 BS1
Cdc13 BS2
Core 1
Core 2
BS1 Mut 5′-aaaaaaaaaaaaaaaaaaCCTTTGTTCATCGACAAGGACTCGGGTAAAGGCGGTGGCGGTGGTGGTGGTGG(116bp)GTGGAGGAGGGGGAGGTGG-3′
BS2 Mut 5′-AAATCGTGATTGGAGGGGCCTTTGTTCATCGACAAaaaaaaaaaaaaaaaaGGTGGCGGTGGTGGTGGTGG(116bp)GTGGAGGAGGGGGAGGTGG-3′
C
Absolute frequency (%) of GCR events
0.025
0.020
0.015
0.01
0.05
0
SiRTA 5L-35
SiRTA 9L-44
D
% of total GCR events
80
70
60
50
40
30
20
10
0
centromere proximal
SiRTA 9L-44
telomere proximal
E
Fraction of probe bound
1.2
1.0
0.8
0.6
0.4
0.2
0
0 5 10 20 30 40 50 60 70 80 90
Cdc13 (nM)
Probe IX
Cdc13 BS1
Cdc13 BS2
F
Absolute frequency (%) of GCRs in SiRTA 9L-44
0.025
0.02
0.015
0.01
0.005
0
*
WT
BS1 mut
BS2 mut
G
other
telomere
GCR events within SiRTA 9L-44 (%)
40
35
30
25
20
15
10
5
0
* *
* *
WT
BS1 mut
BS2 mut

Figure 2-8: A site at which *de novo* telomere addition occurs at high frequency on chromosome IX (SiRTA 9L-44) has a similar organization to SiRTA 5L-35. (A) Schematic of the left arm of chromosome IX. Sizes of the regions between SiRTA 9L-44 and either the HO cleavage site (telomere-proximal) or the most distal essential gene (*MCM10*; centromere-proximal) are indicated. (B) Top schematic: Sequence of SiRTA 9L-44 with vertical arrows indicating sites of *de novo* telomere addition. The sequence is oriented with the telomere to the right so that the DNA strand depicted is the direct 3' primer upon which telomerase acts. In each case, the most 3' chromosomal nucleotide with identity to the cloned *de novo* telomere is indicated. Numbers above arrows indicate the number of independent telomere addition events mapped to each site. Sequences predicted to bind Cdc13 are underlined (Cdc13 BS1 and Cdc13 BS2). Bottom schematic: Mutations created in SiRTA 9L-44. Uppercase letters represent unchanged nucleotides, lowercase letters enclosed in box represent mutated nucleotides. (C) The absolute frequency (%) of GCR events within SiRTA 5L-35 or SiRTA 9L-44 is shown. (D) The percentage of GCR events occurring in each indicated region on chromosome IX is shown. No GCR events were observed in the region centromere-proximal to SiRTA 9L-44. Values in panels C and D are averages of three independent experiments with standard deviation. (E) Binding of the indicated concentration of recombinant Cdc13-DBD to single-stranded probe IX (see Figure 2-6A) or single-stranded probes corresponding to the underlined sequences in panel B. The average fraction of probe bound was determined from three independent experiments. Error bars represent standard deviations. (F) The BS1 mut and BS2 mut sequences shown in (B) were inserted at the endogenous SiRTA 9L-44 locus on chromosome IX and the absolute frequency (%) of GCR formation within SiRTA 9L-44 was determined. (G) The percent of total GCR events that occur within SiRTA 9L-44 for WT and the indicated mutant strains is shown. GCR events involving *de novo* telomere addition were identified by Southern blot; any event that does not involve telomere addition is classified as "other." Results in panels F and G are the averages and standard deviations of three independent experiments. Samples with statistically different values by ANOVA with *post-hoc* Tukey HSD are indicated (* $p<0.05$; ** $p<0.01$). Contributing authors: EAE.

occurred within Core 1, while 4.8 ± 4.4% occurred in Core 2 (data not shown), suggesting that Core 1 is more efficiently targeted. No GCR events occurred within the ~16 kb region between SiRTA 9L-44 and the first essential gene (Figure 2-8D).

Given that we identified a stimulatory sequence within SiRTA 5L-35 capable of binding to Cdc13 (Figures 2-3 and 2-5), we sought to identify similar sequence(s) that may contribute to

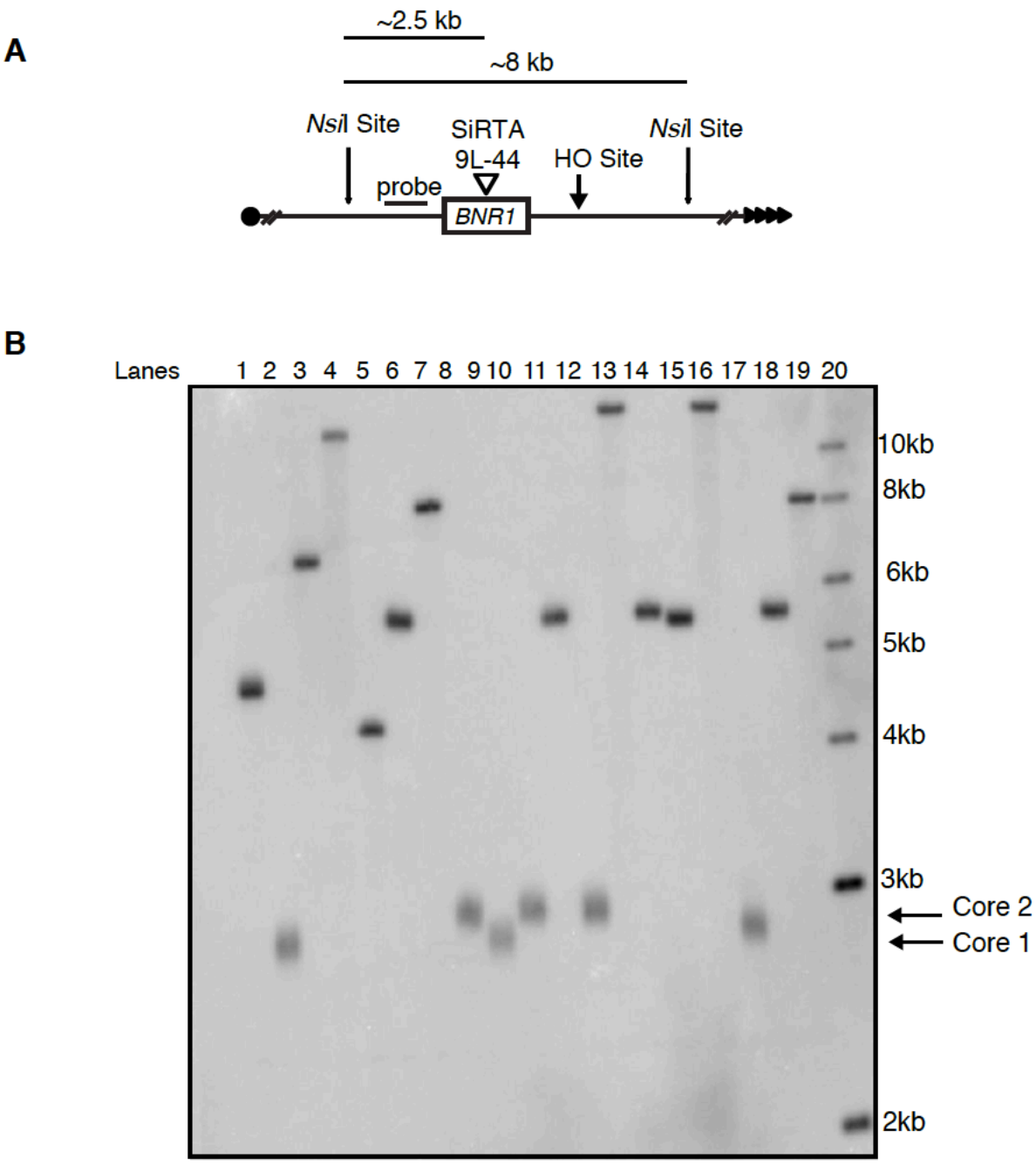

Figure 2-9: Southern blot analysis of GCR events in or near SiRTA 9L-44. (A) Map of region containing SiRTA 9L-44. Genomic DNA was cleaved with *Nsi*I; the location of the probe is shown. (B) Southern blot analysis of 18 independent GCR events on chromosome IX. Arrows indicate bands indicative of *de novo* telomere addition at either Core1 (lanes 2, 9 and 17) or Core 2 (lanes 8, 10, 12). Lane 19 contains the DNA isolated from the parent strain prior to selection for GCR events. Note detection of the expected band of ~8 kb. Lane 20 contains molecular weight marker as indicated. Contributing authors: EAE.

telomere addition at SiRTA 9L-44. Using EMSA, we identified two sites that bind Cdc13-DBD *in vitro* (Cdc13 BS1 and Cdc13 BS2; Figure 2-8B and E). Mutation of Cdc13 BS1 to poly-adenine had no effect on the overall frequency of GCR events at SiRTA 9L-44 relative to WT (Figure 2-8F), although the fraction of GCR events that occurred within SiRTA 9L-44 was significantly reduced (from 33.0 ± 1.4% to 21.4 ± 6.2%; Figure 2-8G). This reduction occurred specifically at Core 1, since the fraction of events at Core 2 remained similar to WT (4.8 ± 4.4% in WT versus 7.5 ± 1.5% in BS1). 4.6 ± 4.2% of the GCR events that occurred at SiRTA 9L-44 when Cdc13 BS1 was mutated were not *de novo* telomere addition events, a phenomenon never observed in WT cells (Figure 2-8G). Together, these results suggest a minor contribution by Cdc13 BS1 to the high rate of *de novo* telomere addition at SiRTA 9L-44.

In contrast, mutation of Cdc13 BS2 to poly-adenine strongly reduced the overall rate of GCR formation at SiRTA 9L-44 (~18-fold; Figure 2-8F). Only 3.5 ± 1.3% of GCR events occurred within SiRTA 9L-44 (Figure 2-8G) and none were within Core 2. Cdc13-DBD binds similarly to BS1 and BS2 *in vitro*, suggesting that the efficacy of these sequences in stimulating telomere addition correlates poorly with the strength of binding by Cdc13 (compare Figure 2-8E to 2-8F and G). The functional difference between these sequences may be explained, at least in part, by their differing proximity to the sites of *de novo* telomere addition at Core 1 and Core 2.

In conclusion, we identified a SiRTA on chromosome IX that bears striking similarities to the SiRTA on chromosome V. Both SiRTAs contain TG-rich tracts within which telomere addition occurs and the high rate of *de novo* telomere addition at these SiRTAs relative to neighboring sequences can be attributed to stimulatory sequences that lie centromere-proximal to the major sites of telomere addition. Finally, EMSA analysis shows that Cdc13 binds these

stimulatory sequences *in vitro*. Thus, increased telomerase activity at SiRTAs is likely achieved, at least in part, by the association of Cdc13 with one or more stimulatory sequences upstream of the sites of actual *de novo* telomere addition.

2.3 Discussion

Endogenous sites of *de novo* telomere addition can affect genome stability and have been associated with cancer [223] and congenital disorders [224–226]. While *S. cerevisiae* provides a useful model system to study mechanisms of *de novo* telomere addition, most studies utilize artificial sequences to stimulate telomere formation. The goal of this study was to examine naturally occurring sites at which *de novo* telomere addition is greatly favored and to identify *cis*- and *trans*-acting factors contributing to this property. We characterized two genomic sites (SiRTAs) at which *de novo* telomere addition occurs at a remarkably (at least 200-fold) increased rate compared to neighboring sequences. Zakian and colleagues reported a third hot spot of *de novo* telomere addition on chromosome VII at a location 50 kb internal to an HO cleavage site [196]. Unlike the two sequences studied here, the chromosome VII site lies internal to the last essential gene on the chromosome arm (a disomic strain lacking *RAD52* was used to maintain viability and limit homologous recombination). Given the ease with which these sites have been found, it seems likely that additional SiRTAs remain to be identified.

While many assays of *de novo* telomere addition utilize short telomeric tracts placed immediately adjacent (within 20 to 30 nucleotides [nt]) to the HO cleavage site (for examples, see references [206] and [202,227,228], the natural SiRTAs described here are located several kilobases internal to the induced break, requiring extensive resection prior to telomere

addition. In our assays, we also observe telomere addition at or very close to the HO cut site (data not shown). This propensity is at least partially a consequence of the TGTT-3' overhang produced by HO endonuclease cleavage. When the recognition site is inverted to generate the complementary ACAA-3'overhang, *de novo* telomere addition at the HO site is reduced and the fraction of events at SiRTA 5L-35 is increased (data not shown). Given these observations, studies of telomere addition at endogenous sites located at a distance from an induced break may more faithfully capture the mechanism of repair of a random chromosomal break than models in which a telomeric seed sequence is intentionally placed adjacent to the HO cleavage site.

We observe that both SiRTA 5L-35 and 9L-44 contain sequences that enhance telomerase action but act rarely, if ever, as the direct target of telomerase action (SiRTA Stim sequences). Because the telomere-binding proteins Cdc13 and Rap1 stimulate *de novo* telomere addition at artificial sequences in *S. cerevisiae* [206,213–215,228]), we hypothesized that one or both of these proteins could be responsible for the enhancing activity of the Stim sequence. Although Cdc13 and Rap1 bind similar sequences, we were able to design artificial sequences that bind with great preference to one protein as measured *in vitro*. Using this approach, we found that a sequence designed to facilitate Cdc13 binding is much more effective in the stimulation of *de novo* telomere addition than one binding primarily Rap1 (Figure 2-6D). Importantly, artificial recruitment of GBD-Cdc13 to SiRTA 5L-35 (Figure 2-7) led to high frequencies of telomere addition, suggesting that Cdc13 binding, and not the TG-rich sequences *per se*, stimulates *de novo* telomere addition. Replacement of Stim with the "Rap1 only" sequence did not reduce telomere addition as dramatically as the replacement of Stim

with a poly (A)sequence or with the Gal4 UAS (compare Figure 2-6D with Figures 2-3B and 2-7B), so binding by Rap1 may also contribute to the stimulation of *de novo* telomere addition. Consistent with the proposal that binding by Cdc13 is important for the stimulatory effect of the Stim sequence, we find that high levels of telomere addition at SiRTA 9L-44 require a sequence capable of binding Cdc13 (BS2, Figure 2-8B) and that this sequence stimulates telomere addition over a distance of more than 100 bp. Rap1 does not bind to the BS2 sequence *in vitro* (data not shown), suggesting that Cdc13 is sufficient to stimulate *de novo* telomere addition at this SiRTA.

The stimulation of *de novo* telomere addition by telomere-like sequences located internal to the site of telomerase action has been previously observed in both artificial and natural contexts. For example, *de novo* telomeres generated following DNA cleavage by HO endonuclease near a TG-rich seed sequence are frequently added at the 3' overhang of the HO endonuclease target site rather than within the telomeric seed itself [229]. At the SiRTA on chromosome VII reported by Mangahas *et al*. [199], telomere addition occurs at several closely spaced sequences located 37 to 49 bp distal to a 35-bp GT dinucleotide repeat. This sequence matches the GXGT$(T/G)_7$ consensus for Cdc13 binding [230], consistent with the GT dinucleotide repeat acting as a Stim sequence in the manner that we report here for SiRTAs 5L-35 and 9L-44. However, as is the case at SiRTA 5L-35, the TG dinucleotide tract on chromosome VII may also bind Rap1 [231], so a contribution of Rap1 to Stim function cannot be ruled out.

Kramer and Haber reported that *de novo* telomere addition occurs 15 to 100 bp distal to an ectopic tract of 13 T_2G_4 repeats (*Tetrahymena thermophila* telomeric sequence), and a similar phenomenon was reported for plasmid substrates [195,232]. The *Tetrahymena*

telomeric sequence contains the GXGT$(T/G)_7$ consensus sequence for Cdc13 binding [230], although a $(T_2G_4)_3$ oligonucleotide was shown to compete poorly with the yeast telomeric sequence for Cdc13 binding *in vitro* [219]. This short sequence is predicted to contain only a single Cdc13 binding site, while the tract of 13 repeats utilized by Kramer and Haber has multiple potential binding sites [195]. Combined with our observation that the Stim sequences in both SiRTA 5L-35 and 9L-44 bind Cdc13 with lower affinity than an optimized sequence from the yeast telomere (Figures 2-6C and 2-8E), it is reasonable to suggest that the stimulatory effect observed by Kramer and Haber is due to Cdc13 binding to the ectopic T_2G_4 tract.

How might the bipartite structure of both SiRTA 5L-35 facilitate *de novo* telomere addition? Genetic and biochemical analyses suggest that Cdc13 protects telomeres from extensive 5'strand degradation [29,84,233] [234]. One possibility is that Cdc13 bound to the Stim sequence inhibits resection past SiRTA, thereby providing a grace period to allow for the formation of a stable telomere at the Core sequence. However, inhibition of resection alone does not account for the increased efficacy of Stim when it is brought in close proximity to Core (Figure 2-4B). Another possibility is that Cdc13 must be bound to both the Stim and Core sequences to stably recruit telomerase to the SiRTA. This proposal is congruent with the results of Hirano and Sugimoto that show greatly increased stimulation of telomerase recruitment and *de novo* telomere addition when two tandem Cdc13 binding sites are placed adjacent to an HO-induced break, compared to the effect of a single site [228].

In addition to its C-terminal oligonucleotide/oligosaccharide binding (OB) fold domain (also known as its DNA-binding domain), Cdc13 contains an N-terminal OB fold that is involved in Cdc13 dimerization [203]. The minimal binding site for both full- length Cdc13 and its isolated

DBD is an 11-mer TG_{1-3} sequence. However, as demonstrated by EMSA, the Cdc13 N-terminal OB fold, which exists as a stable dimer in solution, does not bind to this 11-mer but binds with stronger affinity to single-stranded DNA (ssDNA) sequences at least 37 nucleotides long [203]. These observations support a model in which each Cdc13 monomer binds to a separate site on a single molecule of ssDNA, with optimal binding depending on the distance between the two sites. Finally, mutations that disrupt Cdc13 dimerization *in vitro* cause telomere shortening when introduced *in vivo* [203]. We propose that dimerization between Cdc13 monomers bound to the Stim and Core sequences is required to stably recruit telomerase to the SiRTA. This model additionally accounts for the increased efficacy of Stim when it is juxtaposed with Core, since in that context, the distance between the two monomers may be more optimally suited to stable telomerase recruitment.

2.4 Materials and methods

2.4.1 Yeast strains and plasmids

Table 2-1 contains a complete list of strains used in this study. Unless otherwise noted, strains were grown in yeast extract/peptone/dextrose (YEPD) at 30˚C. In strains utilized for HO cleavage assays (YKF1310 and YKF1308), the *HMRa* sequence on chromosome III was replaced with *nat*, which confers resistance to nourseothricin. All gene deletions were generated by one-step gene replacement with a selectable marker and were confirmed by PCR. $hxt13::URA3$ disruptions were created by using a plasmid in which the *Kpn*I-*Sph*I restriction fragment from *HXT13* was replaced with *URA3* or by amplifying the *hxt13::URA3* locus from an existing strain

using primers hxt13::URA3 F and hxt13::URA3 R (Table 2-2). The HO cleavage site was integrated on chromosomes VII and IX by one-step gene replacement using plasmid pJH2017 (*HOcs::HPH*; gift of J. Haber) as template with selection for hygromycin B resistance. *URA3* was integrated on chromosome VII by one-step gene replacement at the *PAU11* locus and on chromosome IX by one-step gene replacement at the *SOA1* locus. Primers utilized for PCR are listed in Table 2-2. Strain YKF1409 (*rad52*::*LEU2*) was generated by transformation with BamHI-digested plasmid pSM20, which contains the *rad52*::*LEU2* disruption allele [29].

Mutations in SiRTA 5L-35 described in Figures 2-3 and 2-4 were introduced by two-step gene replacement [235]. DNA fragments containing each mutation were generated by PCR using Gene Splicing by Overlap Extension (Gene SOEing;). Met-NPR2 For primer was used with a reverse primer containing the desired mutation to generate fragment I and NPR2 mid-Rev primer was used with a forward primer containing the same mutation to generate fragment II (Table 2-2). Fragments I and II were extended by mutually primed synthesis using the Met *NPR2* For and Mid *NPR2* Rev primers to generate a final PCR product that was cleaved with *Hin*dIII and *Xba*I for ligation into pRS306. The integration plasmid was linearized with *BamH*I or *Bcl*I prior to transformation and selection for Ura^+ integrants. To facilitate the identification of strains containing the desired mutations following selection on media containing 5-FOA, two-step integration was first used to create strain YKF1366 in which SiRTA 5L-35 is deleted. Subsequent strains were created by reintroducing mutated versions of SiRTA 5L-35 into strain YKF1366 by two-step integration. The resulting 5-FOA^R isolates were screened by PCR and candidates were sequenced to confirm the presence of the desired mutations.

For mutations described in Figure 2-6 and 2-7, a portion of SiRTA 5L-35 including the Stim sequence was replaced with *URA3* in strain YKF1323 by one-step gene replacement to generate strain YKF1585. Sequences to be integrated were generated by PCR using the HS forward and HS reverse primers and transformed into strain YKF1585. After allowing cells to recover for 24 - 48 hours on rich media, cells were replica plated to media containing 5-FOA. Mutations were confirmed by sequencing.

SiRTA 5L-35 spacerΔ was integrated on chromosome VII and mutations were introduced at SiRTA 9L-44 by two-step gene replacement essentially as described above. Table 2-2 contains the sequences of primers used for strain construction.

Plasmid pAB180 (pRS414-ADHpromoter-GBD-*CDC13*) was a gift from A. Bianchi. pAB180-Rap1 was created by replacing the *CDC13* open reading frame in pAB180 with the full-length *RAP1* open reading frame at the *Nco*I and *Aat*II sites. All amplified regions were confirmed by sequencing.

2.4.2 GCR assays

For spontaneous GCR assays, cells cultured overnight in synthetic drop-out medium lacking uracil (SD-Ura) were used to inoculate YEPD cultures (approximately 30 per strain). YEPD cultures were grown overnight to saturation (approximately 24 hours) and plated to medium containing 5-FOA and canavanine to isolate GCRs (5-FOA^R Can^R colonies). Only one colony was analyzed from each plate to ensure independence. The approximate location and nature of GCR events was determined by multiplex PCR ([234]and Figure 2-2) and Southern blot (see below).

For HO-cleavage GCR assays, cells were grown in SD-Ura media (with 2% raffinose) to

OD_{600} of ~ 0.3 – 1. Cells were plated on yeast extract/peptone medium with 2% galactose (YEPG) and a dilution was plated on YEPD to determine total cell number. After three days, colonies were counted and galactose-resistant colonies were transferred to SD medium containing 5-FOA to isolate GCR events. At least 100 gal^R colonies were individually plated on media containing 5-FOA to determine the rate of *URA3* loss. If necessary, additional colonies were obtained by replica plating. The approximate location and nature of GCR events was determined by multiplex PCR ([236]; see Figure 2-2)and Southern blot (see below).

The absolute frequency at which GCR events occur within a SiRTA is calculated by multiplying the rate of survival on galactose (colonies on galactose/colonies on glucose, corrected for dilution factor) by the fraction of Gal^R colonies capable of growth on media containing 5-FOA and the fraction of Gal^R 5-FOA^R colonies in which the GCR event occurred within the SiRTA as measured by PCR. Approximately 30 Gal^R 5-FOA^R colonies were analyzed for each experiment and averages and standard deviations presented are derived from a minimum of three independent experiments. In a few cases, rates shown are upper estimates because no 5-FOA resistant colonies were detected among 100 colonies analyzed or no events were obtained within the SiRTA sequence among ~30 Gal^R 5-FOA^R colonies. These cases are indicated in the figure legend where applicable.

2.4.3 Southern blotting

For the characterization of GCR events, approximate locations determined by multiplex PCR were used to design restriction enzyme digests and probes for Southern blot analysis. Information about the restriction enzymes and primers utilized are available upon request.

Digested fragments were separated on a 0.7% agarose gel, transferred to nylon membrane (Hybond N+), and probed with [32P] dCTP-labelled telomeric DNA. Radioactive membranes were exposed to Phosphor screens (Molecular Dynamics) and screens were scanned with Typhoon TRIO Variable Mode Imager (GE Healthcare). Telomere addition was determined by visualization of the characteristic smear generated by the heterogeneous telomere sequence at a size consistent with the PCR result.

2.4.4 Protein purification

Plasmid pET21a-Cdc13-DBD-His_6 [222]was a gift from Deborah Wuttke [University of Colorado, Boulder, CO]. BL21 (DE3) *Escherichia coli* transformed with pET21a-Cdc13-DBD-His_6 were grown at 37°C in LB media with ampicillin (50 mg/L) to an OD_{600} of ~0.6. Cdc13-DBD-His_6 expression was induced with IPTG (isopropyl-β-d-thiogalactopyranoside) at a final concentration of 1 mM at 22°C for approximately 6 hours, after which cells were harvested by centrifugation. Cells were resuspended in buffer A [25 mM HEPES-NaOH, 10% glycerol, 300 mM NaCl, 0.01% NP-40, 20 mM imidazole, 1 mM benzamidine, 0.2 mM phenylmethylsulfonyl fluoride] and cell lysis was achieved by incubation with lysozyme solution [1 mg/mL lysozyme, 1 mM Tris-HCl pH 8.0, 0.1 mM EDTA, 10 mM NaCl, 0.5% Triton-X-100], followed by sonication for 60 sec (two 30-sec cycles) using a Branson 450 Sonifier (power setting 3, 70% duty cycle). Supernatant was separated from cellular debris by centrifugation, and Cdc13-DBD-His_6 was purified from supernatant with Ni-NTA (Ni-nitrilotriacetic acid) agarose beads. Beads were washed in buffer A and protein was eluted from beads in buffer B [25 mM HEPES-NaOH, 10% glycerol, 300 mM NaCl, 0.01% NP-40, 200 mM imidazole, 1 mM benzamidine, 0.2 mM phenylmethylsulfonyl

fluoride]. Eluted protein was dialyzed overnight in buffer C [25 mM HEPES-NaOH, 10% glycerol, 300 mM NaCl]. Protein concentration was estimated by polyacrylamide gel electrophoresis, using bovine serum albumin as standard. Purification of Rap1 has been previously described [237].

2.4.5 Electrophoretic mobility shift assays (EMSA)

To generate EMSA probes, oligonucleotide pairs were mixed in equimolar ratios, boiled in 1X annealing buffer (10 mM Tris-HCl pH 7.5, 100 mM NaCl, 1 mM EDTA), and slowly cooled to room temperature. Probes were radiolabelled with T4 polynucleotide kinase or by fill-in synthesis with Klenow polymerase. For Rap1 EMSAs, each 20 µl EMSA reaction contained binding buffer (20 mM Tris-HCl pH 7.5, 1 mM DTT, 70 mM KCl, 1 mM EDTA, 5% glycerol, 2.5 ng/µl BSA), 1.5 µg herring sperm DNA (Sigma-Aldrich), labeled probe (30 - 50 nM), and the indicated amounts of Rap1. Reactions were separated by 5% native polyacrylamide gel electrophoresis (PAGE) in 0.5X TBE at 100V for 45 min. Gels were fixed in 10% acetic acid/20% methanol and then exposed to Phosphor Screens. Screens were scanned using the Typhoon TRIO Variable Mode Imager and results were analyzed with ImageQuant TL 7.0 software (GE Heathcare). For Cdc13 EMSAs, each 20 µl EMSA reaction contained binding buffer (50 mM Tris-HCl pH 7.5, 1 mM DTT, 75 mM KCl, 75 mM NaCl, 0.1 mM EDTA, 15% glycerol, 1 mg/ml BSA), labeled probe (62.5 nM), and the indicated amount of Cdc13-DBD protein. Reactions were separated on 6% native polyacrylamide gels (containing 5% glycerol) in 1X TBE buffer at 200V for 30 min. Subsequent steps were as described for Rap1 above.

2.4.6 Cloning and sequencing of *de novo* telomeres

Cloning of telomeric DNA was performed as previously described [229] with minor modifications. Blunting of genomic DNA ends was done with T4 DNA polymerase (NEB) in the presence of 0.1 mM dNTPs. Sequences for 'ds oligo 1' and' ds oligo 2' (used to create the double-stranded oligonucleotide that was ligated to the blunted DNA ends) can be found in Table 2-2. Telomere PCR was performed with ds oligo 2 and a primer internal to the *de novo* telomere (Table 2-2). PCR products were separated in 2% agarose gels, purified, and ligated into pGEM-T Easy vector (Promega) or pDrive Vector (Qiagen). Sequencing of inserts was carried out by GenHunter (Nashville, TN) or Genewiz (South Plainfield, NJ) using the primer M13F (-20) (Table 2-2).

TABLE 2-1: List of strains used in Chapter 2

Strain	Genotype	Source
YKF201	*MAT**a** trp1 leu2 ura3 his7*	T. Formosa [238]
YKF870	YKF201 *hxt13*::*URA3* (Fig. 1A, B)	This study
YKF1310	CL11-7: *MAT**a**::ΔHOcs::hisG hmlΔ::hisG HMRa-stk ura3Δ851 trp1Δ63 leu2Δ*::*KAN*^{R} *ade3*::*GAL10*::*HO*	J.E. Haber [217]
YKF1308	JRL017: *MAT**a**::ΔHOcs::hisG hmlΔ::hisG HMRa-stk ura3Δ851 trp1Δ63 leu2Δ*::*KAN*^{R} *ade3*::*GAL10*::*HO can1,1-1446*::*HOcs*::*HPH*^{R}	J.E. Haber [217]
YKF1333	YKF1310 *hmra-stkΔ*::*NAT*^{R}	This study
YKF1323	YKF1308 *hmra-stkΔ*::*NAT*^{R}	This study
YKF1342	YKF1323 *hxt13*::*URA3* (Fig. 1C, D; Fig. 2, 3, 4, 5)	This study
YKF1366	YKF1323 SiRTA 5L-35	This study
YKF1403	YKF1366* SiRTA 5L-35 core mut *hxt13::URA3* (Fig. 2, mutation a)	This study
YKF1401	YKF1366* SiRTA 5L-35 spacer mut *hxt13::URA3* (Fig. 2, mutation b)	This study
YKF1385	YKF1366* SiRTA 5L-35 stim::polyA *hxt13::URA3* (Figs. 2 and 6, mutation c)	This study
YKF1464	YKF1366* SiRTA 5L-35 spacer/core *hxt13::URA3* (Fig. 2, mutation d)	This study
YKF1477	YKF1366* SiRTA 5L-35 spacer *hxt13::URA3* (Fig. 3)	This study
YKF1459	YKF1366* SiRTA 5L-35 stim subst *hxt13::URA3* (Fig. 4)	This study
YKF1517	YKF1366* SiRTA 5L-35 stim subst inv *hxt13::URA3* (Fig. 4)	This study
YKF1585	YKF1323 SiRTA 5L-35::*URA3*	This study
YKF1592	YKF1585** SiRTA 5L-35 Rap1 only *hxt13::URA3* (Fig. 5)	This study
YKF1630	YKF1585** SiRTA 5L-35 Cdc13 only *hxt13::URA3* (Fig. 5)	This study
YKF1588	YKF1585** SiRTA 5L-35 stim::2X UAS *hxt13::URA3* (Fig. 6)	This study
YKF1510	YKF1333 spacer (chr. VII) *pau11::URA3* (Fig. 3)	This study
YKF1518	YKF1333 SiRTA 9L-44 *soa1*::*URA3* (Fig 7)	This study
YKF1610	YKF1333 SiRTA 9L-44 Cdc13 BS Mut1 *soa1*::*URA3* (Fig 7)	This study

YKF1652	YKF1333 SiRTA 9L-44 Cdc13 BS Mut2 *soa1*:: *URA3* (Fig 7)	This study

* Strain YKF1366 contains a deletion of the complete SiRTA 5L-35 sequence. This strain was used as the recipient strain for two-step integration of the indicated SiRTA 5L-35 mutations to facilitate the identification of correct strains following growth on media containing 5-FOA.

** Strain YKF1585 contains a *URA3* cassette replacing a portion of SiRTA 5L-35. This strain was used as the recipient for one-step gene replacement by the indicated SiRTA 5L-35 mutations, with selection for integration on media containing 5-FOA.

Table 2:2: List of primers utilized in Chapter 2

Name	Sequence	Reference and/or Use
hxt13::URA 3 F	5'-CCCCTGGATATATGCGC-3'	Amplify *hxt13::URA3* allele from existing strain for one-step integration
hxt13::URA 3 R	5'-CCCCATATCATTTCACTCC-3'	
hmra-stkΔ::NATR F	5'-ACAAATCTAGAAATTACCAGAGCTATCCATCTTGTTCAAGAAGGTAGGCGCGGATCCCCGGGTTAATTAA-3'	Replace sequences with homology to the HO cleavage site with nat gene
hmra-stkΔ::NATR R	5'-TTGAATAAACCTGGTCTCAAATAAAATTGGTAGAATGACCGAATTCGAGCTCGTTTAAAC-3'	
Met-NPR2 For	5'-CATGTCTAGAATGCTAAGCTATTTCCAAGGG-3'	Fragment I
NPR2-mid Rev	5'-GTACAAGCTTGTGGATCAGTCAAAAAATTCC-3'	Fragment II
stim::polyA fragment I	5'-GGATGTAG**AAAAAAAAAAAAAAAAAA**TACTACTAGGATTTGGCGTG-3'	Use with Met-NPR2 For and NPR2-mid Rev. Fig. 2, mutation c and Fig. 6.
stim::polyA fragment II	5'-GTA**TTTTTTTTTTTTTTTTTT**CTACATCCGAAAAGGATACAAAGG-3'	
core mut fragment I	5'-**CACCTCCCACAACAACACCTCAA**TTCCAACACCTTCAAATCGAAG-3'	Use with Met-NPR2 For and NPR2-mid Rev. Fig. 2, mutation a.
core mut fragment II	5'-**TTGAGGTGTTGTTGTGGGAGGTG**GCAGGTCCTTCATCCACGCC-3'	
spacer mut fragment I	5'-**ATGATGATCCTAAACCGCACCTACTTCCTGCACCA**GTGGAGGGTGTTGTTGTGG-3'	Use with Met-NPR2 For and NPR2-mid Rev. Fig. 2, mutation b.
spacer mut fragment II	5'-**GGTGCGGTTTAGGATCATCAT**ACACCACACCAACTCATCCTAC-3'	
spacer/coreD fragment I	5'-GGTGTGGTGTTTTCCAACACCTTCAAATCGAAG-3'	Use with Met-NPR2 For and NPR2-mid Rev. Fig. 2, mutation d.
spacer/coreD fragment II	5'-AGGTGTTGGAAAACACCACACCAACTCATCCTACATCCG-3'	

spacerD fragment I	5'-GTAGGATGAGTTGGTGTGGTGTGTGGAGGGTGTTGTTGTGGAGTTTTC-3'	Use with Met-NPR2 For and NPR2-mid Rev. Fig. 3 (chr. V).
spacerD fragment II	5'-ACACCACACCAACTCATCCTAC-3'	
stim subst fragment I	5'-GGATGTAG**AATGTATGGGTGT**AACACC**AATGTATGGGTGT**TACTACTAGGATTTGGCGTG-3'	Use with Met-NPR2 For and NPR2-mid Rev. Fig 4G.
stim subst fragment II	5'-GTA**ACACCCATACATT**GGTGTT**ACACCCATACATT**CTACATCCGAAAAGGATACAAAGG-3'	
stim subst inv fragment I	5'-GGATGTAG**ACACCCATACATT**GGTGTT**ACACCCATACATT**TACTACTAGGATTTGGCGTG-3'	Use with Met-NPR2 For and NPR2-mid Rev. Fig 4G.
stim subst inv fragment II	5'-GTA**AATGTATGGGTGT**AACACC**AATGTATGGGTGT**CTACATCCGAAAAGGATACAAAGG-3'	
stim::URA3 for	5'-CACTGTATCTGCTGCTTCTCATATCCTTTGTATCCTTTTCGTACTGAGAGTGCACCACGC-3'	Use to replace SiRTA 5L-35 stim with URA3 by one-step gene replacement.
stim::URA3 rev	5'-AACAACACCCTCCACTGCAGGTCCTTCATCCACGCCAAATCTCCTTACGCATCTGTGCGG'3'	
HS forward	5'-TACTGCATTTCCCTCATCAATTG-3'	fragment I
HS reverse	5'-GACGTCTCCCTACGAACCAG-3'	fragment II
Cdc13 only fragment I	5'-ATCCTAGTAGTA**CACACACACTC**GGTGTT**CACACACACTC**CTACATCCGAAAAGGATACAAAG-3'	Use with HS forward and HS reverse to replace URA3 in stim::URA3. Fig. 5D.
Cdc13 only fragment II	5'-**GAGTGTGTGTG**AACACC**GAGTGTGTGTG**TACTACTAGGATTTGGCGTGG-3'	
Rap1 only fragment I	5'-**CCAAATCCTAGGTGTTGCACCCATACATTGGTGTTGCACCCATACATT**CTACATCCGAAAAGGATACAAAG-3'	Use with HS forward and HS reverse to replace URA3 in stim::URA3. Fig. 5D.
Rap1 only fragment II	5'-**GGTGCAACAC**CTAGGATTTGGCGTGGATGAAG-3'	
stim::2X UAS fragment I	5'-CTAGTAGTA**GTGTCGGCGCAGAGATCTCCGAGTGTCGGCGCAGAGATCTCCGA**GAAAAGGATACAAAGGATATGAG-3'	Use with HS forward and HS reverse to replace URA3

stim::2X UAS fragment II	5'-**GCGCCGACAC**TACTACTAGGATTTGGCGTGG-3'	in stim::URA3. Fig. 6.
Rap1 for	5'-AGGCGCCATGGCTTCTAGTCCAGATGATTTTGAAAC-3'	Use to clone full-length *RAP1* into pAB180.
Rap1 rev	5'-TAGTGACGTCACTGCAATTTGGCACCGCCGCGTTGGGCTGCGCGGATCATGTCTCATAACAGGTCCTTCTCAAAAAATC-3'	
Adj HO for	CATGCTCGAGGAGCTCATGTCGCCGTAATC	Fragment I
Adj HO rev	GTACACTAGTGCGCAAATTGAAAAGTCGGG	Fragment II
SpacerΔ ChrVII fragment I	CAACACCCTCCACACACCACACCAACTCATCCTACATCCGGAAAACAAGCGGCACCAATCTTCAATTGG	Use with Adj HO for and Rev. Fig 3, spacerΔ ChrVII
SpacerΔ ChrVII fragment II	TTGGTGTGGTGTGTGGAGGGTGTTGTTGTGGAGTTGGAAACTGAATTAACTGCTGTGATACAGAAC	
ChrVII HO for	CAATTTCACCTAATCTCTTCTTGGCCTTTGGACATTGCATGTTGGCCTCTCCAGCTGAAGCTTCGTACGC	Use to integrate Hocs on chromosome VII, 3kb away from SIRTA SpacerΔ
ChrVII HO rev	CCGCCTCTAACCCAATCACCGATGCCTGTGCTTTGAAGGGTATTGATTTGCGCATAGGCCACTAGTGGATCTG	
PAU11:URA3 for	CAAATTAACTTCAATCGAAGCTGGTGTCGCTGCCATCGCTGCTACTGCTTCCGCGTACTGAGAGTGCACCACGC	Use to replace *PAU11* with URA3 by one-step gene replacement on ChrVII
PAU11:URA3 rev	GATGAAAATGCTGTCCACGGTGAATTATATTTTAACACATATGGGGGGTTGCTCCTTACGCATCTGTGCGG	
BNR1 for	GTACAAGCTTGGACAATGTCGTTATCACAGTTC	Fragment I
BNR1 rev	CATGTCTAGACTCTGCCCAAGCGTTCAACTAG	Fragment II
Cdc13 BS Mut1 fragment I	CT**AAAAAAAAAAAAAAAAA**CCTTTGTTCATCGACAAGGACTCGGG	Use with BNR1 for and Rev. Fig. 7, mutation Cdc13 BS Mut1
Cdc13 BS Mut1 fragment II	CAAAGG**TTTTTTTTTTTTTTTTT**AGTTACTCCTCCAGCTCCACC	
Cdc13 BS Mut2 fragment I	GGAGGGGCCTTTGTTCATCGAC**AAAAAAAAAAAAAAAAAA**GGTGGCGGTGGTGGTGGTGGAACGGCGCCCAAGTTTTAG	Use with BNR1 for and Rev. Fig. 7, mutation Cdc13 BS Mut1
Cdc13 BS Mut2 fragment II	CTAAAACTTGTGGCGCCGTTCCACCACCACCACCGCCACC**TTTTTTTTTTTTTTTTTT**GTCGATGAACAAAGGCCCCTCC	

SOA1:URA3 for	CCTCGAGCAAATAGGCTACATTTGCTGCTGCACCCCTTTACAGCACAAAGTCGGTACTGAGAGTGCACCACGC	Use to replace *SOA1* with *URA3* by one-step gene replacement on ChrIX.
SOA1:URA3 rev	GCGTAGGTCCTCTACGCATTAAATAAAAGGATGCCACGCCAACAGAAAGGACCTCCTTACGCATCTGTGCGG	
ChrIX HO for	AATTTCGAGCGGTTTTTAAGATACACCATGTTTCAAGTAACCACCTTTCGCGCATAGGCCACTAGTGGATCTG	Use to integrate Hocs on chromosome IX, 3kb away from SIRTA 9L-44
ChrIX HO rev	TATGTAGTGTTATATTCACTCTGTACTCAGAGCCACAAGAAATAACCATTCGCATAGGCCACTAGTGGATCTG	
ds oligo 1	5'-GGGTTCGAATGACCGGCAGCAGCAAAATG-3'	Telomere cloning
ds oligo 2	5'-CATTTTGCTGCTGCCGGTCATTCGAACCC-3'	Telomere PCR/cloning
9L-44 mapping for	5'GTCTGGTTATTGATAGACACTGAGG-3'	Telomere PCR/cloning chr. IX
ChrV telomere-internal	5'-CTGATAATGTAACACACTTATAG-3'	Telomere PCR/cloning chr. V
M13F (-20)	5'-GTAAAACGACGGCCAG-3'	Telomere sequencing
HS TELO rev1	5'-CACGCCAAATCCTAGTAGTA-3'	Used to determine the proportion of telomere addition events in the SiRTA Stim vs. SiRTA Core. Fig. E6
Internal NPR2 rev2	5'-CTTAGTTTAGAAATTTTGGCAATG-3'	

CHAPTER 3

INTERACTION OF YEAST RAD51 AND RAD52 RELIEVES RAD52-MEDIATED INHIBITION OF *DE NOVO* TELOMERE ADDITION[2]

3.1 Introduction

The ends of most linear eukaryotic chromosomes are organized into special nucleoprotein structures, telomeres, that are essential for the maintenance of genome stability and integrity. In association with telomere binding proteins, telomeres protect the ends of the chromosomes from being recognized as DNA double-strand breaks (DSBs), preventing inappropriate nucleolytic processing, fusion, and recombination [52]. Telomeres also counteract loss of sequences due to the 'end-replication problem' by serving as a primer for telomere synthesis by the specialized ribonucleoprotein enzyme telomerase [208]. The telomerase reverse transcriptase utilizes its intrinsic RNA component as a template for the addition of TG-rich sequence repeats ($TG_{1\text{-}3}$ in yeast) to the overhanging 3' strand at the chromosome terminus [208].

DNA DSBs are among the most toxic forms of DNA lesion, with failed or incorrect repair carrying a high likelihood of sequence loss, rearrangement, and cell death. Therefore, appropriate detection and repair of DSBs is crucial for the maintenance of genome stability. DSBs are generated due to exposure to exogenous agents such as ionizing radiation and

[2] This chapter represents my current work submitted to Plos Genetics 08/06/2019. Authors Esther A Epum, Michael Mohan, Nicholas Ruppe and Katherine Friedman.

radiomimetic drugs or endogenous agents such as reactive oxygen species and replication errors [166]. There are two major, mechanistically distinct, pathways of DSB repair – homologous recombination (HR) and non-homologous end joining (NHEJ) – that are defined primarily on the basis of the requirement for sequence homology. HR utilizes a homologous template such as a homologous chromosome or sister chromatid for repair, while NHEJ involves direct ligation of broken ends with minimal processing [161]. During HR, the 5' terminating strands are resected to generate 3' single-stranded DNA that is rapidly bound by replication protein A (RPA), a three-protein complex that in yeast is encoded by the genes *RFA1-3* [166,239,240]. Association of yeast Rad52 with RPA-coated single-stranded DNA results in the displacement of RPA and formation of the Rad51 nucleoprotein filament [166,241,242]. This Rad51 nucleoprotein filament initiates the homology search and coordinates strand invasion into homologous duplex DNA to facilitate repair [166,243]. In addition to serving as a mediator of Rad51 filament formation, Rad52 also contributes to HR by facilitating annealing between complementary RPA-coated single strands [244,245].

While NHEJ and HR are the primary pathways of DSB repair in eukaryotic cells, other forms of less accurate repair such as single-strand annealing (SSA) [166], microhomology-mediated end joining (MMEJ) [181], and break-induced replication (BIR) [173] have also been observed. These 'non-conservative' repair pathways lead to formation of gross chromosomal rearrangements (GCRs) including deletions, inversions, and translocations. The genetic requirements for these pathways are different, but overlapping, and are influenced by the extent and location of available homologies [246]. Since genome rearrangements influence both cancer and genetic disease through changes in gene dosage, formation of fusion proteins,

and/or changes in gene regulation, an understanding of how these non-conservative pathways are regulated and how they may compete during repair of a DSB is essential.

While the pathways described above require interaction of the DSB with an intra- or inter-chromosomal sequence to facilitate repair, terminal deletions can arise through direct addition of a *de novo* telomere by telomerase to an internal DSB [189,194]. In fact, GCR events within a non-essential terminal region of yeast chromosome V are more likely to involve *de novo* telomere addition than any other type of rearrangement, whether they occur spontaneously or in response to a single DSB [63,192,197,202]. Sites of *de novo* telomere addition in yeast typically contain at least a single TG-dinucleotide, likely reflecting a requirement for base pairing between the 3' end of the DSB and the telomerase RNA (which in yeast contains the sequence 5'-CACCACACCCACACAC3') [63,202,247]. However, this interaction is insufficient and telomerase recruitment to a DSB occurs through at least two (perhaps non-exclusive) mechanisms. At sites containing very short TG tracts (<4 nt), *de novo* telomere addition depends on interaction between the TLC1 telomerase RNA and yeast Ku70/80 [63], a heterodimeric complex that interacts in a non-sequence specific manner with both telomeres and DSBs. The telomere-binding protein Cdc13 also recruits telomerase to DSBs via its interaction with the telomerase component Est1 [40,42,202,205]. Cdc13 displays a marked preference for TG-rich, telomere-like sequences [92]. However, even in the absence of obvious TG-rich sequences, chromatin immunoprecipitation (ChIP) experiments reveal association of both Cdc13 and telomerase with regions surrounding a DSB under conditions that encourage the generation of substantial resection (*i.e*. when HR is restricted) [248]. The ability of telomerase to successfully add a *de novo* telomere at TG-repeats of ≤11 nt is moderated by the

Mec1-dependent phosphorylation of Cdc13 [202]. DNA damage-dependent phosphorylation of the helicase Pif1 by Mec1 also inhibits telomere addition at DNA breaks [200], although such inhibition is overcome at sites containing at least 34 bp of telomeric sequence in a manner dependent on Cdc13 function [201]. Together, these mechanisms limit frequencies of *de novo* telomere addition at most internal sequences.

We have previously characterized two endogenous hotspots of *de novo* telomere addition on the left arms of yeast chromosomes V and IX. These TG-rich sequences, termed SiRTAs (Sites of Repair-associated Telomere Addition), undergo *de novo* telomere addition at frequencies ~200-fold higher than neighboring regions [197], even when the initiating chromosome break is located several kilobases distal to the eventual site of telomere addition. [197]. The nomenclature for these sites (SiRTAs 5L-35 and 9L-44) reflects the distance each is located (35kb and 44kb, respectively) from the nearest telomere on that chromosome arm. Both sites display a bipartite structure consisting of a Core sequence within which telomerase acts to initiate *de novo* telomere addition and a Stim sequence that enhances telomere addition at the Core by providing binding site(s) for Cdc13 [197]. The identification of these sequences as hotspots of *de novo* telomere addition provides a tractable system in which to examine the interplay between alternative non-conservative repair pathways.

Telomere addition at SiRTA following a distal chromosome break must involve extensive 5’ end resection to expose Cdc13 binding sites in single-stranded DNA and to generate a 3’ terminus that can prime telomere addition by telomerase. Since such extensive single-stranded DNA is expected to form a Rad51 nucleoprotein filament, in this chapter we investigated roles of the HR-associated proteins Rad51 and Rad52 in *de novo* telomere addition at these SiRTAs.

Indeed, previous work showed that recruitment of Cdc13 to DSBs lacking extensive TG repeats is reduced in the absence of Rad51 [248]. In this chapter, we show that Rad51, but not Rad52, is required for normal levels of *de novo* telomere addition at two different SiRTA sites after DNA DSB induction. Surprisingly, *de novo* telomere addition is restored in the absence of both proteins, suggesting that Rad51 counteracts an inhibitory effect of Rad52. This activity requires the ability of Rad51 to interact with Rad52, but not its ability to bind single-stranded DNA. Additionally, an allele of *RFA1,* that by genetic criteria reduces the interaction between Rfa1 and Rad52, blocks the inhibitory effect of Rad52. The reduction in *de novo* telomere addition in the absence of Rad51 correlates with reduced association of Cdc13 with SiRTA and is rescued by the forced recruitment of Cdc13, suggesting that association of Rad52 with RPA-bound single-stranded DNA directly or indirectly inhibits Cdc13 binding in a manner relieved by Rad51. In the course of these experiments, we found that the genetic manipulations described above also affect the probability of Rad52-mediated microhomology-mediated repair (MHMR) in the region proximal to SiRTA 9L-44, indicating that direct interactions between Rad51 and Rad52 modulate the relative use of alternative repair pathways in a context-dependent manner.

3.2 Results

3.2.1 Rad52 inhibits telomere addition at SiRTA in the absence of Rad51

The ability of a particular sequence to function as a SiRTA is monitored in haploid cells using an inducible HO endonuclease cleavage assay previously described [197,217]. Briefly, a

recognition site for the HO endonuclease is integrated approximately 3 kb distal to the SiRTA, homologous sequences on chromosome III at the *MAT*, *HML*, and *HMR* loci are deleted to prevent repair of the break by gene conversion, and the *URA3* gene is integrated approximately 7 kb distal to the HO cleavage site to monitor loss of the chromosome end. The HO endonuclease is expressed under control of a galactose-inducible promoter. In assays described here, cells are plated on media containing galactose, resulting in persistent HO cleavage. Correct repair through NHEJ or HR using the sister chromatid as a template restores the cleavage site and causes the cell to enter a repair-cleavage cycle that is often lethal; colonies form when incorrect repair results in the mutation or removal of the HO recognition site (Figure 3-1A). Strains in which the HO site is removed due to a large internal deletion, translocation, or loss of the chromosome terminus by *de novo* telomere addition cause the cell to acquire 5-fluoroorotic acid (5-FOA) resistance through loss of the distal *URA3* marker (referred to as Gal^R $5\text{-}FOA^R$ colonies or GCR events) (Figure 3-1A) [197]. The proximal rearrangement junctions thus formed are constrained between the HO cleavage site and the last essential genes *PCM1* or *MCM10,* located ~43kb and ~60kb from telomeres V-L and IX-L, respectively. Repair junctions are mapped by PCR to the SiRTA itself or to the centromere-proximal (between the SiRTA and the essential gene) or telomere-proximal (between the SiRTA and the HO site) regions (Figure 3-1A). These regions are not equal in size, with the SiRTA encompassing only a small fraction of the total region in which repair could occur (<1% in each case). The propensity for repair to occur within a particular region is expressed either as the percent of total GCR events (relative frequency), or as the percent of total cells that incur a GCR event (absolute frequency) [197]. The latter calculation accounts for differences between genotypes in the frequency of survival

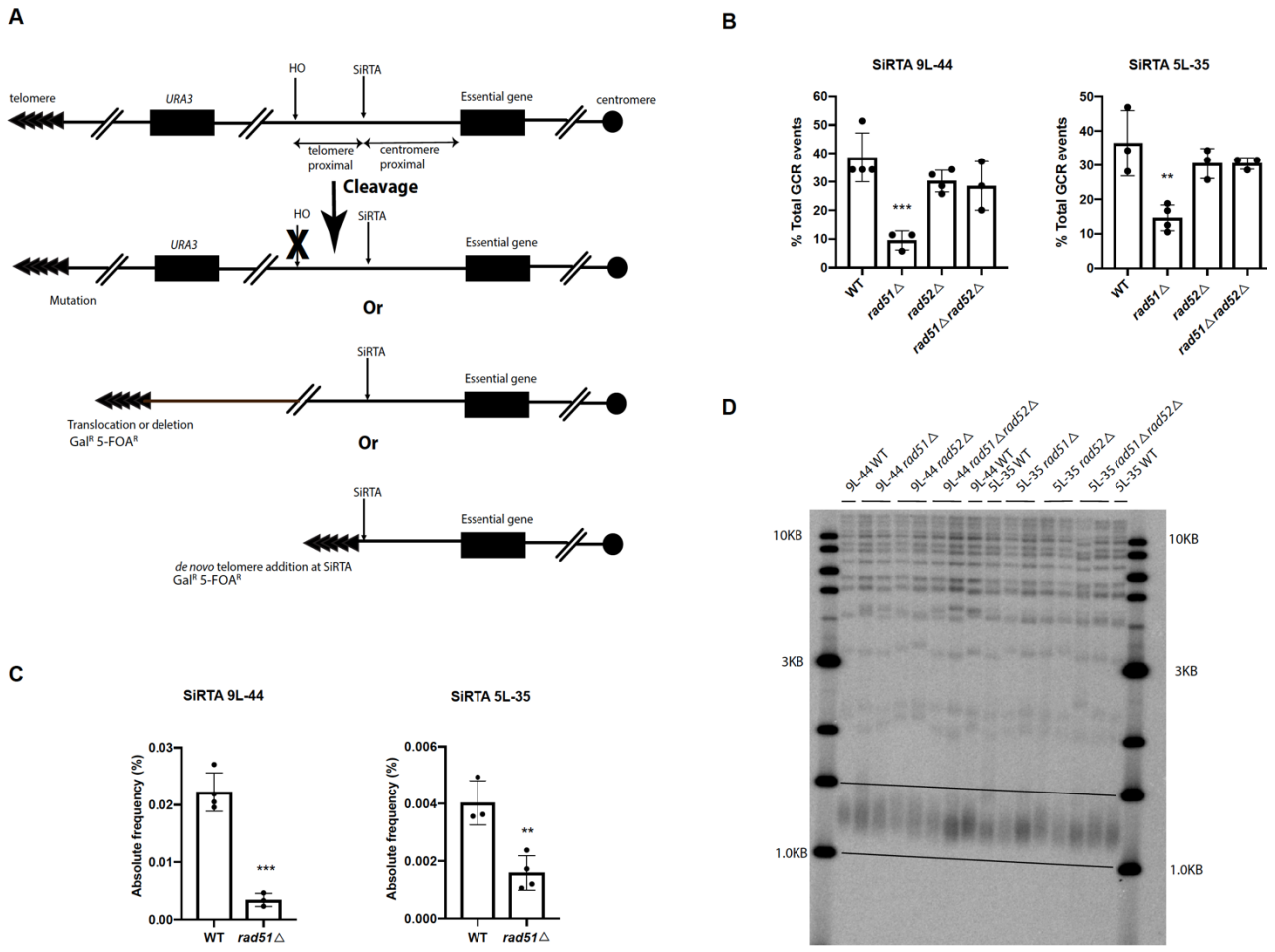

Figure 3-1: Rad51 promotes *de novo* telomere addition at SiRTAs 9L-44 and 5L-35 by inhibiting Rad52 function. (A) Schematic of the HO cleavage assay system. *MCM10* and *PCM1* are the essential genes on the left arms of chromosome IX and V located ~16.7kb and 8.4kb respectively from the SiRTAs. The HO cut site is placed ~3.2kb and 2.9kb distal to the SiRTA on chromosome IX and V respectively. Cleavage is induced by the expression of HO endonuclease upon plating on galactose-containing medium, surviving colonies lacking *URA3* function are selected on media containing 5-FOA, and the approximate location of each GCR event is mapped by PCR to the SiRTA, the region centromere-proximal to the SiRTA, or the region telomere-proximal to the SiRTA (see Materials and methods). (B) The percent of total GCR events occurring within the indicated SiRTA is shown for WT and mutant strains. Averages from at least three independent experiments are shown with standard deviations. Strains statistically different from WT by ANOVA with Dunnett's multiple comparisons test are indicated by asterisks (**p <0.01; ***p <0.001). (C) Data in panel B expressed as absolute frequency (% total cells) for WT and *rad51* strains only (see Materials and methods for calculation). Statistical significance is determined by unpaired t-test (**p<0.01; ***p<0.001). (D) Southern blot analysis of WT, *rad51Δ, rad52Δ* and *rad51Δ rad52Δ* strains. 9L-44 and 5L-35 indicate the YKF1752 and YKF1342 strain backgrounds, respectively (Table 3-1). The first and last lanes contain molecular weight marker as indicated. Contributing authors: EAE.

on galactose- and/or 5-FOA-containing media. In previous work, we found that the vast majority of GCR events mapping to SiRTAs 9L-44 and 5L-35 are the result of *de novo* telomere additions [197] (and see below).

Because *de novo* telomere addition at SiRTA requires resection from the site of the DSB to expose single-stranded DNA as a template for telomere addition, we examined the role of Rad51, which forms a nucleoprotein filament on single-stranded DNA to facilitate the homology search during HR [243]. Indeed, previous work suggested that Rad51 facilitates *de novo* telomere addition, although the mechanism is not understood [248]. Loss of *RAD51* reduces the relative frequency of GCR events at SiRTA 9L-44 by 4-fold (WT: 38.6% $\pm$ 8.6%; *rad51Δ*: 9.5% $\pm$ 3.3%; p<0.001) and at SiRTA 5L-35 by 2.5-fold (WT: 36.4% $\pm$ 9.6%; *rad51Δ*: 14.6% $\pm$ 3.8; p <0.01) (Figure 3-1B; absolute frequencies shown in Figure 3-1C). If formation of the Rad51 nucleoprotein filament contributes to telomere addition at SiRTAs, then loss of Rad52 (required for filament formation [241,242]) should have the same effect. Notably, deletion of *RAD52* does not decrease the frequency of *de novo* telomere addition at either SiRTA 9L-44 (WT: 38.6% $\pm$ 8.6%; *rad52Δ*: 30.3% $\pm$ 3.9%; p=0.24) or 5L-35 (WT: 36.4% $\pm$ 9.6%; *rad52Δ:* 30.5% $\pm$ 4.4%; p=0.44) (Figure 3-1B), consistent with a previous report [197]. The effect of deleting *RAD51* is unique among the genes of the RAD52 epistasis group since deleting *RAD54*, *RAD55*, *RAD57* or *RAD59* does not consistently reduce the frequency of GCR formation at either SiRTA (Figure 3-2).

We then examined the epistatic relationship between *RAD51* and *RAD52*. Surprisingly, deletion of *RAD52* completely suppresses the telomere addition defect associated with *rad51Δ* at both SiRTA 9L-44 (WT: 38.6% $\pm$ 8.6%; *rad51Δ rad52Δ*: 28.6% $\pm$ 8.6%; p=0.18) and SiRTA 5L-35

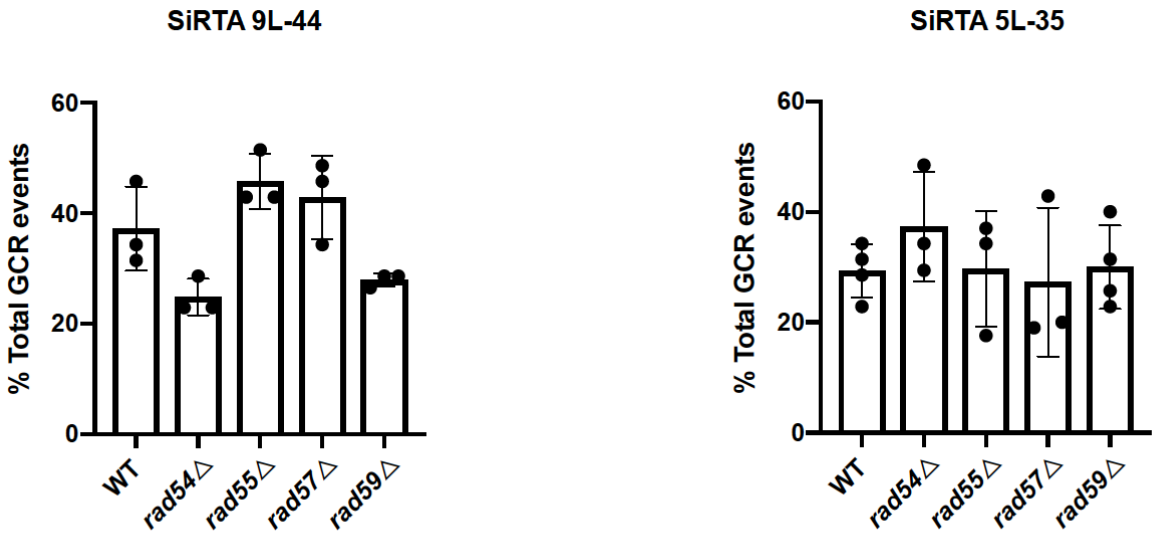

Figure 3-2: *De novo* telomere addition is unaffected by loss of Rad54, Rad55, Rad57 and Rad59. The percent of total GCR events occurring within SiRTA 9L-44 and 5L-35 is shown for the indicated strains. Data are from at least three independent experiments. Error bars represent standard deviation. Statistical significance calculated by ANOVA with Dunnett's multiple comparison test. No significant differences were observed. Contributing authors: EAE.

(WT: 36.4% ± 9.6%; *rad51Δ rad52Δ*: 30.5% ± 1.6%; p=0.44) (Figure 3-1B). This epistatic relationship is incompatible with a model in which Rad51 directly promotes *de novo* telomere addition at SiRTAs and instead suggests that Rad52 inhibits telomere addition, but only in the absence of Rad51. Importantly, the effects observed at SiRTAs are not due to impaired telomerase activity *per se*, as endogenous telomere length is unaffected by the deletions of *RAD51* and/or *RAD52* (Figure 3-1D). We conclude that the effects reported here are specific to the disruption of Rad51 function, with Rad52 functioning as a downstream effector.

Analysis of the GCR events mapping to SiRTA 9L-44 revealed that the effect on *de novo* telomere addition is even more pronounced than reflected in the GCR frequency alone. Using

Southern blotting, the chromosome rearrangements in multiple Gal^R 5-FOA^R colonies were broadly classified as '*de novo* telomere addition' or 'translocation' (although large internal deletions cannot be distinguished from translocations without additional analysis; Figure 3-3). In WT cells, 46 of 50 GCR events (92%) mapping to SiRTA 9L-44 involve *de novo* telomere addition, while the remainder are non-reciprocal translocations or large deletions that remove *URA3*. Similar results were observed in cells lacking *RAD52* only or both *RAD51* and *RAD52* [39 of 41 (95%) in *rad52Δ* and 29 of 29 in *rad51Δ rad52Δ*]. In contrast, only 10 of 19 (53%) events mapping to SiRTA 9L-44 in *rad51Δ* cells involve *de novo* telomere addition. We have previously observed that *cis*-acting mutations reducing SiRTA function likewise reduce the proportion of repair events in the SiRTA that involve *de novo* telomere addition [197], consistent with the effect observed upon *RAD51* deletion.

3.2.2 Rad51 inhibits Rad52-dependent repair events proximal to SiRTA

Concomitant with a decrease in the fraction of GCR events in SiRTA upon deletion of *RAD51*, centromere-proximal events are elevated. This effect is particularly pronounced within the region centromere-proximal of SiRTA 9L-44 (WT: 3.6% $\pm$ 3.6%; *rad51Δ*: 52.4% $\pm$ 3.3%; $p<0.0001$) (Figure 3-4A and Figure 3-5A). Again, deletion of *RAD52* suppresses this increase in centromere-proximal events (*rad51Δ rad52Δ*: 1.0% $\pm$ 1.6%, p=0.70 compared to WT) (Figure 3-4A). As a result, *rad52Δ* and *rad51Δ rad52Δ* strains show relative distributions of GCR events in all three regions (SiRTA, centromere-proximal, and telomere-proximal) that are essentially unchanged compared to WT (Figure 3-5B and C). At SiRTA 5L-35, there is a trend toward

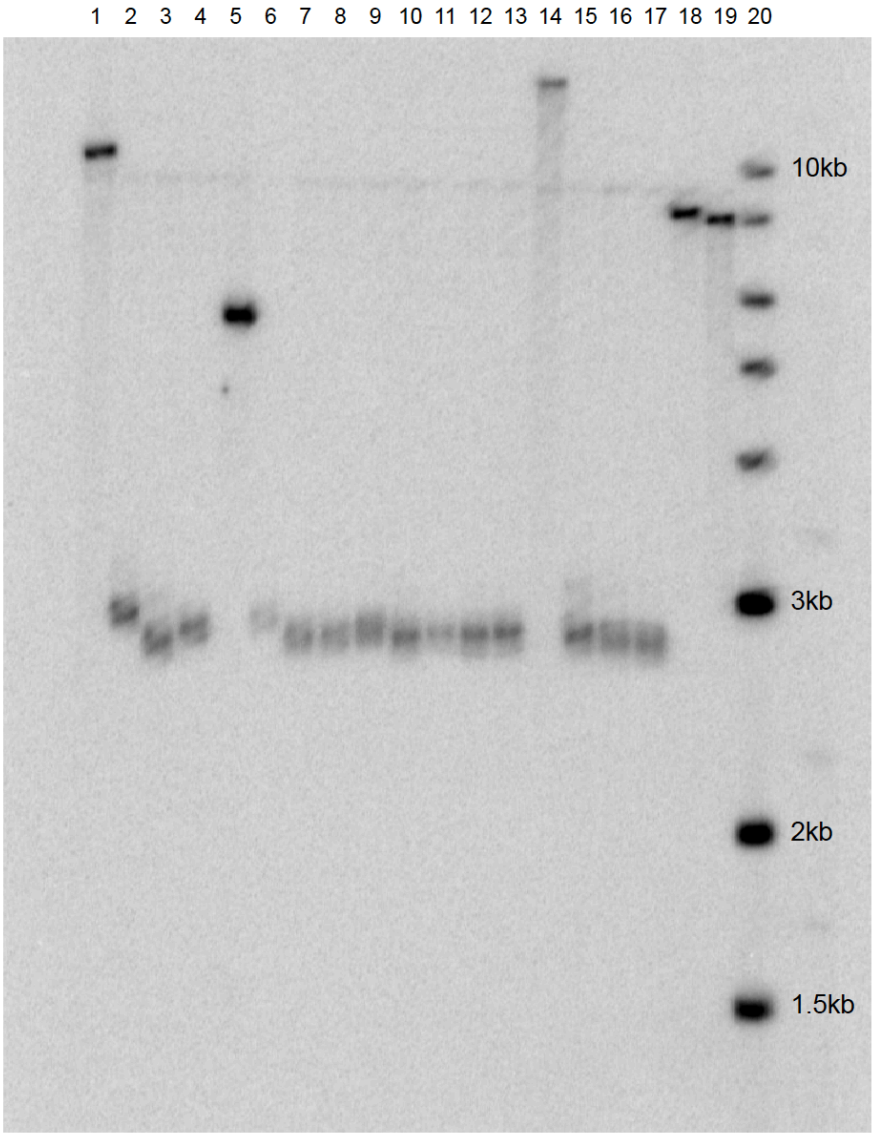

Figure 3-3: Southern blot analysis of GCR events occurring within SiRTA 9L-44. A representative Southern blot is shown. Southern blot was conducted on 18 independent GCR events that mapped to SiRTA 9L-44 by PCR. Candidates in lanes 1, 5, 14 and 18 are classified as translocations. Lane 19 shows a WT strain before HO cleavage. Lane 20 contains molecular weight marker as indicated. All other lanes show GCR events classified as telomere additions following HO cleavage assay. Contributing authors: EAE.

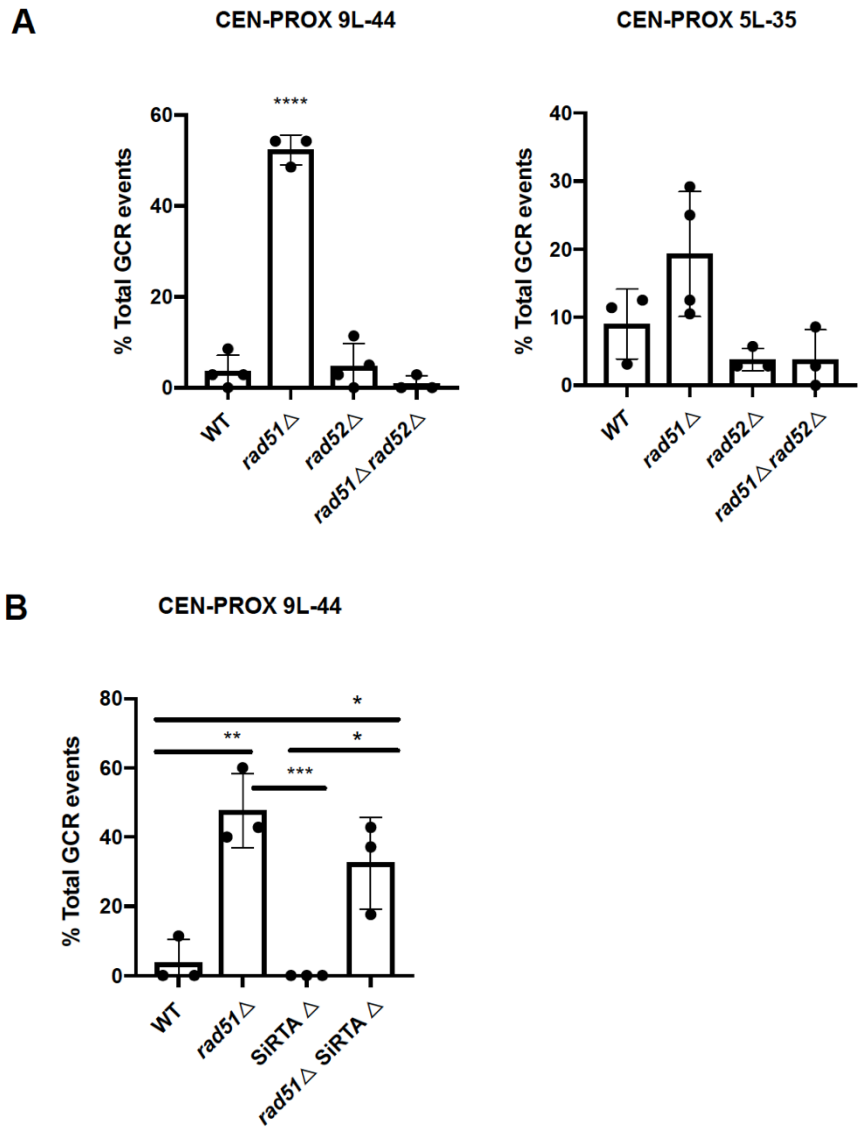

Figure 3-4: Rad52-dependent repair events increase in frequency upon deletion of *RAD51*. (A) The percent of total GCR events occurring centromere-proximal to SiRTAs 9L-44 and 5L-35 is shown for the indicated strains. The strain statistically different from WT by ANOVA with Dunnett's multiple comparisons test is indicated by asterisks (****p <0.0001). (B) The percent of total GCR events occurring centromere-proximal to SiRTA 9L-44 is shown for the indicated strains. In the SiRTAΔ strain, no GCR events were observed in the centromere-proximal region. Values are averages from three independent experiments; error bars represent standard deviation. Averages indicated by asterisks are statistically different by ANOVA with Tukey's multiple comparisons test (*p<0.05; **p <0.01; ***p<0.001). Contributing authors: EAE.

increased GCR frequency in the centromere-proximal region, but the difference is not statistically significant compared to WT (Figure 3-4A and Figure 3-5A). We do not fully understand this discrepancy between the results generated at the two SiRTAs, but speculate that differences in the sequence and/or size of the centromere-proximal regions may play a role (the centromere proximal region on chromosome IX is twice the size of the corresponding region on chromosome V).

We were concerned that the shift to centromere-proximal events in the *rad51Δ* strain might cause the apparent decrease in *de novo* telomere addition at SiRTA when expressing the data as relative GCR frequencies. However, when the absolute frequency of repair in each region is determined, the same pattern is observed, with a 6-fold reduction in the frequency of GCR formation ($p<0.001$) at SiRTA 9L-44 and a 2.5-fold reduction ($p<0.01$) at SiRTA 5L-35 (Figure 3-1C) upon deletion of *RAD51*. We also considered that reduced telomere addition at SiRTA in the absence of *RAD51* might directly cause the increase in centromere-proximal events by allowing resection to proceed internally in a higher fraction of cells. If true, cells completely lacking SiRTA sequences (SiRTAΔ) should undergo more events in the proximal region. Instead, we found no centromere-proximal GCR events in SiRTAΔ 9L-44 cells (WT: 3.8% ± 6.6%; SiRTAΔ: 0%; $p= 0.95$) (Figure 3-4B). However, such events are not dependent on the SiRTA, since centromere-proximal events are observed in SiRTAΔ *rad51Δ* cells at a frequency comparable to that of the *rad51Δ* strain (*rad51Δ*: 47.62% ± 10.8%; SiRTA*Δ* *rad51Δ*: 32.55% ± 13.2%; $p=0.25$) (Figure 3-4B). We conclude that the phenomena observed at the SiRTA and centromere-proximal regions are independent.

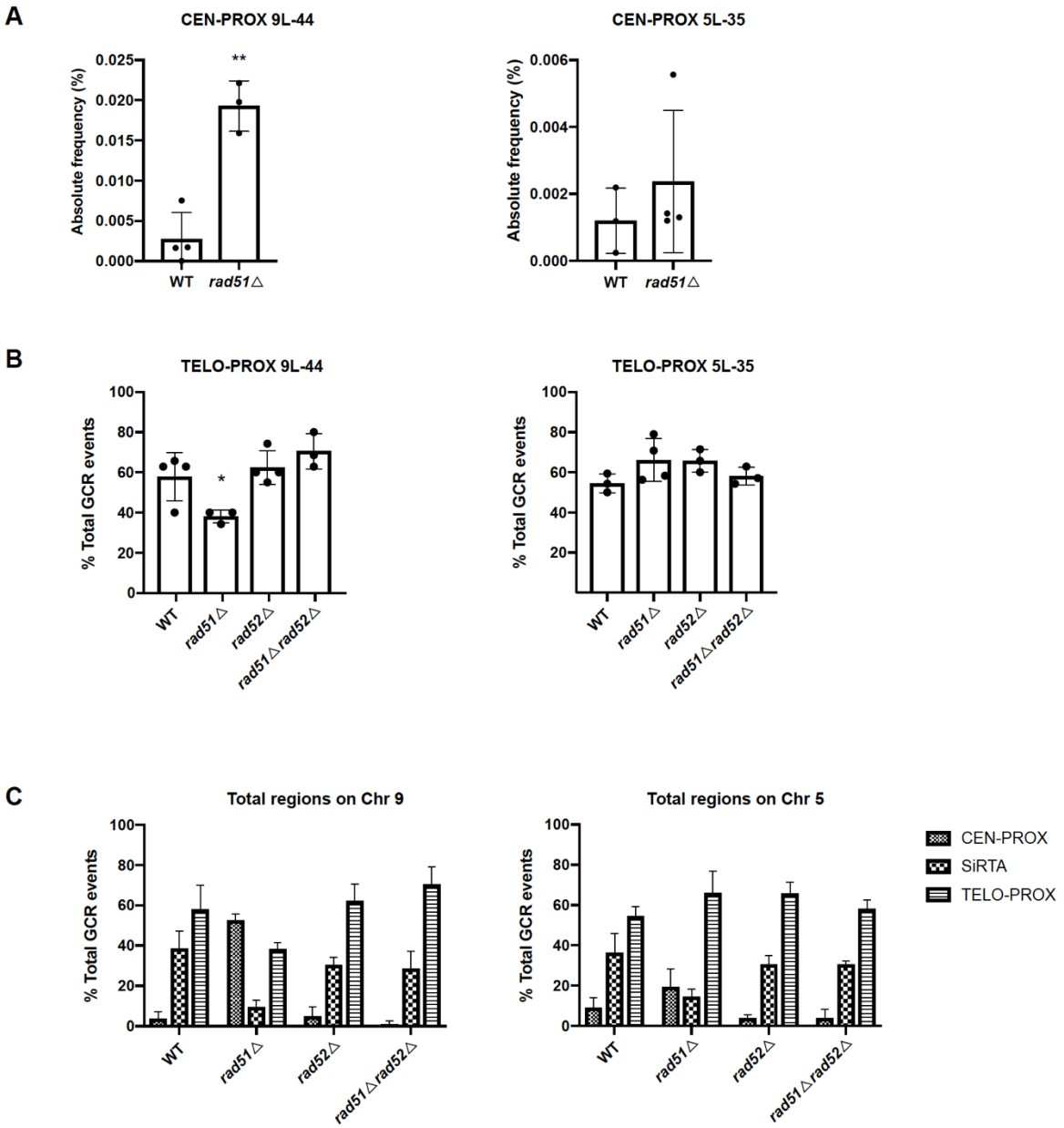

Figure 3-5: Loss of Rad51 alters the distribution of repair events in and centromere-proximal to the SiRTA. (A) Data from Figure 3-4A expressed as absolute frequency (% total cells) for WT and *rad51* strains only (see methods for calculation). Averages and standard deviations are from at least three independent experiments. Statistical significance calculated by unpaired t-test (**p<0.01). (B) The percent of total GCR events occurring within the region telomere-proximal to SiRTAs 9L-44 and 5L-35 is shown for the indicated strains. Data are from the same experiments shown in Figures 3-1B and 3-4A. Averages shown are from at least 3 independent experiments with standard deviation. Strains statistically different from WT by ANOVA with Dunnett's multiple comparisons test are indicated by asterisks (*p <0.05). (C) The percent of total GCR events occurring in each region (see legend) is shown for regions surrounding SiRTA 9L-44 (left graph) and 5L-35 (right graph). The same data are presented in Figures 3-1B, 3-4A, and panel B. Contributing authors: EAE.

3.2.3 Rad51-inhibited repair events require Rad59 and Pol32

To gain insight into the mechanism of repair, genomic DNA was analyzed from twelve independent *rad51Δ* strains containing breakpoints in the centromere-proximal region (between SiRTA 9L-44 and the last essential gene). We used nanopore sequencing at low coverage to obtain very long (up to 54 kb) sequence reads (see Materials and methods). In each case, at least one (and in most cases, multiple) reads span the breakpoint, allowing identification of the sequences involved. Each rearrangement was subsequently verified by PCR amplification across the breakpoint. As shown in Figure 3-6A (repair junctions i-iii), three of the strains contain translocations between the left arm of chromosome IX and chromosome arms V-L, XI-R, or XIV-L, respectively. These strains survived cleavage of chromosome IX by acquiring ~50-70 kilobases of terminal sequence, including the telomere, from a non-homologous chromosome. Sequence reads from the intact chromosome (V, XI, or XIV) are also present in the dataset, indicating that the translocations are nonreciprocal. Microhomology is evident at each breakpoint (Fig 3-6A), with two of the translocations (to XI and XIV) involving the same trinucleotide repeat on chromosome IX. All three translocations occurred after resection of 10 kb or more from the HO cleavage site, which is inserted ~41.5 kb from the left telomere of chromosome IX.

One additional strain contains a 23 kb deletion on chromosome IX (Figure 3-6A, repair junction iv), while at least four, and likely all eight, of the remaining strains contain an identical 39 kb internal deletion (Figure 3-6A, repair junction v). There is some ambiguity in the latter case because the left termini of chromosomes IX and X are nearly identical over more than 15 kb, including the position of the distal breakpoint [249]. A single base polymorphism between

the two chromosomes at nucleotide position 8415 (chromosome IX) could be used in four strains to determine unambiguously that the rearrangement is a deletion, rather than a non-reciprocal translocation to chromosome X. Appropriate sequence reads were lacking in the remaining four strains to make a determination, but we consider it likely that these are also internal deletions on chromosome IX. Like the translocations, the deletions occur at regions of microhomology (Figure 3-6A). Using primers designed to amplify across the breakpoint of the common 39kb deletion, we found that 45% (30 of 67) of all centromere-proximal GCR events in the *rad51Δ* background are of this type, while the same deletion accounted for only one of 45 centromere-proximal events (~2%) in the wild-type strain. We conclude that much of the increase in centromere-proximal events upon loss of *RAD51* is driven by an increase in the likelihood of an internal deletion.

The inhibition of centromere-proximal events is unique to Rad51 as individual deletion of *RAD54*, *RAD55*, *RAD57* or *RAD59* results in little or no increase in the fraction of repair events occurring proximal to SiRTAs 9L-44 or 5L-35 (Figure 3-7). However, as described above, the increase in centromere-proximal events in the *rad51Δ* strain requires *RAD52*, consistent with a homology-driven repair process (Figure 3-4A). *RAD59* is required for some Rad51-independent homologous repair pathways [250–253]. Indeed, deletion of *RAD59* suppresses the increase in centromere-proximal events observed in the absence of *RAD51,* while deletion of *RAD54* has no effect (Figure 3-6B). Strikingly, the telomere addition defect at SiRTA 9L-44 is not suppressed in the *rad59Δ* strain (Figure 3-6B), further supporting our conclusion that events occurring in the centromere-proximal region are independent of SiRTA function. We also examined the role of *POL32*, which encodes a nonessential subunit of DNA polymerase δ [254], and is required

A

i. TEL-CTTGAAAAGCTGATGGGT-GTCAAGCACGCCCATCAGCGCATCTGAA — Chr. 5, 51941

GGACGACGACGTCGAGGTCGTCGAGCACGCCCGCGACGCAGTCAAAC-CEN — Chr. 9, 54181

ii. TEL-AGCGGCGAATCTTCAAGCAGCAGCAGCAGCAGCAGCAGCAGCAGCAGTGACA — Chr. 11, 613726

CGCGCTTACAACAGGAGCAGCAGCAGCAGCAGCAGCCGGATTCTCAGGACTC-CEN — Chr. 9, 49508

iii. TEL-TTCTCAACGATCTTTGCAGCAGCAGCAGCAGCAGCAGCAGCAACAAAAACAAC — Chr. 14, 70027

GCGCTTACAACAGGAGCAGCAGCAGCAGCAGCAGCCGGATTCTCAGGACT-CEN — Chr. 9, 49509

iv. TEL-ATGATGGTGCTGAGTTTACCGAGGCAAAATTCCCATATGATGAAGATAT — Chr. 9, 14297

TAGATTTGGACGACGTTCCCGAGGCAAAAT-CCCCCTTTTCAACAAGGG-CEN — Chr. 9, 53396

v. TEL-CTTTGGAGCAAAAAAAAATGGTGGTTGCTCTTGGTCGCGAAGTGA — Chr. 9, 26690

CAACAAGATGTATCTAAATGGTGGTTGCTCAGTTGTCCCAACAGG-CEN — Chr. 9, 50109

B

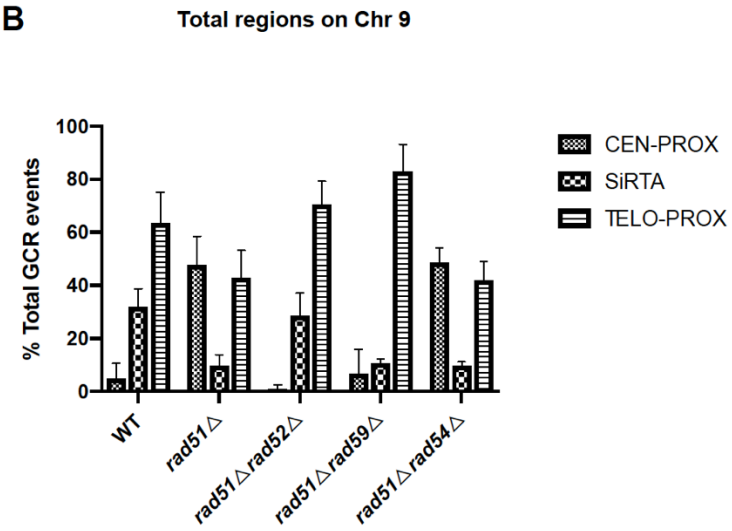

C

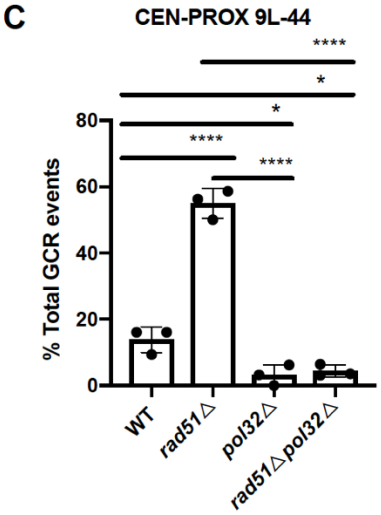

Figure 3-6: Microhomology-mediated repair requires Rad52, Pol32, and Rad59 and is inhibited by Rad51. (A) Unique breakpoint sequences identified by nanopore sequencing in twelve independent *rad51Δ* strains are shown. Event (iv) was recovered independently eight times, while the other rearrangements occurred once. Bases in gray are present on the original chromosome, while bases in black are those retained in the rearranged chromosome. The shaded regions indicate microhomologies utilized in mediating repair. The chromosome coordinate of each rearrangement is indicated. (B) The percent of total GCR events occurring in each region on chromosome IX (see legend) is shown in the indicated strains. Data for *rad51Δ rad52Δ* are repeated from Figs 3-1B, 3-4A and 3-5B for comparison. (C) The percent of total GCR events occurring centromere-proximal to SiRTA 9L-44 is shown for the indicated strains. Averages indicated by asterisks are statistically different by ANOVA with Tukey's multiple comparisons test (*p<0.05; ****p<0.0001). Contributing authors: EAE, KLF, NR.

for some repair events requiring extensive replication [183,216]. Even in a WT *RAD51* background, GCR events in the centromere-proximal region are reduced upon deletion of *POL32* (WT = 13.8% ± 3.9%; *pol32Δ* = 3.2% ± 3.1%; p<0.05) and this phenotype is epistatic to *rad51Δ* (Figure 3-6C). We conclude that nearly all of the centromere-proximal events, in both the presence and the absence of *RAD51*, require *POL32*.

3.2.4 The negative effect of Rad52 on *de novo* telomere addition requires interaction with Rad51

The incongruence between the effects of *RAD51* and *RAD52* deletion on *de novo* telomere addition at SiRTAs implies that the requirement for Rad51 is independent of nucleoprotein filament formation. To test this idea, we took advantage of the *rad51-K191A* allele, previously shown to prevent ssDNA binding and DNA strand exchange [255,256]. Remarkably, the reduced frequency of GCR formation at SiRTA 9L-44 in the *rad51Δ* strain is fully complemented when this allele is expressed in a *rad51Δ* strain from a low-copy number

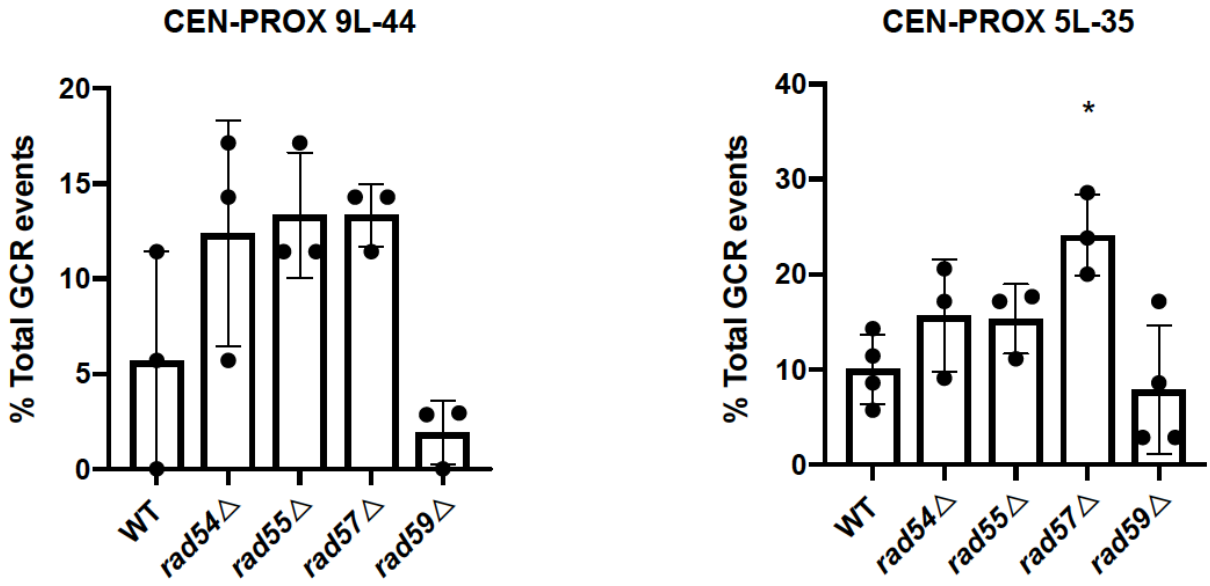

Figure 3-7: The inhibition of centromere-proximal events is specific to loss of Rad51. The percent of total GCR events occurring within the region centromere-proximal to SiRTAs 9L-44 and 5L-35 is shown. Averages and standard deviations are from at least three independent experiments. Statistical significance is calculated by ANOVA with Dunnett's multiple comparison test. Strain statistically different from WT is indicated by asterisks (*p<0.05). Contributing authors: EAE.

plasmid under the native promoter (*rad51Δ+RAD51*: 35.2% ± 3.3%; *rad51Δ+rad51-K191A*: 25.7% ± 5.0%; p=0.55) (Figure 3-8A).

We speculated that physical association between Rad51 and Rad52 might be required to prevent Rad52 from inhibiting *de novo* telomere addition at SiRTAs. We analyzed cells expressing two different Rad51 variants, Rad51-Y388H and Rad51-G393D, both of which were shown by yeast two-hybrid and biochemical experiments to be defective for interaction with Rad52 (but not with Rad54 or Rad55) [163,257]. The *rad51-Y338H* allele does not complement

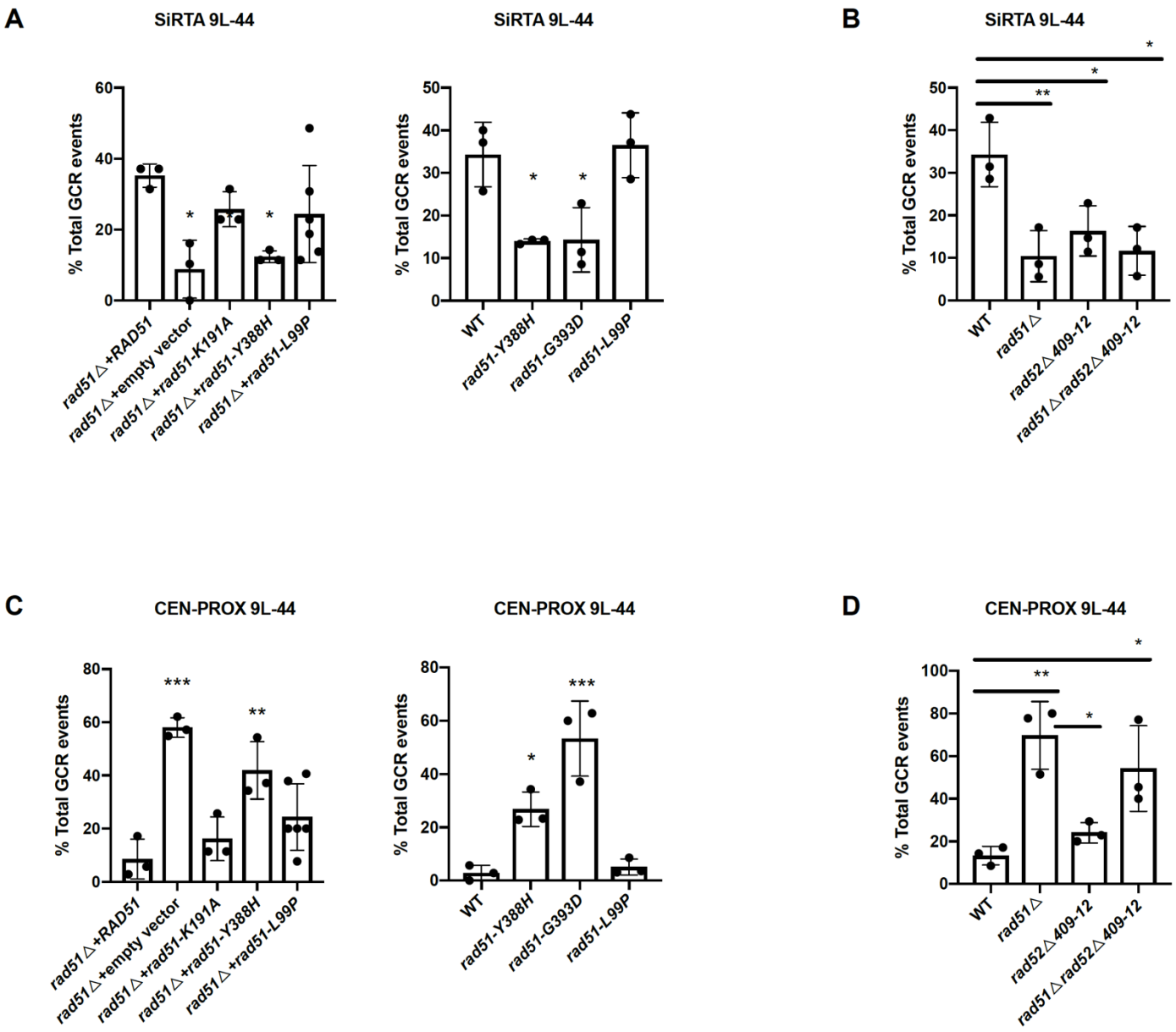

Figure 3-8: The Rad52-dependent effects of Rad51 on telomere addition and micro-homology mediated repair require the Rad51-Rad52 interaction. (A) The percent of total GCR events occurring within SiRTA 9L-44 is shown for *rad51Δ* strains containing plasmids expressing WT *RAD51*, an empty vector, or the indicated *rad51* mutant allele (left graph) or strains containing the indicated mutant allele integrated at the endogenous *RAD51* locus (right graph). Averages and standard deviations are from at least three independent experiments. Strains statistically different from the corresponding WT control strain by ANOVA with Dunnett's multiple comparisons test are indicated by asterisks (*p <0.05). (B) The percent of total GCR events occurring within SiRTA 9L-44 is shown for the indicated strains. Averages indicated with asterisks are significantly different by ANOVA with Tukey's multiple comparison test (*p<0.05,

p<0.01). (C) The percent of total GCR events occurring centromere-proximal to SiRTA 9L-44 is shown for the same experiments presented in panel A. Averages and standard deviations are from at least three independent experiments. Strains statistically different from the WT control by ANOVA with Dunnett's multiple comparison test are indicated by asterisks (p<0.01, ***p<0.001). (D) The percent of total GCR events occurring centromere-proximal to SiRTA 9L-44 is shown for the same experiments presented in panel B. Averages indicated with asterisks are significantly different by ANOVA with Tukey's multiple comparison test (*p<0.05, **p<0.01). Contributing authors: EAE, MM.

the *rad51* deletion strain when expressed on a low-copy number plasmid (Figure 3-8A) and both alleles result in a null phenotype when integrated at the endogenous *RAD51* locus (WT: 34.3% ± 7.6%; *rad51-Y388H*: 14.0% ± 0.6%; *rad51-G393D*: 14.3% ± 7.6%; p<0.05) (Figure 3-8A).

If interaction between the two proteins is critical, we would expect a mutation in Rad52 that disrupts interaction with Rad51 to have a similar effect. Deletion of Rad52 residues 409 to 412 disrupts DNA repair and the association of Rad51 with Rad52, eliminating Rad52 mediator activity, but does not affect DNA binding, ssDNA annealing, and protein oligomerization by Rad52 [258]. Integration of this allele at the *RAD52* locus reduces GCR formation at SiRTA 9L-44 (WT: 34.3% ± 7.6%; *rad52-Δ409-12*: 16.3% ± 5.9%; p<0.05) (Figure 3-8B). Combining this *rad52* allele with a deletion of *RAD51* does not further reduce GCR events at SiRTA 9L-44 (*rad51Δ:* 10.4% ± 6.0%; *rad51Δ rad52Δ409-12*: 11.66% ± 5.7%; p=0.66) (Figure 3-8B), consistent with the requirement that Rad51 interact with Rad52 to block its ability to inhibit *de novo* telomere addition. A single amino acid substitution of tyrosine 409 to alanine in Rad52 similarly reduces the frequency of GCR events at both SiRTA 9L-44 and SiRTA 5L-35 (Figure 3-9A). Finally, consistent with our conclusion that other members of the Rad52 epistasis group are not

required, the *rad51-L99P* allele that disrupts interaction with Rad54 and Rad55 [163] complements the *rad51Δ* defect at SiRTA 9L-44 (Figure 3-8A). Taken together, these results suggest that it is not formation of the nucleoprotein filament or strand exchange by Rad51 *per se* that are required for *de novo* telomere addition, but rather the ability of Rad51 to interact with Rad52.

Interestingly, we see a correlation between those alleles that reduce GCR formation at SiRTA and those that increase GCR formation in the centromere-proximal region. When measured either by complementation of the *rad51Δ* allele or by expression from the endogenous locus, the *rad51-Y388H* and *rad51-G393D* alleles increase centromere-proximal events, whereas no increase in GCR formation in the centromere-proximal region is observed in strains expressing *rad51-L99P* or *rad51-K191A* (Figure 3-8C). The *rad52-Y409A* allele also increases centromere-proximal events (Figure 3-9B), although the increase is not statistically significant in the *rad52Δ409-12* strain (Figure 3-8D). Since our previous results argue that effects at SiRTA and the centromere-proximal region can occur independently, we conclude that the interaction between Rad51 and Rad52 reduces the formation of microhomology-mediated rearrangements, although there is some context dependence to this effect since we do not observe a statistically significant increase in the corresponding region of chromosome V (Figure 3-4A).

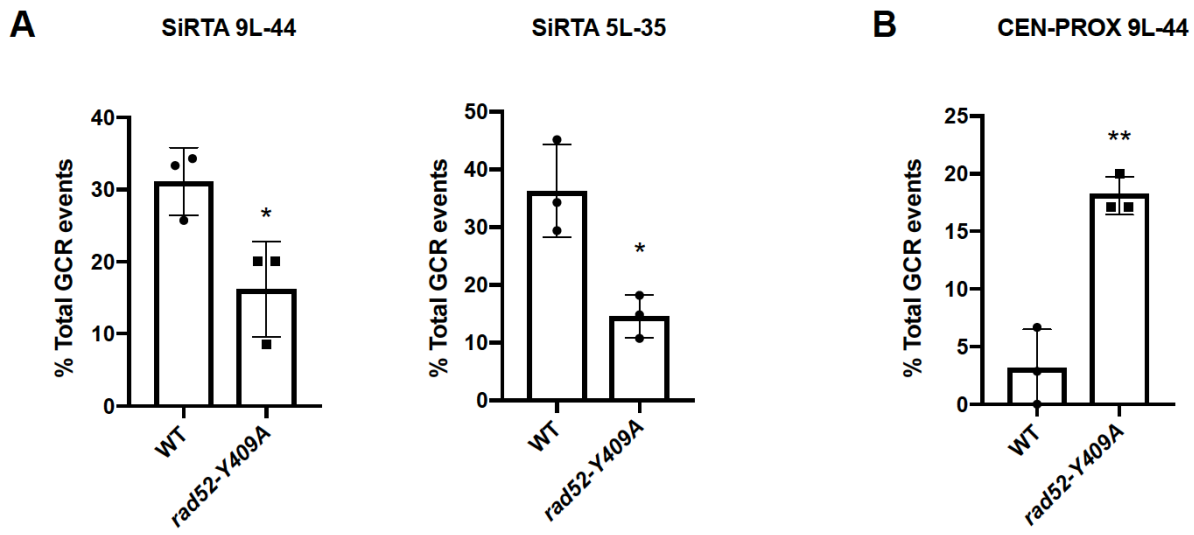

Figure 3-9: *De novo* telomere addition at SiRTAs is mediated by the Rad51-Rad52 interaction. (A) The percent of total GCR events occurring within SiRTA 9L-44 and 5L-35 is shown for the WT and *rad52-Y409A* strains. (B) The percent of total GCR events occurring centromere-proximal to SiRTA 9L-44 is shown for the same experiments presented in panel A. Averages and standard deviation are from at three independent experiments. Statistical significance is calculated by unpaired t-test (*p<0.05; **p<0.01). Contributing authors: EAE, MM.

3.2.5 Rad52 inhibits *de novo* telomere addition at SiRTA by reducing Cdc13 recruitment

Both chromatin immunoprecipitation (ChIP) and immunofluorescence studies show that the association of Cdc13 with DNA breaks (either HO- or chemically-induced) is stimulated by Rad51 [248,259]. We previously observed that high levels of *de novo* telomere addition at SiRTAs correlates with the ability of the SiRTA-stim sequence to bind Cdc13 and that the effect of the stim sequence is mimicked by artificial recruitment of Cdc13 [197]. These observations suggest that reduced *de novo* telomere addition in the absence of *RAD51* likely reflects reduced recruitment of Cdc13 to SiRTA sequences following an HO-induced DSB. To explore this possibility, we monitored recruitment of Cdc13 to the SiRTA 9L-44 locus by chromatin

immunoprecipitation (ChIP). We found that while Cdc13 was efficiently recruited in WT cells, recruitment was decreased 2-fold at the 4 hr ($p<0.05$) and 3-fold at the 8 hr ($p<0.001$) timepoints following HO induction in the absence of Rad51 (Figure 3-10A). Recruitment of Cdc13 was not significantly affected in the absence of Rad52 at the 4 hr timepoint ($p=0.17$) and was modestly reduced compared to WT cells at the 8 hr timepoint ($p<0.05$) (Figure 3-10A). If reduced recruitment of Cdc13 observed by ChIP in the *rad51Δ* strain is related to reduced *de novo* telomere addition at SiRTA, then artificial recruitment of Cdc13 to SiRTA should restore telomere addition in the absence of Rad51. To test this idea, we utilized a system previously described [197,205] in which the stim sequence at SiRTA 5L-35 is replaced with two copies of the Gal4 upstream activating sequence (SiRTA-stim::2XUAS). Cells containing this SiRTA-stim::2XUAS construct were transformed with a plasmid expressing either the GAL4 DNA binding domain only (GBD) or Cdc13 fused to GBD (GBD-Cdc13). As previously demonstrated, SiRTA-stim::2XUAS cells expressing GBD alone support very low levels of GCR formation within SiRTA 5L-35, consistent with the role of the stim sequence in facilitating *de novo* telomere addition at SiRTA (Figure 3-10B) [197]. Expression of the GBD-Cdc13 fusion construct increases the frequency of GCR formation 10-fold when compared to the GBD control (Figure 3-10B). When the same experiment is done in a *rad51Δ* background, two effects are observed. First, in the SiRTA-stim::2XUAS cells expressing GBD alone, deletion of *RAD51* does not further decrease the relative frequency of GCR events at the SiRTA. Second, expression of the GBD-Cdc13 fusion protein fully rescues GCR formation in the *rad51Δ* strain (Figure 3-10B). These results are consistent with a model in which Rad51 contributes (perhaps indirectly) to the binding of Cdc13 to SiRTA sequences following HO-induced DSB breaks.

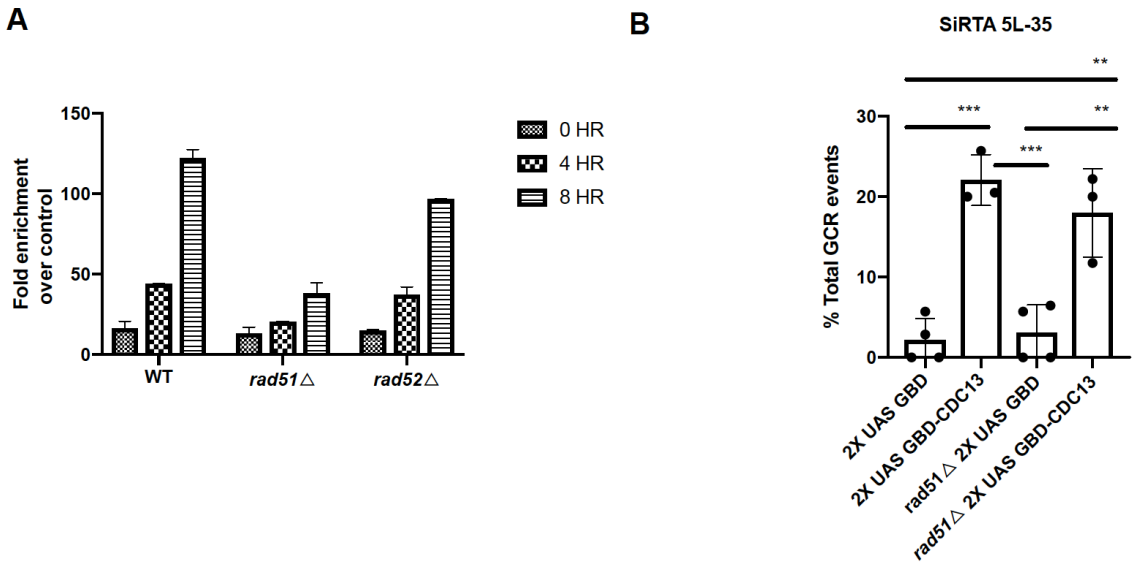

Fig 3-10: Rad51 promotes the recruitment of Cdc13 to SiRTAs. (A) ChIP analyses of Cdc13 binding at SiRTA 9L-44 in WT, *rad51Δ* and *rad52Δ* strains are shown for the indicated timepoints following induction of HO cleavage. SiRTA 9L-44 IP signals are normalized to signal at the control ARO1 locus at the 0 hr timepoint (see Methods). WT is significantly different from *rad51Δ* at the 4 hr timepoint ($p<0.01$) and 8 hr timepoint ($p<0.001$) and *rad52Δ* at the 8 hr timepoint ($p<0.05$) by ANOVA with Dunnett's multiple comparison test. Data shown are averages and standard deviation from two independent experiments. (B) The percent of total GCR events occurring at SiRTA 5L-35 is shown for WT or *rad51Δ* strains containing two copies of the Gal4-UAS sequence integrated in place of the SiRTA-Stim. Cells are transformed with vector expressing GBD only (GBD) or vector expressing full-length Cdc13 fused to the Gal4 DNA binding domain (GBD-Cdc13). Data are averages and standard deviations from at least three independent experiments. Averages indicated by asterisks are statistically different by ANOVA with Tukey's multiple comparisons test (**$p<0.01$; ***$p<0.001$). Contributing authors: EAE, MM.

3.2.6 Rad52-RPA interaction contributes to suppression of *de novo* telomere addition at SiRTAs

Because the interaction of Rad52 with RPA-bound single-stranded DNA persists in the absence of Rad51 [165], we speculated that the interaction between Rad52 and RPA might be important for the ability of Rad52 to inhibit *de novo* telomere addition. To address this possibility, we tested the effect of a mutation in *RFA1*, the gene encoding the largest subunit of the RPA complex. We specifically selected an allele (*rfa1-44*) that is defective in DSB repair and HO-induced gene conversion and is sensitive to both X-ray and UV irradiation, but does not appear to affect DNA replication since cell growth is relatively unaffected in the absence of DNA damage [260]. The effects of this allele are epistatic with *rad52Δ* and suppressed by overexpression of Rad52, consistent with the mutation disrupting interaction between Rad52 and Rfa1 [162]. Strains carrying the *rfa1-44* mutation at the endogenous *RFA1* locus show no defect in the frequency of *de novo* telomere addition at SiRTAs 9L-44 (WT: 31.4 $\pm$ 2.9; *rfa1-44*: 32.9% $\pm$ 14.1%; p=0.99) or 5L-35 (WT: 35.9% $\pm$ 4.0%; *rfa1-44*: 37.7% $\pm$ 16.8%; p=0.99) (Figure 3-11A). Remarkably, in the absence of *RAD51*, the *rfa1-44* mutation completely restores *de novo* telomere addition at both SiRTAs 9L-44 (*rad51Δ rfa1-44*: 31.4% $\pm$ 2.9%; *rad51Δ:* 6.7% $\pm$ 3.3% p<0.01) and 5L-35 (*rad51Δ rfa1-44*: 37.1% $\pm$ 7.6%; *rad51Δ:* 10.0% $\pm$ 2.4%; p<0.05) (Figure 3-11A) in a manner equivalent to the complete knockout of *RAD52* (compare with Figure 3-1B). Furthermore, the *rfa1-44* mutation completely suppresses GCR formation in the centromere-proximal region of SiRTA 9L-44 (*rad51Δ:* 71.4% $\pm$ 4.9%; *rad51Δrfa1-44*: 11;4% $\pm$ 7.6%; p<0.0001) (Figure 3-11B). These results show that the interaction between Rad52 and RPA must be retained for the inhibitory effect of Rad52 on *de novo* telomere addition.

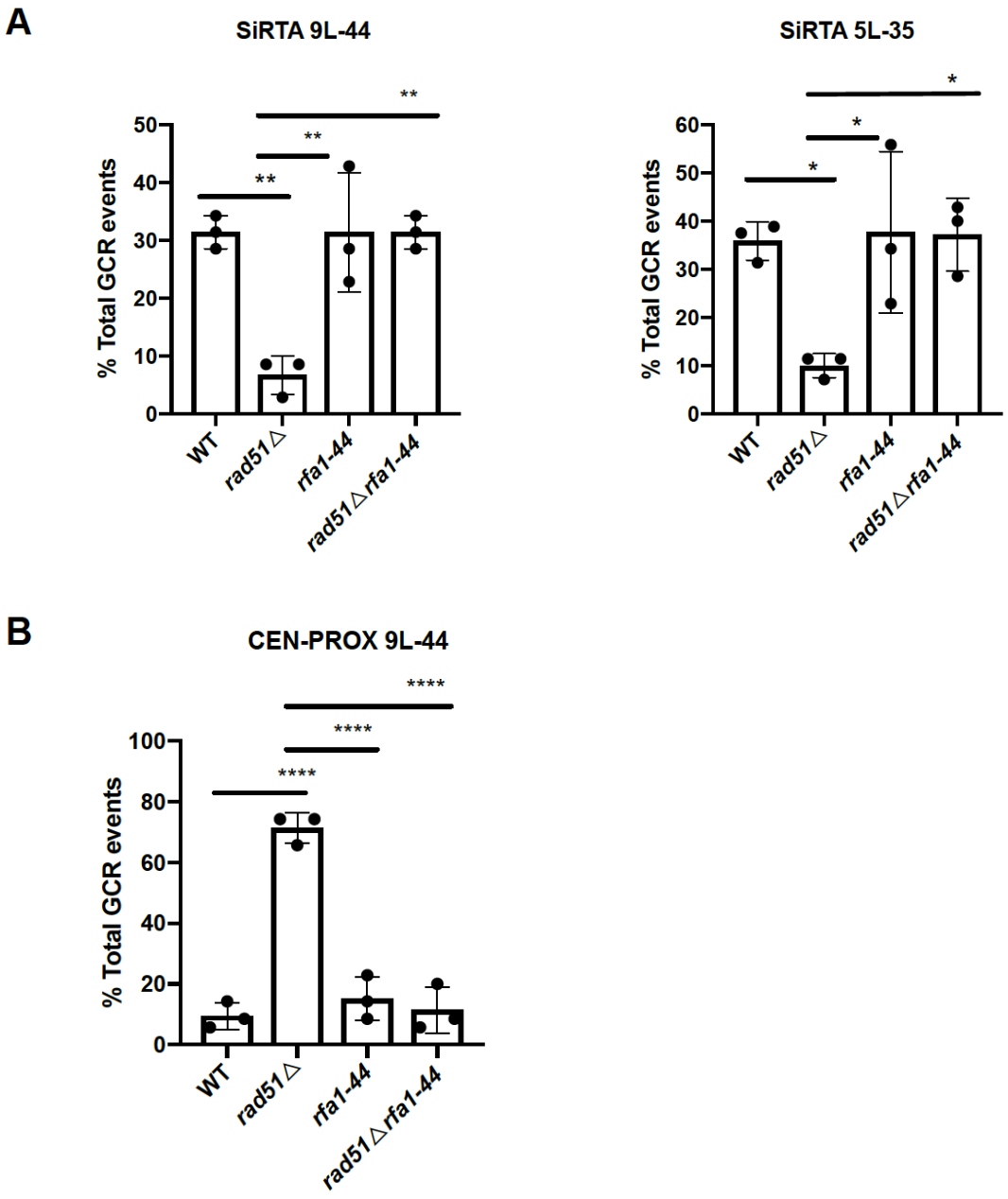

Figure 3-11. Disruption of the Rad52-Rfa1 interaction suppresses the *de novo* telomere addition defect of *rad51Δ.* (A) The percent of total GCR events occurring within SiRTA 9L-44 and 5L-35 is shown for the indicated strains. (B) The percent of total GCR events occurring centromere-proximal to SiRTA 9L-44 is shown for the same experiments presented in panel A. Averages and standard deviations are from three independent experiments. Averages indicated by asterisks are statistically different by ANOVA with Tukey's multiple comparisons test (*p <0.05; **p<0.01; ****p<0.0001). Contributing authors: EAE, MM.

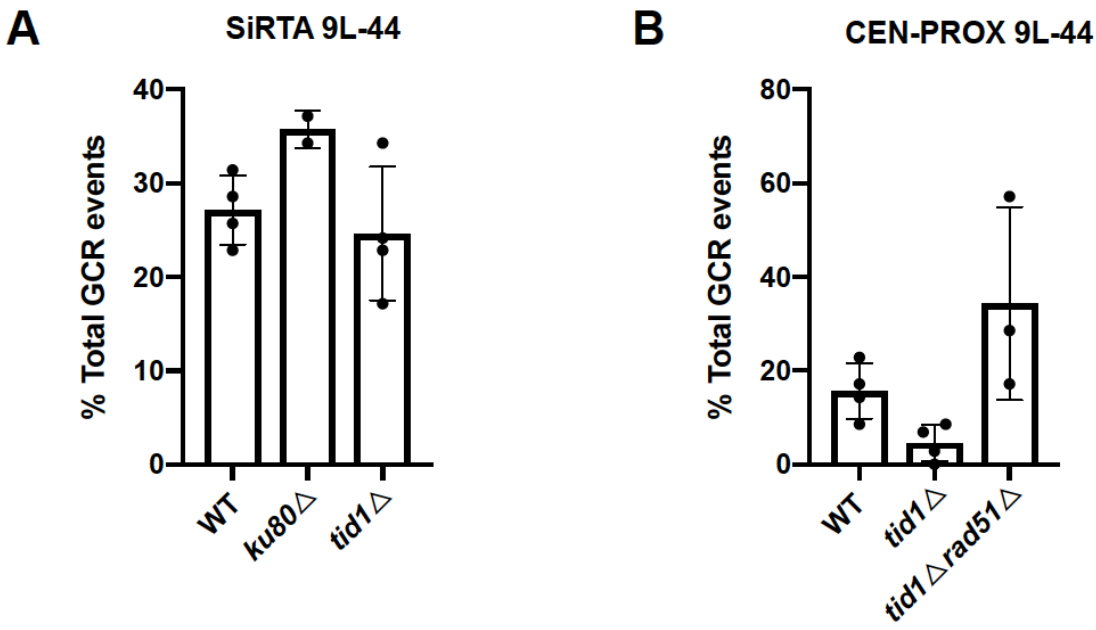

Figure 3-12: Adaptation-defective strains do not show reduced *de novo* telomere addition at SiRTA. (A) The percent of total GCR events occurring within SiRTA 9L-44 is shown for the indicated strains. (B) The percent of total GCR events occurring centromere-proximal to SiRTA 9L-44 is shown for the indicated strains. Averages and standard deviations are from at least two independent experiments. Statistical significance is calculated by ANOVA with Dunnett's multiple comparison test. No significance was observed. Contributing authors: EAE, MM.

3.3 Discussion

In work described in this chapter, we find that Rad51 stimulates *de novo* telomere addition at SiRTAs, endogenous TG-rich sequences previously shown to support unusually high levels of telomere addition. It was previously speculated that formation of the Rad51 nucleoprotein filament on resected 3' ends may facilitate recruitment of telomerase to DSBs [248], but our data are inconsistent with this model. Surprisingly, we find that Rad52 is not required for *de novo* telomere addition at SiRTAs. Indeed, nucleoprotein filament formation is dispensable for telomere addition since a variant of Rad51 that cannot bind single-stranded

DNA retains normal levels of *de novo* telomere addition (Figure 3-8). Furthermore, *de novo* telomere addition is restored by the simultaneous deletion of *RAD51* and *RAD52* (Figure 3-1B). This epistatic relationship suggests that Rad52 suppresses *de novo* telomere addition at SiRTAs in a manner that is normally counteracted by Rad51. Our results further show that the interaction between Rad51 and Rad52 is required for this regulatory function. Variants of Rad51 that retain DNA binding but are defective for interaction with Rad52 fail to sustain *de novo* telomere addition, as does a mutant version of Rad52 that cannot interact with Rad51 (Figure 3-8). The effect is specific to Rad51 and Rad52, since mutation of *RAD59*, a gene that shares homology with the N-terminal domain of *RAD52* but lacks the C-terminal Rad51-interacting domain, neither affects *de novo* telomere addition nor suppresses the effect of deleting *RAD51* (Figure 3-6B). Likewise, mutations in other Rad52-epistasis group genes (*RAD54* and *RAD57*) do not consistently reduce telomere addition at SiRTAs (Figure 3-2).

The Chartrand group has reported that that the intranuclear trafficking of the telomerase (TLC1) RNA is modulated in G2/M phase in response to DNA damage [259]. While TLC1 RNA is predominantly nucleolar in G2/M, nucleoplasmic localization increases moderately in response to DNA damage [259]. Rad52 enforces nucleolar localization, which may sequester telomerase from double-strand breaks. In contrast to cells lacking Rad52 function, which display increased nucleoplasmic localization of TLC1 after DNA damage, cells lacking *RAD51* show little relocalization of TLC1 RNA to the nucleoplasm [259] and association of Cdc13 with DNA damage-induced foci is reduced [248,259]. However, in contrast to our observations, the TLC1 RNA localization phenotype of the *rad51Δ* strain is epistatic to that observed upon loss of *RAD52* [259], indicating that the effects we see on *de novo* telomere addition at SiRTAs in the

absence of *RAD51* and/or *RAD52* cannot be explained by changes in the intranuclear localization of telomerase.

The genetic results presented in this chapter suggest that Rad52 interferes in some manner with the ability of Cdc13 to associate with a persistent DSB, but that this effect is alleviated through Rad52-Rad51 interaction. Haber and colleagues reported the same genetic interaction between *RAD52* and *RAD51* in the context of checkpoint adaptation [256]. Yeast cells subjected to a persistent DSB arrest in G2/M, but eventually release from the checkpoint and proceed into the following cell cycle, even in the absence of repair [256]. Cells lacking *RAD51* have a moderate adaptation defect that is fully suppressed by deletion of *RAD52* and, as we observe for *de novo* telomere addition, suppression requires the Rad52-Rad51 interaction and is independent of Rad51-nucleoprotein filament formation [256]. Despite the similarities in the genetic interactions, the effects that we observe on *de novo* telomere addition cannot be explained as an indirect consequence of the failure of *RAD51* deficient strains to undergo checkpoint adaptation. Strains lacking either the Ku complex or Tid1 are also adaptation-defective through mechanisms distinct from that occurring in the absence of Rad51 [261,262], but we observe no significant reduction in telomere addition at SiRTA 9L-44 in either *yku80Δ* or *tid1Δ* strains (Figure 3-12). Nevertheless, given the strong parallels in the genetic observations between these two phenomena, it is possible that the underlying mechanisms giving rise to both the *de novo* telomere addition defect and adaptation defect in the absence of *RAD51* are similar.

Our data suggest that telomere addition is reduced at SiRTAs in the absence of Rad51 function as a consequence of reduced Cdc13 association with the double-strand break. We find

by ChIP that the association of Cdc13 with sequences near the SiRTA on chromosome IX increases after induction of a double-strand break in WT cells and that binding, while reduced upon deletion of *RAD51*, is largely unaffected in the absence of *RAD52* (Fig 3-10A). Importantly, recruitment of the Cdc13-GBD fusion protein completely suppresses the telomere addition defect of the *rad51Δ* strain (Fig 3-10B), supporting the conclusion that defects in Cdc13 association underlie the reduction in *de novo* telomere addition observed in the absence of Rad51.

How does Rad52 interfere with telomere addition in the absence of Rad51? Based on several *in vitro* observations, we propose the following explanation for our results. Single-molecule experiments reported by the Green and Sung laboratories show that the association of Rad52 with RPA-coated single-stranded DNA alters the binding properties of RPA [263]. When bound to ssDNA, the RPA complex undergoes transient "micro-dissociation" events that facilitate exchange with other single-stranded DNA binding proteins [264,265]. Remarkably, addition of Rad52 stabilizes the association of RPA with the DNA, rendering RPA resistant to displacement by other proteins in a manner that appears to require direct protein-protein contact between RPA and Rad52 [263]. As expected, addition of Rad51 triggers the Rad52-mediated replacement of RPA with Rad51, although some RPA and Rad52 remain associated with the Rad51 nucleoprotein filaments [263]. Perhaps, when Rad52 interacts with RPA in the absence of Rad51, Cdc13 cannot easily displace RPA. Recruitment of Cdc13 to the SiRTA through binding to the Gal4 UAS (which must happen while the DNA remains double-stranded) would be expected to overcome this deficit, as we observe. We also find that the Rfa1-44 variant of RPA prevents Rad52 from inhibiting *de novo* telomere addition in the absence of

RAD51, consistent with data showing that this mutation reduces the interaction between Rfa1 and Rad52 [162,260].

The single-molecule experiments do not directly address the requirement for the Rad51-Rad52 interaction, nor whether Rad51 protein that lacks the ability to bind DNA can still alter the interaction between Rad52 and RPA. In this regard, Sugiyama and Kantake report that RPA-coated ssDNA is aggregated by the addition of Rad52 in a manner that requires the interaction between Rad52 and Rfa1 [266]. Although it is not entirely clear what these interactions represent, Rad51 leads to the dissolution of the aggregate, even when Rad51 is pre-bound to dsDNA and does not replace RPA on the ssDNA. These results may provide an explanation for the ability of a Rad51 variant that itself cannot bind ssDNA to disrupt the inhibitory effect of Rad52 on *de novo* telomere addition, perhaps by altering the interaction of Rad52 with RPA and/or the ability of Rad52 to self-associate.

Although we were initially interested in understanding the influence of HR-associated proteins on *de novo* telomere addition, we observed a striking increase in the fraction of repair events occurring internal to the SiRTA on chromosome IX upon deletion of *RAD51*, suggesting that these events are normally inhibited by Rad51 function (Figure 3-4A). This change does not result directly from reduced repair at the SiRTA because complete deletion of the SiRTA sequence is not associated with increased repair in the centromere-proximal region (Figure 3-4B). Furthermore, the effects at the SiRTA and the internal region are genetically separable--deletion of *RAD59* in the *rad51Δ* background suppresses the events in the centromere-proximal region, but does not restore telomere addition at the SiRTA (Figure 3-6B).

To gain insight into the nature of these events, we used nanopore technology to sequence the entire genomes of twelve independent survivors of HO cleavage (in a *rad51Δ* background). Three of the events were non-reciprocal translocations that in each case were mediated by small (<25 bp) regions of microhomology (Figure 3-6A). Since the intact chromosome was detected in each case and all events occurred within 75 kb of a telomere, these events likely arose through BIR, a repair event in which single-stranded DNA produced on the proximal side of a DSB invades a homologous duplex with subsequent extension of the 3' end in a conservative manner using the invaded strand as template [173]. Consistent with this idea, we find that the increase in centromere-proximal events in the *rad51Δ* background depends strongly on *RAD52*, *RAD59*, and *POL32* (Figures 3-4A and 3-6B,C) and is partially reduced upon deletion of *TID1* (Figure 3-12B), all genes shown previously to contribute to BIR [216,253].

The most common event observed was an internal deletion, with eight of twelve strains showing the identical event, again between a short (19 bp) region of imperfect micro-homology. Having identified this deletion, we analyzed a large number of centromere-proximal events accumulated from the experiments described here and found that the frequency of this particular deletion increases dramatically in the absence of *RAD51*. While it is formally possible that the large internal deletions on chromosome IX are mediated by BIR (with an intrachromosomal invasion event), we favor the idea that these events occur through a variation of microhomology-mediated recombination (MHMR) characterized in detail by Villarreal *et al.* on model substrates [183]. Such events resemble SSA, but are distinguished by the use of very short (15-18 bp) regions of microhomology and strong dependence on *POL32*.

Congruent with our observations, *RAD52* and *RAD59* were shown to stimulate MHMR when microhomologies are 15-18 bp in length, while *RAD51* represses these events [267]. Remarkably, the 39 kb deletion is the result of repair between two micro-homologous sequences that are located 12 kb proximal and 27 kb distal to the site of HO cleavage, demonstrating that such events can occur even after extensive 5' end resection. Our observation that interaction between Rad51 and Rad52 is required to fully repress these SSA-like events is consistent with *in vitro* experiments demonstrating that interaction with Rad51 suppresses the DNA-annealing activity of Rad52 [268].

It is intriguing that we do not see a significant increase in centromere-proximal events on chromosome V. This difference may reflect the relative sizes of the two regions (the distance between the SiRTA and the first essential gene is nearly two times greater on chromosome IX) or the fortuitous existence of microhomologies. We note, however, that all of the events observed on chromosome IX have proximal breakpoints within 4 kb of each other, even though the centromere-proximal region is nearly 17 kb. This observation is reminiscent of a report from the Haber lab of an enhancer on chromosome III that greatly stimulates SSA within a neighboring region [269]. On chromosome III, the enhancing sequence was mapped to a 200 bp region adjacent to, but not including, an origin of replication [269]. There is no origin reported in the region immediately proximal to the breakpoint junctions and no obvious sequence homology with the enhancer on chromosome III. Future studies are required to determine if such enhancing activity is present on chromosome IX.

3.4 Materials and Methods

3.4.1 Yeast strains and plasmids

All strains used in this study are listed in S1 Table and are derivatives of YKF1308 and YKF1310 [197,217]. Unless otherwise indicated, strains were grown in yeast extract/peptone/dextrose medium (YEPD) at 30°C. All gene deletions were derived by one-step gene replacement using a selectable marker and verified by PCR.

Mutations in the *RAD51* gene were introduced by replacing a portion of *RAD51* with *URA3* in strain YKF1508 by one-step gene replacement to create strain YKF1508+URA3. Sequences containing desired mutations were generated by a two-step PCR reaction and PCR products were transformed into YKF1508+URA3. Cells were allowed to recover on rich media overnight and then replica-plated onto medium containing 5-FOA. Candidates were confirmed by sequencing.

Plasmids pRS413 [270] expressing *rad51-Y388H* or *rad51-L99P* and pR51.4 expressing *rad51-K191A* were generously provided by Dr. James Haber [256]. The 3.7 kb *Bam*HI fragment containing the promoter and open reading frame of each mutant allele contained on plasmid pRS413 was cloned into the *Bam*HI site of the *TRP1*-containing centromeric plasmid pRS315 [270]; the 3.2 kb *Hin*dIII fragment containing the promoter and open reading frame on pR51.4 was cloned into the *Hin*dIII site of pRS315 [270]. Plasmid pRS315-*RAD51* was also a gift from Dr. James Haber.

RAD52 and *RFA1* alleles were constructed utilizing the CRISPR-Cas9 cleavage system. gRNAs were designed and cloned into a *Bpi*I-digested plasmid bRA90 constitutively expressing

Cas9 [271] (a gift from Dr. James Haber). Plasmids were verified by PCR and cotransformed into yeast strains with PCR-derived linear DNAs containing the desired mutations. Candidates surviving selection for the bRA90 plasmid were verified by sequencing and screened for loss of bRA90 prior to use.

3.4.2 HO inducible cleavage assay

Yeast cells were grown overnight in synthetic complete media lacking uracil (SC-Ura) containing 2% raffinose to OD_{600} of ~0.6 to 0.8. 10 μl-30 μl aliquots of culture were plated on yeast extract/peptone medium containing 2% galactose (YEPG) and a dilution was plated on rich medium containing 2% glucose (YEPD) to determine total viable cell count. Unless otherwise noted, plates were incubated at 30°C for 3 days. Surviving colonies were counted and at least 100 galactose-resistant (Gal^R) colonies were patched to plates containing 5-FOA to isolate GCR events (Gal^R 5-FOA^R colonies). Additional Gal^R5-FOA^R colonies were obtained by replica plating where necessary. For each experiment, at least 30 Gal^R 5-FOA^R colonies were analyzed to determine the approximate location and/or type of GCR event; averages and standard deviations were derived from a minimum of three independent experiments. The location and nature of GCR events were determined by PCR and Southern blotting as previously described [197]. The relative frequency of GCR formation in a particular region is determined by dividing the number of events observed in that region by the total number of Gal^R 5-FOA^R events. The absolute frequency at which GCR formation occurs in a particular region is derived by multiplying the frequency at which Gal^R colonies are produced (surviving colonies on galactose plates/surviving colonies on glucose plates, adjusted for dilution) by the fraction of

Gal^R colonies that survive on media containing 5-FOA (Gal^R 5-FOA^R) and by the fraction of Gal^R 5-FOA^R colonies that map to that particular region (the relative frequency of GCR formation) [197].

3.4.3 Southern blotting

Total genomic DNA was extracted by glass beads lysis [272]. Extracted DNA was digested overnight with *Nsi*I (NEB) to analyze events occurring at SiRTA 9L-44 or *Xho*I (NEB) to analyze endogenous telomeres and digested fragments were separated on a 0.7% agarose gel and subsequently denatured. Denatured fragments were transferred to nylon membrane (Hybond N+) overnight and prehybridized for several hours. Pre-hybridized membranes were probed overnight with [^{32}P]dCTP-labelled, random-primed DNA derived from PCR amplification of the SiRTA 9L-44 locus or telomeric DNA to detect SiRTA 9L-44 or endogenous telomeres respectively. Membranes were washed and exposed to Phosphor screens (Molecular Dynamics) and screens were scanned with Typhoon TRIO variable mode imager (GE Healthcare). Telomere addition events were identified by the characteristic smear generated by the heterogenous telomere length at the correct size. Primers used to generate probes for Southern blot analysis of GCRs are listed in S2 Table.

3.4.4 Identification of chromosome breakpoints

Genomic DNA was isolated using the MasterpureTM Yeast DNA purification kit (Lucigen) and sequenced using MinION technology from Oxford Nanopore at VANTAGE (Vanderbilt Technologies for Advanced Genomics). Libraries from twelve samples were generated for

MinION sequencing using the Rapid Barcoding Kit (RBK-004) per manufacturer's instructions (Oxford Nanopore). Sequencing was performed on a total of 3 flow cells (type R9.4.1). Sequences were demultiplexed using porechop v0.2.4 (https://github.com/rrwick/Porechop) with default settings.

Sequence reads were analyzed with tools available at UseGalaxy.org. Briefly, each dataset was converted to a BLAST database using NCBI BLAST+ makeblastdb (refs), which allowed a list of reads matching chromosome 9 sequences centromere-proximal to the SiRTA to be generated. Iterative BLAST searches with the tool in the Saccharomyces Genome Database (SGD; https://www.yeastgenome.org) were used to pinpoint the site of the rearrangement and/or to identify sequence reads containing intact chromosomes. Breakpoints were verified by PCR. Primer sequences and additional information about each of the 12 clones can be found in supplementary data (S1 Data). All sequence reads obtained have been submitted to the NCBI Sequence Read Archive (SRA) under BioProject accession number PRJNA557764.

3.4.5 Chromatin immunoprecipitation

Yeast cells were grown in yeast extract/peptone with 2% raffinose to OD_{600} of 0.5 to 0.6. DSB induction was achieved by adding galactose to a final concentration of 2%. At the indicated timepoints, 50 ml of cells were removed and fixed in formaldehyde to final concentration of 1% at room temperature for 30 min. At later timepoints, cells were diluted with media to maintain the initial OD_{600} reading. Quenching was done by adding glycine to a final concentration of 125 mM for 5 min at room temperature. Cells were washed twice with ice-cold HBS (50 mM HEPES at pH 7.6, 140 mM NaCl), frozen in dry ice and stored at -80°C. Cell pellets were resuspended in

400 μl ChIP lysis buffer high salt (Santa Cruz Biotechnologies; sc-45001) containing protease inhibitor cocktail (Roche; 1 tablet/5 ml ChIP lysis buffer) and lysed with an equal volume of glass beads at 4°C by vortexing at maximum speed for 40 min. Cell lysates were sonicated on the Covaris LE220 series with settings 450 peak power, 30% Duty factor, 200 cycles per burst for 15 mins in AFA crimp-cap 130 μl tubes to yield an average fragment size of 0.1 to 0.5 kb. Sonicated lysates were clarified by centrifugation twice (13, 000 rpm for 5 min, then 13,000 rpm for 15 min), supernatant was transferred to a new tube after each centrifugation. A portion of the pre-IP extract was set aside as input sample. The remaining extracts were incubated with 6 μg of anti-myc antibody (Roche; 11667149001) at 4°C overnight. Protein-G magnetic beads (Life Technologies) were added to each sample and incubation continued for 4-6 hours. Beads were washed 2 times with ChIP lysis buffer (Santa Cruz Biotechnologies; sc-45000), 3 times with ChIP lysis buffer high salt (Santa Cruz Biotechnologies; sc-45001) and ChIP wash buffer (Santa Cruz Biotechnolgies; sc-45002) at 4°C for 5 min each. Immunoprecipitated chromatin was eluted off the beads in ChIP elution buffer (50 mM Tris-Hcl pH 7.5, 10 mM EDTA, 1% SDS, 200 mM NaCl) at 65°C for 30 min. Reversal of crosslinks was carried out at 65°C for 14 hr. All samples (pre-IP and IP eluates) were treated with RNAse for 1 hr at 37°C and proteinase K for 2hrs at 55°C. DNA was purified by phenol:chloroform:isoamy alcohol (24:25:1) extraction, followed by ethanol precipitation. Purified DNA was resuspended in buffer EB (Qiagen) and used in qPCR reactions containing 1X SsoAdvanced universal SYBR green supermix (Bio-Rad) and 500 nM of each primer. DNA in each sample was quantified by comparison to a standard curve generated from a dilution of sonicated yeast genomic DNA. qPCR reactions were carried out in a C1000 Thermal Cycler with CFX96 Real-time System (Bio-Rad) and data were analyzed using CFX Manger

software (Bio-Rad). Primer sequences are provided in supplementary information (S2 Table). The amount of IP DNA at the SiRTA 9L-44 locus is divided by the respective time point input DNA from an independent ARO1 locus to correct for the progressive loss of input DNA at the SiRTA locus. The IP SiRTA 9L-44/ARO1 input ratio at each time point is then normalized to the IP ARO1/Input ARO1 signal before HO induction [171,273].

TABLE 3-1. List of strains used in Chapter 3

Strain	Genotype	Source (ref)
YKF1308	JRL017: *MAT**α**::ΔHOcs::hisG hmlaΔ::hisG HMRa-stk ura3Δ851 trp1Δ63 leu2Δ::KAN^R ade3::GAL10::HO can1,1-1446::HOcs::HPH^R*	[29]
YKF1310	CL11-7: *MAT**α**::ΔHOcs::hisG hmlaΔ::hisG HMRa-stk ura3Δ851 trp1Δ63 leu2Δ::KAN^R ade3::GAL10::HO*	[29]
YKF1333	YKF1310 *hmra-stkΔ::NAT^R*	[20]
YKF1323	YKF1308 *hmra-stkΔ::NAT^R*	[20]
YKF1342	YKF1323 *hxt13*::*URA3*	[20]
YKF1508	YKF1310 *hmra-stkΔ::NAT^R*	[20]
YKF1752	YKF1333 SiRTA 9L-44 *soa1*::*URA3*	[20]
YKF1784	YKF1752 *rad51::TRP*	This study
YKF1885	YKF1752 *rad51::LEU2*	This study
YKF1785	YKF1752 *rad52::LEU2*	This study
YKF1791	YKF1784 *rad51::TRP rad52::LEU2*	This study
YKF1718	YKF1342 *rad51::TRP*	This study
YKF1783	YKF1342 *rad52::LEU2*	This study
YKF1835	YKF1718 *rad52::LEU2*	This study
YKF1811	YKF1752 *rad54::TRP*	This study
YKF1841	YKF1752 *rad55::TRP*	This study
YKF1842	YKF1752 *rad57::TRP*	This study

YKF1843	YKF1752 *rad59::TRP*	This study
YKF1867	YKF1885 *rad59::TRP*	This study
YKF1815	YKF1811 *rad51::LEU2*	This study
YKF1821	YKF1342 *rad54::TRP*	This study
YKF1822	YKF1342 *rad55::TRP*	This study
YKF1824	YKF1342 *rad57::TRP*	This study
YKF1826	YKF1342 *rad59::TRP*	This study
YKF1921	YKF1752 SiRTA 9L-44Δ	This study
YKF1923	YKF SiRTA 9L-44Δ *rad51::LEU2*	This study
YKF 1986	YKF1752 *rad51-Y388H*	This study
YKF1954	YKF1752 *rad51-G393D*	This study
YKF1987	YKF1752 *rad51-L99P*	This study
YKF2055	YKF1752 *rad52-Y409A*	This study
YKF2056	YKF1342 *rad52-Y409A*	This study
YKF1989	YKF1752 Cdc13 13 MYC TRP	This study
YKF1990	YKF1885 Cdc13 13 MYC TRP	This study
YKF2048	YKF1882 Cdc13 13 MYC TRP	This study
YKF 2057	YKF1752 *rfa1-44*	This study
YKF2058	YKF1784 *rfa1-44*	This study
YKF2059	YFK1342 *rfa1-44*	This study
YKF2060	YKF1718 *rfa1-44*	This study

YKF2061	YKF1752 *rad52⊿409-12*	This study
YKF2062	YKF1784 *rad52⊿409-12*	This study
YKF2038	YKF1752 *pol32::TRP*	This study
YKF2040	YKF1885 *pol32::TRP*	This study

CHAPTER 4

CONCLUSIONS AND FUTURE DIRECTIONS

4.1 SiRTAs: Endogenous sites of *de novo* telomere addition

Telomeres are the nucleoprotein structures at the ends of many linear eukaryotic chromosomes that distinguish normal chromosome ends from DNA DSBs and thus protect these ends from nucleolytic degradation and chromosome fusions. Also, telomeres facilitate the complete replication of the ends of the chromosome by providing a buffer to counter the loss of sequences due to the end replication problem (Figure 1-1B). The telomere-specific reverse transcriptase, telomerase, counteracts this sequence loss by synthesizing telomeric sequences, utilizing an internal RNA template (reviewed in [52]).

Telomerase activity is not restricted to the ends of the chromosomes. Infrequently, telomerase can also target chromosome-internal telomere-like sequences for extension in a process referred to as *de novo* telomere addition (reviewed in [191]). *De novo* telomere addition events are a part of a broader class of genome rearrangements called GCRs (gross chromosomal rearrangements) that involve large-scale interstitial deletions, inversions and translocations. *De novo* telomere addition results in terminal deletions that have been associated with human diseases (reviewed in [187]). Given these consequences, it is important to understand how these telomere addition events are regulated. In *Saccharomyces cerevisiae*, the majority of studies on telomere addition have been conducted using artificial telomere seed sequences placed immediately adjacent to an inducible cleavage site [105,274]. However, these

artificial systems do not fully recapitulate *in vivo* conditions, as DSBs may occur at a distance from sites of endogenous telomere addition.

In work presented in Chapter 2, we extensively characterized a previously identified hotspot of *de novo* telomere addition on the left arm of chromosome V *in S. cerevisiae*. We also identified and characterized a second hotspot of *de novo* telomere addition on the left arm of chromosome IX. We refer to these hotspots as SiRTAs (Sites of repair-associated telomere addition). SiRTA sequences are telomere-like (Figure 4-1), containing TG-rich repeats and are therefore predicted to facilitate base pairing with the template region of the telomerase RNA. Telomere addition at SiRTA sites can occur following resection from a HO-induced double-strand break (DSB) located at least ~ 3kb distal to these sequences.

Given the small size of the SiRTA sequences on chromosomes V and IX (<100bp), telomere addition is disproportionately likely to occur within these sequences. For example, in WT cells, ~30% of all GCR events occurring in the ~20 kb non-essential region of chromosome IX, (extending from the end of the essential gene *MCM10* to the HO cut site; Figure 2-8A), map to the SiRTA (Figures 2-8D; 3-1B), and over 90% of these GCR events at SiRTA 9L-44 are *de novo* telomere additions. Given that the SiRTA encompasses less than 0.5% of the total DNA in this region, this represents at least a 60-fold increased probability of a GCR event occurring at the SiRTA. 60-70% of the remaining GCRs occur telomere-proximal to the SiRTA (between the SiRTA and the HO site) site while 0-10% occur in the centromere-proximal region of the SiRTA (between the essential gene and the SiRTA) (Figure 2-8D). Further analysis indicates that in wild-type cells, over half of the telomere-proximal GCRs involve *de novo* telomere additions occurring most likely at scattered TG dinucleotides in this region. These results suggest that in

the absence of accurate repair of DSBs, while several non-conservative repair pathways may compete for these DSBs, *de novo* telomere addition is a very likely, maybe even preferred, pathway of repair (see below). In fact, previous works by the Kolodner lab showed that broken chromosomes healed by *de novo* telomere additions dominate over other GCR-promoting pathways [189,190].

However, the absolute frequency of such events is low. In the absence of exogenous damage, GCR events are isolated in 1 of 10^9 wild-type cells in the Kolodner assay. In the HO cleavage assay, ~0.1-0.2% of cells survive growth on galactose-containing medium (Gal^R). We presume that the remaining cells attempt homologous recombination (HR) with the sister chromatid or correct repair by non-homologous end joining (NHEJ), both of which recreate the HO cleavage and result in additional round of cleavage and repair. Since extensive resection from the break is observed in these types of assays, it is likely that many cells die through loss of essential genes in the absence of repair. 20-30% of these Gal^R cells have undergone a GCR event, resulting in terminal deletions and have thereby acquired resistance to the drug 5-fluoorotic acid (Gal^R 5-FOA^R). 25-35% of Gal^R 5-FOA^R cells have added a telomere at SiRTA sequences (Chapters 2 and 3).

The two SiRTAs characterized in Chapter 2 behave in remarkably similar manner. Both SiRTAs contain an upstream stimulatory sequence called the 'SiRTA-Stim' that is TG-rich, but is rarely the actual site of telomere addition events. Rather these SiRTA-Stim sequences facilitate telomere addition events that occur at a downstream TG-rich sequence called the 'Core'. The SiRTA-Stim and Core sequences are both required for normal levels of telomere addition at the SiRTA such that mutation of either sequence drastically reduces *de novo* telomere additions

(Figures 2-3C, mutation c and 2-8F, G). Furthermore, in strains carrying SiRTA-Stim mutations, a subset of the GCRs that map to these SiRTA regions are in fact not *de novo* telomere addition events when further characterized by Southern blot analysis (Figures 2-8G; 2-9). One possibility is that these events initiate as telomere addition, but are then routed to other pathways when telomere addition cannot be completed.

4.2 SiRTAs as informative models of *de novo* telomere formation

Given that *de novo* telomere addition is a rare event, the relatively high frequency of *de novo* telomere addition at SiRTAs and the apparent mechanistic conservation of these sequences suggest that SiRTAs provide a very useful system for the detailed study of *de novo* telomere formation in a natural context. Most previous assays have utilized a galactose-inducible HO endonuclease cleavage site integrated immediately adjacent an 81 bp artificial telomere seed sequence at an ectopic site on chromosome VII (Figure 1-8B) [105]. Chromosome healing by *de novo* telomere addition is very efficient in this system and *de novo* telomeres can be visualized within hours of HO induction by Southern blot analysis. Approximately 90% of cells that incur a DSB have added a telomere within 4 hours of DSB induction [105]. This system has been used to gain a mechanistic understanding into telomerase function and activity and has proven useful again and again [105,202,205,213,215,274,275].

There are, however, limitations to this approach for the study of telomerase activity at DSBs as a mechanism of DSB repair. First, this system utilizes artificial telomere seed sequences that are not represented in the yeast genome (outside of the telomere) and are unlikely to

accurately reflect telomerase activity at endogenous TG sequences. Secondly, this system places the HO recognition site immediately adjacent these artificial TG tracts such that upon HO induction, these TG tracts may mimic shortened telomeres in need of immediate extension. Extensive resection does not occur at these ends and telomerase activity outcompetes other repair pathways [105]. In the orientation commonly utilized in this assay, the HO endonuclease generates a TGTT 3' overhang. In one study, the majority of telomere addition events occurred at the this 4 bp overhang even though the telomere seed is separated from the cleavage site by 8 or more base pairs due to sequences required to allow recognition by the HO endonuclease [229]. In contrast, spontaneous breaks are expected to occur at many possible sites and may often occur within regions lacking extensive TG tracts. In the absence of homologous repair, these DSBs will likely be subject to extensive resection before repair can take place. In our HO cleavage assay (Figure 3-1A), DSBs are induced several kilobases distal to the SiRTA sequences to more accurately mimic endogenous conditions while providing alternative options of repair. Furthermore, as explored in Chapter 3, regulation of telomerase activity immediately adjacent a DSB may differ considerably from a break induced several kilobases away because, in the latter case, the single-stranded DNA (ssDNA) generated after resection is bound by ssDNA-associated repair proteins.

4.3 What is the function of the SiRTA-stim?

What aspects of these SiRTAs make them much better target for *de novo* telomere addition than surrounding sequences? Mangahas *et al*. were the first to establish the ability of endogenous sequences to act as enhancers of telomere addition events. They characterized

repair events in disomic yeast strains carrying two copies of chromosome VII: an unmodified chromosome VII and a modified arm of chromosome VII containing the HO recognition site integrated immediately next to the endogenous telomere. The *URA3* gene was integrated internal to the HO site [199]. In the absence of Rad52 (required for HR), *de novo* telomere addition was the predominant outcome with 70% of *de novo* telomere addition events occurring very close to but not within an endogenous $(TG)_{17}$ tract [199]. All remaining telomere addition events occurred within the integrated *URA3* gene, distal to an 11 bp TG tract [199]. These results strongly suggested that telomere-like TG tracts can promote telomere addition following DSB induction. Although not based on endogenous sequences, Kramer and Haber found that TG-rich sequences derived from ciliate telomeres act as enhancers of *de novo* telomere addition at distal TG sequences (described in section 1.2.4.1) [195]. Both of these studies are consistent with our observations of SiRTAs described in this thesis [197].

Despite the reports above that enhancing sequences exist, the work described in Chapter 2 of this thesis is the first to characterize enhancers of *de novo* telomere addition (the SiRTA-Stim sequences) in detail. Our results suggest that the SiRTA-Stim associates with telomere-binding protein(s) that facilitate either the activity and/or recruitment of telomerase. We show that the ssDNA telomere-binding protein Cdc13 binds the SiRTA-Stim sequences of both SiRTAs with high affinity (Figures 2-6C, 2-8E) [197]. Cdc13 is a single-stranded DNA binding protein with specificity for TG-rich sequences [92]. Cdc13, through interaction of its 'recruitment' domain with Est1, is required for association of the telomerase enzyme with telomeres [40,42]. Tethering either full-length Cdc13, the Cdc13 recruitment domain or Est1 immediately adjacent to a DSB promotes telomere formation at that site [206]. These results

suggest that Cdc13 binding at the SiRTA-Stim may also serve to increase the local concentration of telomerase to allow *de novo* telomere addition. In experiments where the SiRTA-Stim was replaced with two copies of a canonical Cdc13 binding site (Figure 2-5G), the frequency of telomere addition at SiRTA 5L-35 increased compared to the endogenous SiRTA-Stim, presumably due to more efficient recruitment of telomerase. Tethering Cdc13 through a fusion with Gal4 DNA binding domain to the SiRTA-Stim replaced with two copies of a Gal4 UAS sequence also restored telomere addition to wild-type levels (Figure 2-7A, B). Taken together, our results suggest that Cdc13 binding to SiRTA-Stim stimulates *de novo* telomere addition at SiRTA sequences in a dose-dependent manner.

4.4 What is the role of the intervening sequences?

At the two SiRTA sites analyzed in Chapter 2**,** the SiRTA-Stim and Core sequences are separated by 20-30 nucleotides (Figure 4-1). At SiRTA 5L-35, we deleted these intervening sequences (spacerΔ) and found that ~80% of Gal^R 5-FOA^R candidates have added a telomere at the SiRTA [197]. Another 15% have added a telomere very near the Core sequence [197]. In addition, unlike in wild-type cells, where only 20-30% of Gal^R colonies acquire resistance to 5-FOA, in spacerΔ cells, >95% of Gal^R colonies have lost the end of the chromosome (unpublished results). In summary, the vast majority of cells surviving HO cleavage have undergone *de novo* telomere addition in or immediately adjacent to the SiRTA, effectively outcompeting other GCR-promoting pathways. What underlies this striking change in the efficiency of telomere addition? It is unclear that removing the spacer sequence would increase the amount of Cdc13 bound to the SiRTA. In fact, replacing the SiRTA-Stim with two copies of a canonical Cdc13 binding site

increases the frequency of telomere addition but not to the extent observed in the SpacerΔ strain (Figure 2-5G). In the future, ChIP experiments like those shown in Figure 3-10A could be used to determine whether Cdc13 recruitment is increased upon deletion of the spacer. Alternatively, the SiRTA-Stim and Core sequences without the spacer may form secondary structure(s) that are more primed for telomerase activity, may be more effectively recruited to the nuclear periphery for repair (see section 4.6) or may be more resistant to the negative inhibition normally imposed on telomere addition at these SiRTAs.

It is possible that the rate of telomere addition in the spacerΔ strain is so high that it interferes with canonical repair pathways. If so, it seems likely that such an efficient 'hotspot' would be selected against, perhaps providing an explanation for the physical separation of the core and stim sequences. To address this possibility, one could conduct an experiment in strains disomic for chromosome V. One chromosome will contain spacerΔ construct, the HO cut site and the *URA3* gene, while the other chromosome V will be unmodified. The goal of this experiment will be to address if telomere addition at SiRTA sequences competes favorably with homologous recombination (HR), which is accurate and largely favored over other repair pathways in yeast. From experiments done by other groups, repair by HR in this context is the most predominant outcome [80,195,196]. If telomere addition at spacerΔ competes favorably with HR, it will suggest that the intervening sequences decrease the efficiency of SiRTA sites and allow for other repair options. One caveat is that resection may not progress sufficiently to reveal the SiRTA sequence in this experiment since the SiRTA is 3 kb internal to the HO site. To address this, the HO site can be integrated at varying distances from the SiRTA sequence including immediately adjacent to the spacerΔ construct. The experiment described here may

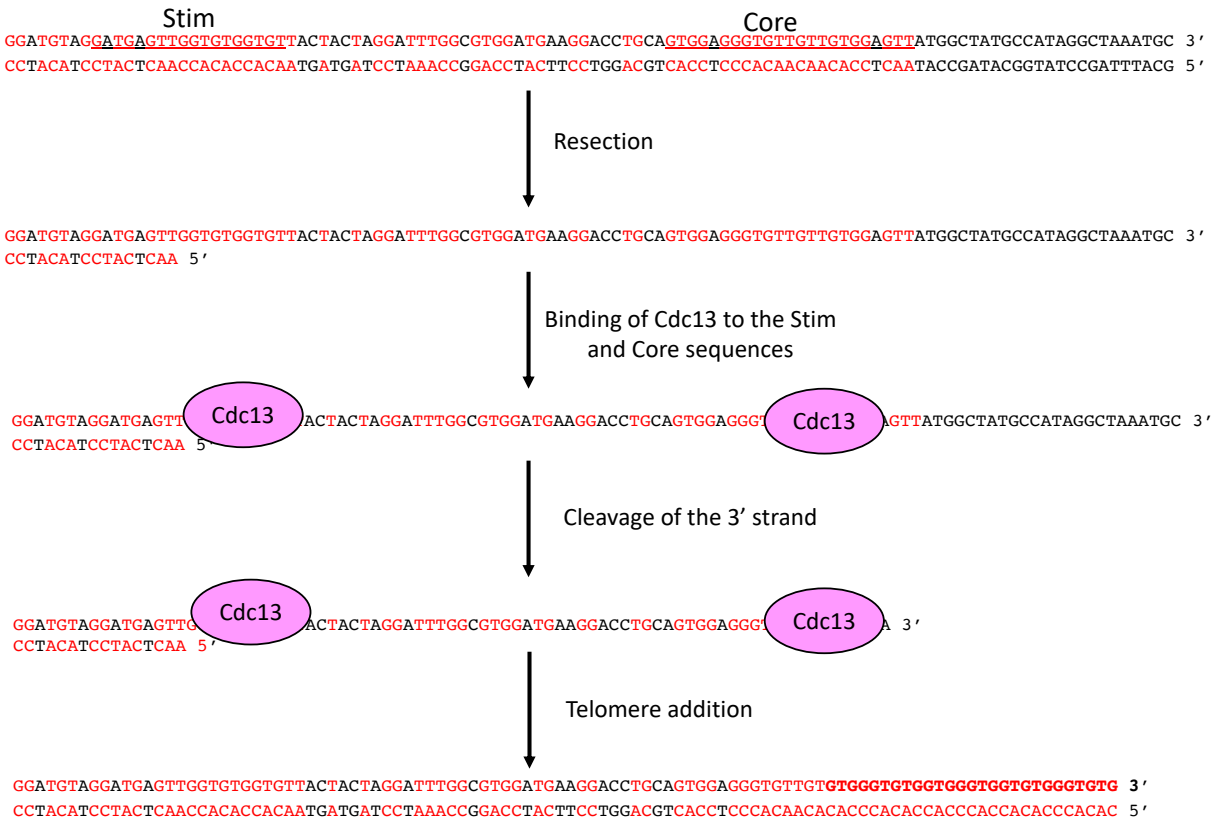

Figure 4:1 *De novo* telomere addition at SiRTAs requires resection of the 5' strand and cleavage of the 3' strand. SiRTA 5L-35 sequences are shown. T and G nucleotides are shown in red while A and C nucleotides are shown in black. The Stim and Core sequences are underlined. Following HO induction, the 5' strand undergoes resection to reveal single-stranded SiRTA sequences to allow Cdc13 binding at the Stim and Core sequences. In this model, I propose that the Cdc13 binding is coupled to the cleavage of the 3'strand. Newly synthesized telomere sequences are shown in bold red. Following de novo telomere addition, the 5' strand is filled in.

address the utilization of both homologous recombination and telomere addition under

conditions that may be ideal for both pathways.

4.5 Resection of DSBs and *de novo* telomere addition at SiRTAs

Our HO cleavage system is designed such that the DSB is induced a few kilobases distal to the SiRTAs. In this system, resection has to extend through the SiRTA sequences since telomerase acts upon single-stranded DNA (Figure 4-1). In yeast, the initial 5' to 3' resection of a HO-induced DSB is carried out by the MRX complex (Mre11, Xrs2 and Rad50) in association with Sae2 (reviewed in [276]) and is followed by extensive resection by Exo1 and Dna2 nucleases [166]. The Gottschling lab reported that *de novo* telomere addition does not occur in the absence of the MRX complex when the DSB is induced immediately adjacent to the TG tracts [274]. Also, they found that Cdc13 binding was abolished in the absence of Rad50, suggesting that the MRX complex is required to generate single-stranded DNA needed for Cdc13 binding [274]. Several years ago, I designed a genetic screen to identify genes required for *de novo* telomere addition at spacerΔ SiRTA 5L-35. In addition to genes encoding the telomerase components *CDC13* and *EST2*, the *MRE11* and *XRS2* genes were identified several times in this screen. Altogether, these results suggest that MRX-dependent 5' to 3' resection of HO-induced DSBs allows *de novo* telomere addition at SiRTAs.

While HO-induced DSBs undergo extensive 5' to 3' resection (Figure 4-1), very little, if any, 3' to 5' exonuclease activity occurs at these ends [166,195]. Since telomerase can only act on the 3' TG-rich strand, this 3' strand has to resected or cleaved to allow telomerase activity (see Figure 4-1 for an illustration). One of the major questions that remains unanswered is how the 3' strand is cleaved to allow Cdc13/telomerase binding and activity at internal sites following DSB induction. Synthesis of the C-rich strand (leading strand) is coupled to telomerase-mediated lengthening of the 3' strand [105]. It is possible that one or more aspects

of 5’ to 3’ resection is coupled to the cleavage of the 3’ strand and/or subsequent telomerase action. I propose that resection of the 5’ strand following HO induction in our system is coupled to the cleavage of the 3’ strand and/or telomerase binding for the reasons explained here.

First, I have observed that under conditions where *de novo* telomere addition is not possible at SiRTA sequences (for example due to complete deletion of the SiRTA sequences (SiRTAΔ)), all GCR events map to telomere-proximal to the SiRTA (data not shown). These observations suggest that resection in these cases may not extend 3kb internal to SiRTA sequences. Second, in situations where telomere addition at SiRTA sequences is very efficient such as in the spacerΔ strains [197], resection almost always proceeds to SiRTA sequences and GCR events do not occur in the telomere-proximal region. In these two scenarios, resection on the 5’ strand may be coupled to GCR SIRTA activity on the 3’ strand. If resection occurs randomly and uncoupled from telomere addition activity at SiRTA, I would expect that the relative rates of GCR events (taking into account the size of the regions and distance to the HO site) would be almost equal in the centromere-proximal and telomere-proximal regions irrespective of the status of the SiRTA sequence. In our system, it appears that a crosstalk exists between the progression of resection, 3’ strand cleavage and *de novo* telomere addition at SiRTA. I imagine a scenario where after extensive resection of the 5’ strand 3 kb internal the HO recognition site, Cdc13 binds and recruits telomerase to TG-rich SiRTA sites on the 3’ strand. Once bound, resection is halted. Cdc13 binds to the ssDNA and recruits telomerase followed by cleavage of the 3’ strand and telomerase-mediated extension of these sequences (see Figure 4-1 for illustration). Currently, an exonuclease has not been identified capable of 3’ strand cleavage under *in vivo* conditions. There are observations of a nuclease activity tightly

associated with telomerase that is detected in *in vitro* telomerase assays (reviewed in [187]). In the absence of the SiRTA sequences (SiRTAΔ; no Cdc13 binding and telomerase recruitment), failure to cleave the 3' strand would allow the single-stranded DNA generated by resection to be quickly taken up into other recombination structures represented as GCR events in the telomere-proximal region.

4.6 Roles of Rad51 and Rad52 in *de novo* telomere addition

Following the published work in Chapter 2, I wanted to further explore and understand the requirements for Cdc13 binding at SiRTA-Stim and Core sequences. 5' to 3' resection of a DSB generates ssDNA that is first bound by the heterotrimeric complex RPA which prevents formation of secondary structures and stabilizes the ssDNA. The Rad52 protein, acts as a mediator of recombination, replacing bound RPA for the Rad51 recombinase (Figure 4-2A). Rad51 forms a nucleofilament on the ssDNA that initiates the homology search and strand invasion into homologous duplex DNA to effect repair (reviewed in [161,166,277]). Since ssDNA is first bound by HR- associated proteins, I wanted to address the impact of these HR-associated proteins on telomere addition at SiRTA sequences and the role of Cdc13 in that process.

Oza *et al.* found that the association of Cdc13 with ssDNA is reduced in the absence of Rad51 following a HO-induced DSB at the *MAT* locus. Interestingly, enrichment of Cdc13 is observed following DNA cleavage even though this chromosome region lacks extensive TG repeats [248]. These authors proposed that the formation of the Rad51 filament may be needed for optimal association of Cdc13 with ssDNA and *de novo* telomere addition [248]. Surprisingly, they never addressed the requirement for Rad52 in this context. In agreement

with their results, I found that deletion of *RAD51* greatly reduced telomere addition at both SiRTAs (Figure 3-1B). However, *RAD52* deletion had no effect, consistent with another report showing that *RAD52* deletion promotes telomere addition events (Figure 3-1B) [278]. My results suggest that Rad51 nucleofilament formation is not required for telomere addition since Rad51 nucleofilament will not form in the absence of Rad52 (reviewed in [166]) and Rad52 deletion has no effect on telomere addition in our strains (Figure 3-1B). Consistent with these results, a Rad51 mutant that is impaired in nucleofilament formation has no effect on telomere addition (Figure 3-8C). Rather, Rad51 mutations that disrupt the Rad51-Rad52 interaction significantly reduce telomere formation (Figure 3-8C), suggesting that this interaction is important in maintaining WT levels of telomere formation.

How does Rad51 promote telomere formation at SiRTAs? Similar to the Oza *et al.* observations [248], I found that Cdc13 recruitment was significantly reduced at SiRTA 9L-44 in the absence of Rad51, implicating a role for Rad51 in Cdc13 recruitment and/or binding (Figure 3-10A). Furthermore, forced recruitment of Cdc13 to a SiRTA lacking SiRTA-Stim promoted telomere formation in the absence of Rad51 (Figure 3-10B). Though not directly addressed by ChIP, these observations suggest, that Cdc13 binding should be restored in the absence of both Rad51 and Rad52. However, it is important to address what portion of Cdc13 binding requires the SiRTA sequences especially since Oza *et al.* report Cdc13 binding at regions lacking specific Cdc13 binding sites in a Rad51-dependent manner. By ChIP, I expect that the association of Cdc13 with SiRTA sequences will be greater than at non-SiRTA sequences. In conclusion, Rad51 does not directly promote telomere addition at SiRTAs but prevents Rad52 from preventing telomere addition at SiRTAs.

4.7 Potential role of Cdc13 in nuclear localization

Oza *et al*. reported that unrepairable or slowly repaired DSBs are localized to the nuclear periphery in a Rad51- and Cdc13-dependent manner for repair. Mps3, an essential inner nuclear envelope protein required for spindle pole body duplication and telomere tethering at the nuclear periphery, also depends on Cdc13 for its efficient recruitment to DSBs [248]. The tethering of DSBs to the nuclear periphery occurs through the N-terminal domain of Mps3 [248]. Previous work established that Mps3 interacts with Est1 [279], the telomerase subunit that interacts with Cdc13 to mediate telomerase recruitment [40]. The Oza *et al.* paper suggested that unrepairable or persistent DSBs are localized to the nuclear periphery through the Mps3-Est1 and Est1-Cdc13 interactions, for repair by telomere addition [248]. In unpublished data, I analyzed the effect of an N-terminal truncation mutant of Mps3 on telomere addition at SiRTA 9L-44 and observed that these events are reduced by at least 50%. Taken together, these results suggest that Rad51 promotes the association of Cdc13 with SiRTA sequences which in turn allows the association of Mps3 with other telomerase components for localization to the nuclear periphery for repair. I found that almost half of the GCRs that occur within SiRTA 9L-44 in the absence of Rad51 are in fact not *de novo* telomere additions (Epum *et al*., submitted). It would appear that, in these cases, these breaks are not effectively localized to the nuclear periphery and may become routed into other GCR-promoting pathways. It would be helpful to analyze the precise nature of these non *de novo* telomere addition events in

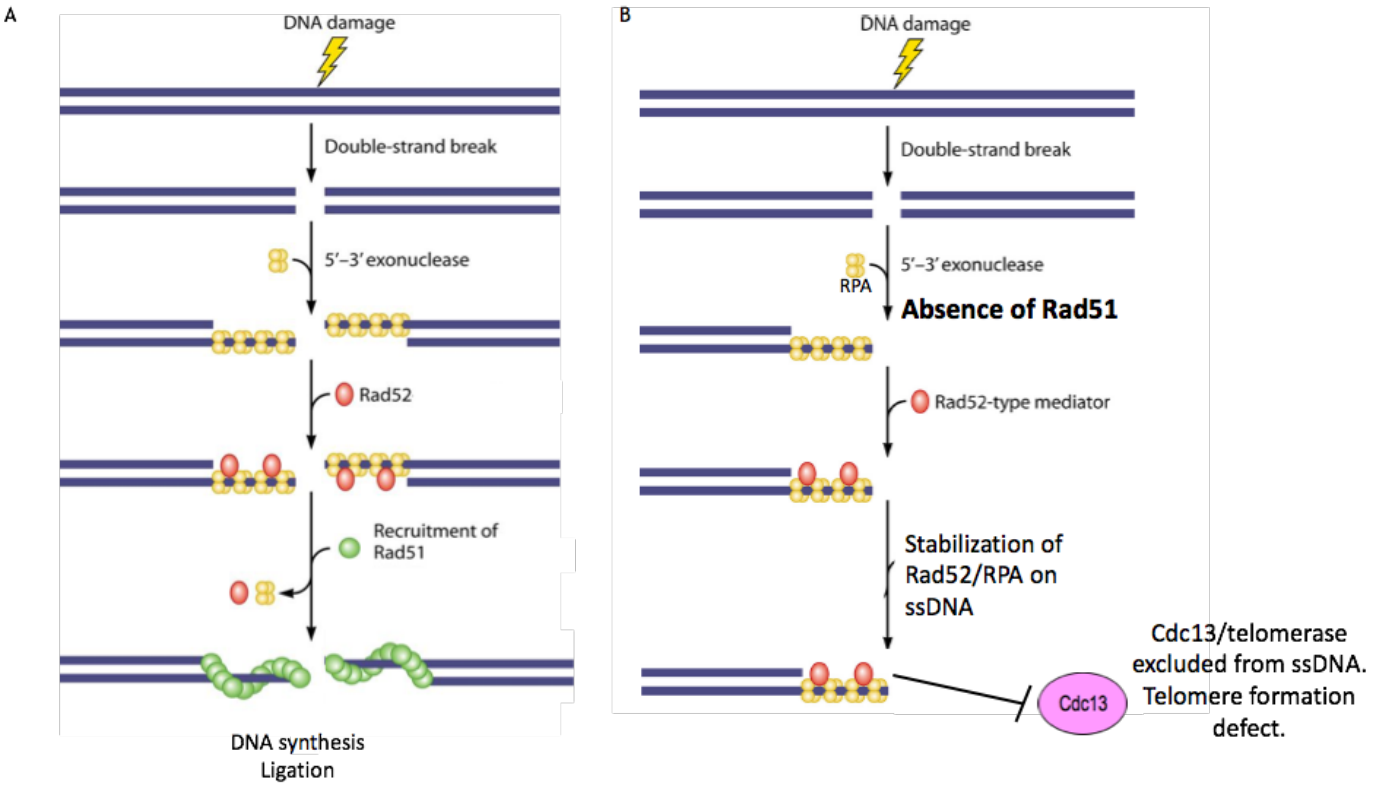

Figure 4.2: Interaction between Rad51, Rad52 and RPA during homologous recombination and *de novo* telomere addition. (A) DSB induction is followed by 5' to 3' resection to expose single-stranded DNA that is bound by RPA. Rad52 replaces RPA with Rad51. Rad51 forms nucleofilament to facilitate repair. (B) In the absence of Rad51, Rad52 stabilizes RPA on the single-stranded DNA, blocking Cdc13 binding (see text more details). Figure modified from [280].

rad51Δ cells which would hint at a more precise role of Rad51 in nuclear localization of DSBs for *de novo* telomere formation.

4.8 How then do we explain the inhibitory role of Rad52 on *de novo* telomere addition?

In the absence of Rad51, some *in vitro* experiments showed that the binding interaction between Rad51 and RPA is altered in a manner that allows both proteins to persist on the ssDNA (Figure 4-2B) [241,263]. Significantly, from these results, Rad52 does not displace RPA but rather binds to it and further stabilizes its association with ssDNA (Figure 4-2B) [241,263]. I propose that this association between both proteins and the ssDNA may inhibit the association of Cdc13 with ssDNA and prevent telomere formation at SiRTAs (Figure 4-2B). Indeed Cdc13 and RPA are both similar in structure since both are a three-part complex and bind ssDNA as well [82,83]. The RPA complex also binds telomeres and may compete with Cdc13 for binding to telomeres and DSBs [82]. Furthermore, in the absence of Rad51, Rad52 promotes annealing of RPA-coated single-stranded DNA to facilitate single-strand annealing (SSA) events [245]. This Rad52-RPA association may inhibit the binding of Cdc13 to promote telomere formation at SiRTAS. I predicted that disrupting the interaction between Rad52 and RPA should overcome some of the inhibition to Cdc13 binding and allow for telomere formation. To test this idea, I analyzed the effect of an allele of *RFA1*, *rfa1-44*, on telomere formation at both SiRTAs. By genetic criteria, this mutant protein does not interact with Rad52. The frequency of telomere formation at both SiRTAs in *rfa1-44* cells was not different from that observed in WT cells (Figure 3-11A). Remarkably, I found that the *rfa1-44* mutation completely suppresses the telomere addition defect of *rad51Δ* at both SiRTAs (Figure 3-11A). These results suggest that the inhibitory effect of Rad52 on telomere formation at SiRTAs can be overcome by disrupting the Rad52-RPA interaction.

Why would the Rad52-RPA interaction prevent telomere formation? In the absence of Rad51, I made a striking observation in the centromere-proximal region of the SiRTA on chromosome IX; the rate of GCR formation in this region was significantly increased from 0-10% in WT cells to 50-75% in the absence of Rad51 (Figure 3-4A). These GCR events are completely dependent on Rad52, Rad59 and Pol32 since deletion of their corresponding genes in a *rad51Δ* background completely prevented these GCR events (Figure 3-6B,C). However, deletion of *RAD59* and *POL32* did not suppress the telomere addition of *rad51Δ* (Figure 3-6B). Sequencing of 12 independent GCR events from this strain revealed that these GCR events are microhomology-mediated (Figure 3-6A). 8 out of 12 of them utilized microhomologies distal to the break site on chromosome IX and represent a type of SSA, known as microhomology mediated repair (MHMR) [183] while the others utilized microhomologies on other chromosomes and are most likely break-induced replication (BIR) (section 1.3.3.4). I analyzed 67 other GCR events occurring in the centromere-proximal region of SiRTA 9L-44 in *rad51Δ* strains and found that about 45% of these GCR events are due to MHMR. Importantly, Rad51 has been shown to inhibit the single-strand annealing activity of Rad52 (Figure 4-3) [268]. Taken together, my results suggest that in the absence of Rad51, Rad52 interacts with RPA, perhaps to promote single-strand annealing of RPA-coated ssDNA (Figure 4-3). This Rad52-RPA interaction blocks Cdc13 binding and *de novo* telomere addition (Figures 4-2, 4-3). One future experiment will be to test the competition between Cdc13 and RPA in *in vitro* binding assays. For example, using single molecule imaging on ssDNA curtains containing binding sites for Cdc13, competition between these proteins can be explored. I predict that, in the absence of Rad51, Rad52-RPA complexed to ssDNA should prevent the association of Cdc13. However, Cdc13

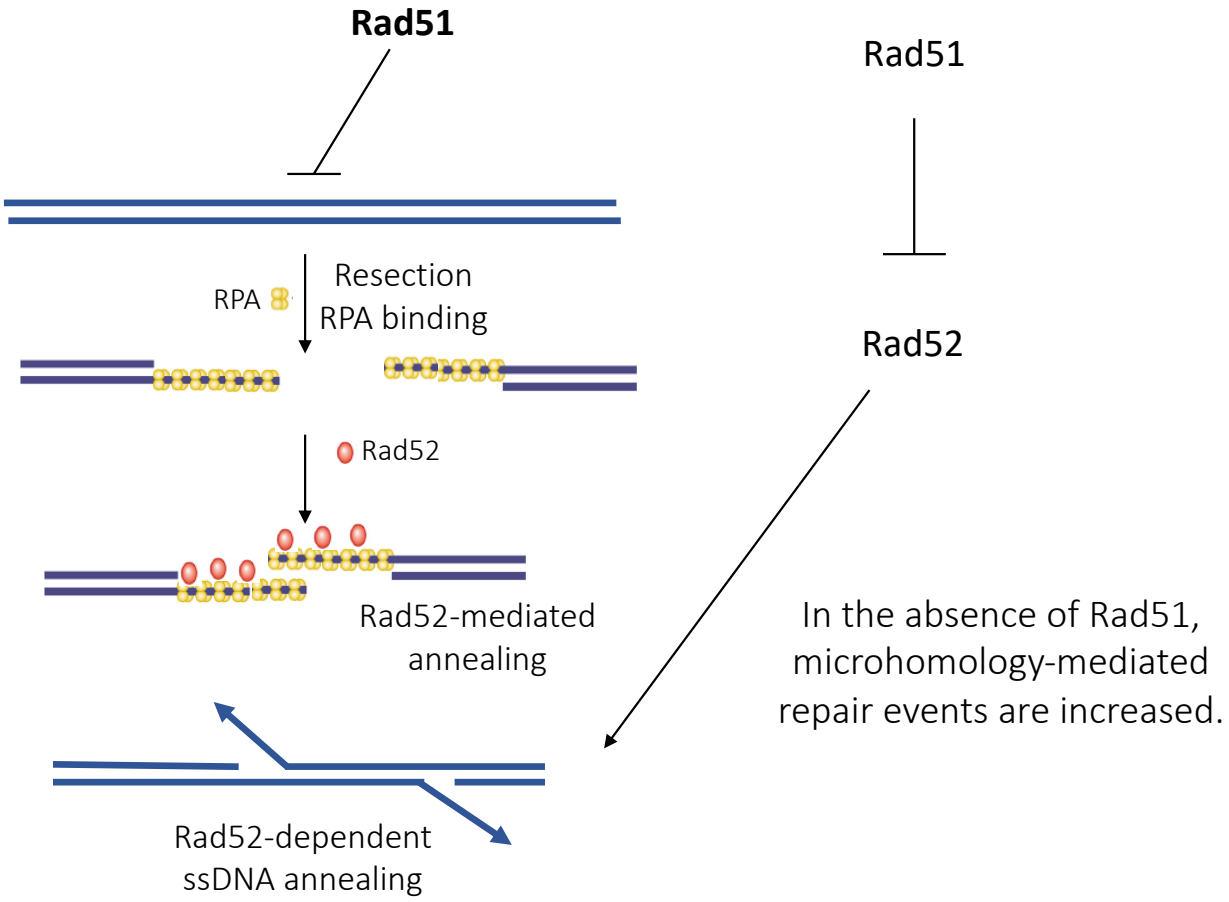

Figure 4-3: Rad51 inhibits Rad52 annealing of RPA-coated single-stranded DNA to inhibit microhomology mediated repair. Following resection of a DSB, RPA binds to exposed single-stranded DNA. In the absence of Rad51, Rad52 promotes the annealing of complementary RPA-coated single-stranded DNA. These annealing events are represented as microhomology-mediated repair in the absence of Rad51 (see text for more details).

should be able to displace RPA from the ssDNA in the absence of Rad52. With the addition of Rad51, Rad52-mediated displacement of RPA should allow Cdc13 association with the ssDNA. However, other possibilities exist that could account for my observations.

4.9 Opposing roles for Rad51 and Rad52

The Haber lab reported similar genetic interactions between Rad51 and Rad52 in adaptation [256]. Adaptation describes a cellular process where, following a DSB, yeast cells are able to initiate cell division after a period of checkpoint arrest even if the DSB is not repaired. Cells deleted for *RAD51* are adaptation-deficient while *RAD52* deleted cells are proficient in adaptation. Similar to *de novo* telomere addition at SiRTAs, *RAD52* deletion completely suppresses the adaptation defect of *RAD51* deletion [256]. Adaptation deficiency itself does not explain my observations because deleting either *TID1* or *KU80* also causes a severe adaptation defect by a different mechanism from that of *RAD51* deletion [256,262]. However, *ku80*Δ and *tid1*Δ cells do not show any telomere addition defect at both SiRTAs (Figure 3-12A). The Haber paper showed that adaptation in yeast is controlled by two different pathways involving Rad52 and RPA. Both proteins are engaged with the checkpoint and require Rad51 and Tid1 respectively to turn the checkpoint off, allowing adaptation. The Haber paper showed that adaptation is dependent on a functional checkpoint system (in a sense, adaptation is defined by the ability of a cell to arrest in response to DNA damage). In preliminary results, I found that the effect of *RAD51* deletion on *de novo* telomere addition is dependent on a functional checkpoint as cells lacking both *RAD51* and *RAD9* (required for checkpoint signaling) exhibit fully wild-type phenotypes. The significance of this result is not completely understood. It would be interesting to explore the roles of other genes in the checkpoint signaling pathway and to ask whether it is arrest in G2/M *per se* that is important or signaling events that occur upon checkpoint activation. These results suggest that the association of Rad52 with RPA on the single-stranded

DNA may be responsible for regulating adaptation and *de novo* telomere addition by an unclear mechanism.

4.10 Competition between non-conservative repair pathways

Telomere formation has been regarded as a 'last-ditch' effort to save the cells from death in the absence of other accurate pathways following DNA damage. Other non-conservative repair pathways involving microhomology usage such as SSA, BIR and MMEJ are also typically used by yeast in these situations. It is not clear which of these pathways is favored when yeast cells are presented with an unrepairable DSB. Most studies on BIR, MMEJ and SSA have utilized artificial sequences containing homologies/microhomologies of various lengths to probe the sequence requirements of these different pathways [180,181,267,281]. While very informative, such studies have not queried how repair pathway choices are made in the context of endogenous sequences. In our system, I found that *de novo* telomere formation at SiRTAs is more favored over these other types of GCR-promoting pathways. At SiRTA 9L-44, only in the absence of Rad51, do I find an upregulation of MHMR (a type of SSA) events. In fact, *de novo* telomere formation at SiRTAs does not directly compete with these events since deletion of the SiRTA sequences does not lead to an increase in occurrence of MHMR (Figure 3-4B). The SiRTA on chromosome IX can be used as a model system to further characterize and detail the endogenous competition between repair pathways following induction of an otherwise unrepairable DSB. These experiments can test the involvement of other genes known to act in these pathways or explore the competition between repair pathways by varying the distance between the sequences utilized for telomere addition and MHMR.

In conclusion, the work presented in Chapter 2 shows that endogenous hotspots of *de novo* telomere addition (SiRTAs) follow a bipartite structure in which Cdc13 binding at an upstream Stim sequence stimulates *de novo* telomere addition at a downstream core sequence. In Chapter 3, I show that Rad51 indirectly promotes the binding of Cdc13 to SiRTA sequences by altering the interaction of Rad52 with RPA. *De novo* telomere addition is associated with some human genetic diseases [187,191,194]. Mini-satellite sequences that increase the frequency of telomere addition in yeast in a Cdc13-dependent manner [207] are often found in human subtelomeric regions where telomere additions are observed (reviewed in [191]). These human subtelomeric regions contain sequences prone to formation of secondary structures and hard to replicate sequences that may increase the frequency of breakage and/or repair by *de novo* telomere addition. Therefore, the regulation of *de novo* telomere addition described in this thesis may be conserved in mammalian cells as well.

REFERENCES

1. HJ Muller. The remaking of chromosomes. The Collecting Net-Woods Hole. 1938. 13: 181-198.
2. McClintock B. The behavior in successive nuclear divisions of a chromosome broken at meiosis. Proc Natl Acad Sci U S A. 1939 Aug;25(8):405–16.
3. McClintock B. The stability of broken ends of chromosomes in *Zea Mays*. Genetics. 1941 Mar;26(2):234–82.
4. McKnight TD, Shippen DE. Plant telomere biology. Plant Cell. 2004 Apr;16(4):794–803.
5. J. Watson and F. Crick. A structure for deoxyribose nucleic acid. Nature. 1953;(4356):737–8.
6. Meselson M, Stahl FW. The replication of DNA. Cold Spring Harb Symp Quant Biol. 1958;23:9–12.
7. Olovnikov AM. Principle of marginotomy in template synthesis of polynucleotides. Dokl Akad Nauk SSSR. 1971;201(6):1496–9.
8. Watson JD. Origin of concatemeric T7DNA. Nat New Biol. 1972 Oct;239(94):197–201.
9. LeBel C, Wellinger RJ. Telomeres: What's new at your End? J Cell Sci. 2005 Jul 1;118(13):2785–8.
10. Sfeir AJ, Shay JW, Wright WE. Fine-tuning the chromosome ends: The Last Base of Human Telomeres. Cell Cycle. 2005 Nov 22;4(11):1467–70.
11. Sfeir AJ, Chai W, Shay JW, Wright WE. Telomere-end processing. Mol Cell. 2005 Apr

1;18(1):131–8.

12. Hayflick L, Moorhead PS. The serial cultivation of human diploid cell strains. Exp Cell Res. 1961 Dec;25(3):585–621.

13. Opresko PL, Shay JW. Telomere-associated aging disorders. Ageing Res Rev. 2017 Jan;33:52–66.

14. Hoffman DC, Anderson RC, DuBois ML, Prescott DM. Macronuclear gene-sized molecules of hypotrichs. Nucleic Acids Res. 1995 Apr 25;23(8):1279–83.

15. Blackburn EH, Gall JG. A tandemly repeated sequence at the termini of the extrachromosomal ribosomal RNA genes in Tetrahymena. J Mol Biol. 1978 Mar 25;120(1):33–53.

16. Klobutcher LA, Swanton MT, Donini P, Prescott DM. All gene-sized DNA molecules in four species of hypotrichs have the same terminal sequence and an unusual 3’ terminus. Proc Natl Acad Sci U S A. 1981 May;78(5):3015–9.

17. Szostak JW, Blackburn EH. Cloning yeast telomeres on linear plasmid vectors. Cell. 1982 May 1;29(1):245–55.

18. Shampay J, Szostak JW, Blackburn EH. DNA sequences of telomeres maintained in yeast. Nature. 1984 Jul;310(5973):154–7.

19. Moyzis RK, Buckingham JM, Cram LS, Dani M, Deaven LL, Jones MD, et al. A highly conserved repetitive DNA sequence, (TTAGGG)n, present at the telomeres of human chromosomes. Proc Natl Acad Sci U S A. 1988 Sep 1;85(18):6622–6.

20. Meyne J, Ratliff RL, Moyzis RK. Conservation of the human telomere sequence (TTAGGG)n among vertebrates. Proc Natl Acad Sci. 1989 Sep 1;86(18):7049–53.

21. Greider CW, Blackburn EH. Identification of a specific telomere terminal transferase activity in Tetrahymena extracts. Cell. 1985 Dec;43(2 Pt 1):405–13.

22. Greider CW, Blackburn EH. The telomere terminal transferase of *Tetrahymena* is a ribonucleoprotein enzyme with two kinds of primer specificity. Cell. 1987 Dec 24;51(6):887–98.

23. Greider CW, Blackburn EH. A telomeric sequence in the RNA of *Tetrahymena* telomerase required for telomere repeat synthesis. Nature. 1989 Jan 26;337(6205):331–7.

24. Yu GL, Bradley JD, Attardi LD, Blackburn EH. In vivo alteration of telomere sequences and senescence caused by mutated *Tetrahymena* telomerase RNAs. Nature. 1990 Mar 8;344(6262):126–32.

25. Shippen-Lentz D, Blackburn E. Functional evidence for an RNA template in telomerase. Science. 1990 Feb 2;247(4942):546–52.

26. Lundblad V, Szostak JW. A mutant with a defect in telomere elongation leads to senescence in yeast. Cell. 1989 May 19;57(4):633–43.

27. Singer MS, Gottschling DE. TLC1: template RNA component of *Saccharomyces cerevisiae* telomerase. Science. 1994 Oct 21;266(5184):404–9.

28. Lendvay TS, Morris DK, Sah J, Balasubramanian B, Lundblad V. Senescence mutants of *Saccharomyces cerevisiae* with a defect in telomere replication identify three additional *EST* genes. Genetics. 1996 Dec;144(4):1399–412.

29. Garvik B, Carson M, Hartwell L. Single-stranded DNA arising at telomeres in cdc13 mutants may constitute a specific signal for the RAD9 checkpoint. Mol Cell Biol. 1995 Nov;15(11):6128–38.

30. Lingner J, Hughes TR, Shevchenko A, Mann M, Lundblad V, Cech TR. Reverse Transcriptase Motifs in the Catalytic Subunit of Telomerase. Science. 1997 Apr 25;276(5312):561–7.

31. Morin GB. The human telomere terminal transferase enzyme is a ribonucleoprotein that synthesizes TTAGGG repeats. Cell. 1989 Nov 3;59(3):521–9.

32. Kim N, Piatyszek M, Prowse K, Harley C, West M, Ho P, et al. Specific association of human telomerase activity with immortal cells and cancer. Science. 1994 Dec 23;266(5193):2011–5.

33. Nakamura TM, Morin GB, Chapman KB, Weinrich SL, Andrews WH, Lingner J, et al. Telomerase catalytic subunit homologs from fission yeast and human. Science. 1997 Aug 15;277(5328):955–9.

34. Harley CB, Futcher AB, Greider CW. Telomeres shorten during ageing of human fibroblasts. Nature. 1990 May 31;345(6274):458–60.

35. Bodnar AG, Ouellette M, Frolkis M, Holt SE, Chiu CP, Morin GB, et al. Extension of Life-Span by Introduction of Telomerase into Normal Human Cells. Science. 1998 Jan 16;279(5349):349–52.

36. de Lange T, Shiue L, Myers RM, Cox DR, Naylor SL, Killery AM, et al. Structure and variability of human chromosome ends. Mol Cell Biol. 1990 Feb;10(2):518–27.

37. Cohn M, Blackburn E. Telomerase in yeast. Science. 1995 Jul 21;269(5222):396–400.

38. Lin JJ, Zakian VA. An *in vitro* assay for *Saccharomyces* telomerase requires *EST1*. Cell. 1995 Jun 30;81(7):1127–35.

39. Steiner BR, Hidaka K, Futcher B. Association of the Est1 protein with telomerase activity

in yeast. Proc Natl Acad Sci. 1996 Apr 2;93(7):2817–21.

40. Evans SK, Lundblad V. Est1 and Cdc13 as Comediators of Telomerase Access. Science. 1999 Oct 1;286(5437):117–20.

41. Qi H, Zakian VA. The *Saccharomyces* telomere-binding protein Cdc13p interacts with both the catalytic subunit of DNA polymerase alpha and the telomerase-associated Est1 protein. Genes Dev. 2000 Jul 15;14(14):1777–88.

42. Pennock E, Buckley K, Lundblad V. Cdc13 delivers separate complexes to the telomere for end protection and replication. Cell. 2001 Feb 9;104(3):387–96.

43. Chan A, Boulé J-B, Zakian VA. Two pathways recruit telomerase to *Saccharomyces cerevisiae* telomeres. PLoS Genet. 2008 Oct 24;4(10):e1000236.

44. Seto AG, Livengood AJ, Tzfati Y, Blackburn EH, Cech TR. A bulged stem tethers Est1p to telomerase RNA in budding yeast. Genes Dev. 2002 Nov 1;16(21):2800–12.

45. Tuzon CT, Wu Y, Chan A, Zakian VA. The *Saccharomyces cerevisiae* telomerase subunit Est3 binds telomeres in a cell cycle– and Est1–dependent manner and Interacts directly with Est1 *In Vitro*. PLoS Genet. 2011 May 5;7(5):e1002060.

46. Virta-Pearlman V, Morris DK, Lundblad V. Est1 has the properties of a single-stranded telomere end-binding protein. Genes Dev. 1996 Dec 15;10(24):3094–104.

47. DeZwaan DC, Freeman BC. The conserved Est1 protein stimulates telomerase DNA extension activity. Proc Natl Acad Sci. 2009 Oct 13;106(41):17337–42.

48. Taggart AKP, Teng S-C, Zakian VA. Est1p as a cell cycle-regulated activator of telomere-bound telomerase. Science. 2002 Aug 9;297(5583):1023–6.

49. Wu Y, Zakian VA. The telomeric Cdc13 protein interacts directly with the telomerase

subunit Est1 to bring it to telomeric DNA ends in vitro. Proc Natl Acad Sci. 2011 Dec 20;108(51):20362–9.

50. Osterhage JL, Talley JM, Friedman KL. Proteasome-dependent degradation of Est1p regulates the cell cycle–restricted assembly of telomerase in *Saccharomyces cerevisiae*. Nat Struct Mol Biol. 2006 Aug 23;13(8):720–8.

51. Ferguson JL, Chao WCH, Lee E, Friedman KL. The Anaphase Promoting Complex Contributes to the Degradation of the S. cerevisiae Telomerase Recruitment Subunit Est1p. PLoS One. 2013 Jan 25;8(1):e55055.

52. Wellinger RJ, Zakian VA. Everything you ever wanted to know about *Saccharomyces cerevisiae* telomeres: beginning to end. Genetics. 2012 Aug;191(4):1073–105.

53. Friedman KL, Cech TR. Essential functions of amino-terminal domains in the yeast telomerase catalytic subunit revealed by selection for viable mutants. Genes Dev. 1999 Nov 1;13(21):2863–74.

54. Talley JM, DeZwaan DC, Maness LD, Freeman BC, Friedman KL. Stimulation of Yeast Telomerase Activity by the Ever Shorter Telomere 3 (Est3) Subunit Is Dependent on Direct Interaction with the Catalytic Protein Est2. J Biol Chem. 2011 Jul 29;286(30):26431–9.

55. Hughes TR, Weilbaecher RG, Walterscheid M, Lundblad V. Identification of the single-strand telomeric DNA binding domain of the *Saccharomyces cerevisiae* Cdc13 protein. Proc Natl Acad Sci. 2000 Jun 6;97(12):6457–62.

56. Friedman KL, Heit JJ, Long DM, Cech TR. N-terminal Domain of Yeast Telomerase Reverse Transcriptase: Recruitment of Est3p to the Telomerase Complex. Mol Biol Cell. 2003

Jan;14(1):1–13.

57. Lee J, Mandell EK, Tucey TM, Morris DK, Lundblad V. The Est3 protein associates with yeast telomerase through an OB-fold domain. Nat Struct Mol Biol. 2008 Sep;15(9):990–7.

58. Zappulla DC, Goodrich K, Cech TR. A miniature yeast telomerase RNA functions in vivo and reconstitutes activity in vitro. Nat Struct Mol Biol. 2005 Dec 20;12(12):1072–7.

59. Livengood AJ, Zaug AJ, Cech TR. Essential regions of *Saccharomyces cerevisiae* telomerase RNA: separate elements for Est1p and Est2p interaction. Mol Cell Biol. 2002 Apr;22(7):2366–74.

60. Dandjinou AT, Lévesque N, Larose S, Lucier J-F, Elela SA, Wellinger RJ. A Phylogenetically Based Secondary Structure for the Yeast Telomerase RNA. Curr Biol. 2004 Jul 13;14(13):1148–58.

61. Lin J, Ly H, Hussain A, Abraham M, Pearl S, Tzfati Y, et al. A universal telomerase RNA core structure includes structured motifs required for binding the telomerase reverse transcriptase protein. Proc Natl Acad Sci. 2004 Oct 12;101(41):14713–8.

62. Qiao F, Cech TR. Triple-helix structure in telomerase RNA contributes to catalysis. Nat Struct Mol Biol. 2008 Jun 25;15(6):634–40.

63. Stellwagen AE, Haimberger ZW, Veatch JR, Gottschling DE. Ku interacts with telomerase RNA to promote telomere addition at native and broken chromosome ends. Genes Dev. 2003 Oct 1;17(19):2384–95.

64. Fisher TS, Taggart AKP, Zakian VA. Cell cycle-dependent regulation of yeast telomerase by Ku. Nat Struct Mol Biol. 2004 Dec 7;11(12):1198–205.

65. Vega LR, Phillips JA, Thornton BR, Benanti JA, Onigbanjo MT, Toczyski DP, et al. Sensitivity

of yeast strains with long G-Tails to levels of telomere-bound telomerase. PLoS Genet. 2007 Jun;3(6):e105.

66. Gallardo F, Olivier C, Dandjinou AT, Wellinger RJ, Chartrand P. TLC1 RNA nucleo-cytoplasmic trafficking links telomerase biogenesis to its recruitment to telomeres. EMBO J. 2008 Mar 5;27(5):748–57.

67. Seto AG, Zaug AJ, Sobel SG, Wolin SL, Cech TR. *Saccharomyces cerevisiae* telomerase is an Sm small nuclear ribonucleoprotein particle. Nature. 1999 Sep 9;401(6749):177–80.

68. Harari Y, Kupiec M. Genome-wide studies of telomere biology in budding yeast. Microb cell. 2014 Mar 1;1(3):70–80.

69. Larrivee M, LeBel C, Wellinger RJ. The generation of proper constitutive G-tails on yeast telomeres is dependent on the MRX complex. Genes Dev. 2004 Jun 15;18(12):1391–6.

70. Wellinger RJ, Wolf AJ, Zakian VA. Origin activation and formation of single-strand TG1-3 tails occur sequentially in late S phase on a yeast linear plasmid. Mol Cell Biol. 1993 Jul;13(7):4057–65.

71. Makarov VL, Hirose Y, Langmore JP. Long G tails at both ends of human chromosomes suggest a C strand degradation mechanism for telomere shortening. Cell. 1997 Mar 7;88(5):657–66.

72. Griffith JD, Comeau L, Rosenfield S, Stansel RM, Bianchi A, Moss H, et al. Mammalian Telomeres End in a Large Duplex Loop. Cell. 1999 May 14;97(4):503–14.

73. Bochman ML, Paeschke K, Zakian VA. DNA secondary structures: stability and function of G-quadruplex structures. Nat Rev Genet. 2012 Nov 3;13(11):770–80.

74. Smith JS, Chen Q, Yatsunyk LA, Nicoludis JM, Garcia MS, Kranaster R, et al. Rudimentary

G-quadruplex–based telomere capping in *Saccharomyces cerevisiae*. Nat Struct Mol Biol. 2011 Apr 13;18(4):478–85.

75. Zahler AM, Williamson JR, Cech TR, Prescott DM. Inhibition of telomerase by G-quartet DMA structures. Nature. 1991 Apr 25;350(6320):718–20.

76. Zaug AJ, Podell ER, Cech TR. Human POT1 disrupts telomeric G-quadruplexes allowing telomerase extension in vitro. Proc Natl Acad Sci. 2005 Aug 2;102(31):10864–9.

77. Oganesian L, Moon IK, Bryan TM, Jarstfer MB. Extension of G-quadruplex DNA by ciliate telomerase. EMBO J. 2006 Mar 8;25(5):1148–59.

78. Louis EJ, Borts RH. A complete set of marked telomeres in *Saccharomyces cerevisiae* for physical mapping and cloning. Genetics. 1995 Jan;139(1):125–36.

79. Walmsley RW, Chan CSM, Tye B-K, Petes TD. Unusual DNA sequences associated with the ends of yeast chromosomes. Nature. 1984 Jul;310(5973):157–60.

80. Sandell LL, Zakian VA. Loss of a yeast telomere: arrest, recovery, and chromosome loss. Cell. 1993 Nov 19;75(4):729–39.

81. Lundblad V, Blackburn EH. An alternative pathway for yeast telomere maintenance rescues *est1*- senescence. Cell. 1993 Apr 23;73(2):347–60.

82. Gao H, Cervantes RB, Mandell EK, Otero JH, Lundblad V. RPA-like proteins mediate yeast telomere function. Nat Struct Mol Biol. 2007 Mar 11;14(3):208–14.

83. Gelinas AD, Paschini M, Reyes FE, Heroux A, Batey RT, Lundblad V, et al. Telomere capping proteins are structurally related to RPA with an additional telomere-specific domain. Proc Natl Acad Sci. 2009 Nov 17;106(46):19298–303.

84. Grandin N, Damon C, Charbonneau M. Cdc13 prevents telomere uncapping and Rad50-

dependent homologous recombination. EMBO J. 2001 Nov 1;20(21):6127–39.

85. Luciano P, Coulon S, Faure V, Corda Y, Bos J, Brill SJ, et al. RPA facilitates telomerase activity at chromosome ends in budding and fission yeasts. EMBO J. 2012 Apr 18;31(8):2034–46.

86. Grandin N, Reed SI, Charbonneau M. Stn1, a new *Saccharomyces cerevisiae* protein, is implicated in telomere size regulation in association with Cdc13. Genes Dev. 1997 Feb 15;11(4):512–27.

87. Petreaca RC, Chiu H-C, Nugent CI. The role of Stn1p in *Saccharomyces cerevisiae* telomere capping can be separated from its interaction with Cdc13p. Genetics. 2007 Nov;177(3):1459–74.

88. Xu L, Petreaca RC, Gasparyan HJ, Vu S, Nugent CI. *TEN1* Is essential for *CDC13* -mediated telomere capping. Genetics. 2009 Nov;183(3):793–810.

89. Vodenicharov MD, Wellinger RJ. DNA degradation at unprotected telomeres in yeast Is regulated by the CDK1 (Cdc28/Clb) Cell-Cycle Kinase. Mol Cell. 2006 Oct 6;24(1):127–37.

90. Vodenicharov MD, Wellinger RJ. The cell division cycle puts up with unprotected telomeres: cell cycle regulated telomere uncapping as a means to achieve telomere homeostasis. Cell Cycle. 2007 May 15;6(10):1161–7.

91. Vodenicharov MD, Laterreur N, Wellinger RJ. Telomere capping in non-dividing yeast cells requires Yku and Rap1. EMBO J. 2010 Sep 1;29(17):3007–19.

92. Nugent CI, Hughes TR, Lue NF, Lundblad V. Cdc13p: a single-strand telomeric DNA-binding protein with a dual role in yeast telomere maintenance. Science. 1996 Oct 11;274(5285):249–52.

93. Petreaca RC, Chiu H-C, Eckelhoefer HA, Chuang C, Xu L, Nugent CI. Chromosome end protection plasticity revealed by Stn1p and Ten1p bypass of Cdc13p. Nat Cell Biol. 2006 Jul 11;8(7):748–55.

94. Sun J, Yu EY, Yang Y, Confer LA, Sun SH, Wan K, et al. Stn1-Ten1 is an Rpa2-Rpa3-like complex at telomeres. Genes Dev. 2009 Dec 15;23(24):2900–14.

95. Puglisi A, Bianchi A, Lemmens L, Damay P, Shore D. Distinct roles for yeast Stn1 in telomere capping and telomerase inhibition. EMBO J. 2008 Sep 3;27(17):2328–39.

96. Grossi S, Puglisi A, Dmitriev P V, Lopes M, Shore D. Pol12, the B subunit of DNA polymerase, functions in both telomere capping and length regulation. Genes Dev. 2004 Apr 22;18(9):992–1006.

97. Shore D, Nasmyth K. Purification and cloning of a DNA binding protein from yeast that binds to both silencer and activator elements. Cell. 1987. Dec 4;51(5):721–32.

98. Wright JH, Zakian VA. Protein-DNA interactions in soluble telosomes from *Saccharomyces cerevisiae*. Nucleic Acids Res. 1995 May 11;23(9):1454–60.

99. Marcand S, Gilson E, Shore D. A protein-counting mechanism for telomere length regulation in yeast. Science. 1997 Feb 14;275(5302):986–90.

100. Levy DL, Blackburn EH. Counting of Rif1p and Rif2p on *Saccharomyces cerevisiae* telomeres regulates telomere length. Mol Cell Biol. 2004 Dec 15;24(24):10857–67.

101. Marcand S, Pardo B, Gratias A, Cahun S, Callebaut I. Multiple pathways inhibit NHEJ at telomeres. Genes Dev. 2008 May 1;22(9):1153–8.

102. Kupiec M. Biology of telomeres: lessons from budding yeast. FEMS Microbiol Rev. 2014 Mar;38(2):144–71.

103. Bonetti D, Clerici M, Anbalagan S, Martina M, Lucchini G, Longhese MP. Shelterin-like proteins and Yku inhibit nucleolytic processing of *Saccharomyces cerevisiae* Telomeres. PLoS Genet. 2010 May 27;6(5):e1000966.

104. Mimitou EP, Symington LS. Ku prevents Exo1 and Sgs1-dependent resection of DNA ends in the absence of a functional MRX complex or Sae2. EMBO J. 2010 Oct 6;29(19):3358–69.

105. Diede SJ, Gottschling DE. Telomerase-mediated telomere addition in vivo requires DNA primase and DNA polymerases alpha and delta. Cell. 1999 Dec 23;99(7):723–33.

106. Marcand S, Brevet V, Gilson E. Progressive cis-inhibition of telomerase upon telomere elongation. EMBO J. 1999 Jun 15;18(12):3509–19.

107. Peterson SE, Stellwagen AE, Diede SJ, Singer MS, Haimberger ZW, Johnson CO, et al. The function of a stem-loop in telomerase RNA is linked to the DNA repair protein Ku. Nat Genet. 2001 Jan;27(1):64–7.

108. Gallardo F, Laterreur N, Cusanelli E, Ouenzar F, Querido E, Wellinger RJ, et al. Live cell imaging of telomerase RNA Dynamics reveals cell cycle-dependent clustering of telomerase at elongating telomeres. Mol Cell. 2011 Dec 9;44(5):819–27.

109. Teixeira MT, Arneric M, Sperisen P, Lingner J. Telomere length homeostasis is achieved via a switch between telomerase- extendible and -nonextendible states. Cell. 2004 Apr 30;117(3):323–35.

110. Sabourin M, Tuzon CT, Zakian VA. Telomerase and Tel1p preferentially associate with short telomeres in S. cerevisiae. Mol Cell. 2007 Aug 17;27(4):550–61.

111. Hector RE, Shtofman RL, Ray A, Chen B-R, Nyun T, Berkner KL, et al. Tel1p Preferentially

Associates with Short Telomeres to Stimulate Their Elongation. Mol Cell. 2007 Sep 7;27(5):851–8.

112. McGee JS, Phillips JA, Chan A, Sabourin M, Paeschke K, Zakian VA. Reduced Rif2 and lack of Mec1 target short telomeres for elongation rather than double-strand break repair. Nat Struct Mol Biol. 2010 Dec 7;17(12):1438–45.

113. Faure V, Coulon S, Hardy J, Géli V. Cdc13 and Telomerase bind through different mechanisms at the lagging- and leading-strand telomeres. Mol Cell. 2010 Jun 25;38(6):842–52.

114. Mallory JC, Petes TD. Protein kinase activity of Tel1p and Mec1p, two *Saccharomyces cerevisiae* proteins related to the human ATM protein kinase. Proc Natl Acad Sci. 2000 Dec 5;97(25):13749–54.

115. de Lange T. Shelterin: the protein complex that shapes and safeguards human telomeres. Genes Dev. 2005 Sep 15;19(18):2100–10.

116. Baumann P, Cech TR. Pot1, the putative telomere end-binding protein in fission yeast and humans. Science (80-). 2001 May 11;292(5519):1171–5.

117. de Lange T. Shelterin-mediated telomere protection. Annu Rev Genet. 2018 Nov 23;52(1):223–47.

118. Palm W, de Lange T. How Shelterin Protects Mammalian Telomeres. Annu Rev Genet. 2008 Dec 4;42(1):301–34.

119. van Steensel B, de Lange T. Control of telomere length by the human telomeric protein TRF1. Nature. 1997 Feb 20;385(6618):740–3.

120. Smogorzewska A, van Steensel B, Bianchi A, Oelmann S, Schaefer MR, Schnapp G, et al.

Control of Human Telomere Length by TRF1 and TRF2. Mol Cell Biol. 2000 Mar 1;20(5):1659–68.

121. Doksani Y. The Response to DNA Damage at Telomeric Repeats and Its Consequences for Telomere Function. Genes (Basel). 2019;10(4).

122. Nandakumar J, Bell CF, Weidenfeld I, Zaug AJ, Leinwand LA, Cech TR. The TEL patch of telomere protein TPP1 mediates telomerase recruitment and processivity. Nature. 2012 Dec 13;492(7428):285–9.

123. Schmidt JC, Dalby AB, Cech TR. Identification of human TERT elements necessary for telomerase recruitment to telomeres. Elife. 2014 Oct 1;3.

124. Artandi SE, DePinho RA. Telomeres and telomerase in cancer. Carcinogenesis. 2010 Jan;31(1):9–18.

125. Wang Z, Yi J, Li H, Deng LF, Tang XM. Extension of life-span of normal human fibroblasts by reconstitution of telomerase activity. Shi Yan Sheng Wu Xue Bao. 2000 Jun;33(2):129–40.

126. Cong Y-S, Wright WE, Shay JW. Human Telomerase and Its Regulation. Microbiol Mol Biol Rev. 2002 Sep 1;66(3):407–25.

127. Hahn WC, Counter CM, Lundberg AS, Beijersbergen RL, Brooks MW, Weinberg RA. Creation of human tumour cells with defined genetic elements. Nature. 1999 Jul 29;400(6743):464–8.

128. Calado RT, Young NS. Telomere Diseases. N Engl J Med. 2009 Dec 10;361(24):2353–65.

129. Walne AJ, Vulliamy T, Kirwan M, Plagnol V, Dokal I. Constitutional Mutations in RTEL1 Cause Severe *Dyskeratosis Congenita*. Am J Hum Genet. 2013 Mar 7;92(3):448–53.

130. Kajtár P, Méhes K. Bilateral coats retinopathy associated with aplastic anaemia and mild dyskeratotic signs. Am J Med Genet. 1994 Feb 15;49(4):374–7.

131. Kappei D, Londoño-Vallejo JA. Telomere length inheritance and aging. Mech Ageing Dev. 2008 Jan;129(1–2):17–26.

132. Misteli T. Beyond the Sequence: Cellular organization of genome function. Cell. 2007 Feb 23;128(4):787–800.

133. Peterson CL, Almouzni G. Nucleosome dynamics as modular systems that integrate DNA damage and repair. Cold Spring Harb Perspect Biol. 2013 Sep 1;5(9).

134. Vilenchik MM, Knudson AG. Endogenous DNA double-strand breaks: Production, fidelity of repair, and induction of cancer. Proc Natl Acad Sci. 2003 Oct 28;100(22):12871–6.

135. Pfeiffer P, Goedecke W, Obe G. Mechanisms of DNA double-strand break repair and their potential to induce chromosomal aberrations. Mutagenesis. 2000 Jul 1;15(4):289–302.

136. Chen J, Stubbe J. Bleomycins: towards better therapeutics. Nat Rev Cancer. 2005 Feb;5(2):102–12.

137. Shrivastav M, De Haro LP, Nickoloff JA. Regulation of DNA double-strand break repair pathway choice. Cell Res. 2008 Jan 24;18(1):134–47.

138. Jackson SP. Sensing and repairing DNA double-strand breaks. Carcinogenesis. 2002 May 1;23(5):687–96.

139. Jackson SP, Bartek J. The DNA-damage response in human biology and disease. Nature. 2009 Oct 22;461(7267):1071–8.

140. Van Gent DC, Hoeijmakers JH, Kanaar R. Chromosomal stability and the DNA double-stranded break connection. Nat Rev Genet. 2001 Mar;2(3):196–206.

141. Khanna KK, Jackson SP. DNA double-strand breaks: signaling, repair and the cancer connection. Nat Genet. 2001 Mar;27(3):247–54.

142. Fugmann SD, Lee AI, Shockett PE, Villey IJ, Schatz DG. The RAG proteins and V(D)J recombination: complexes, ends, and transposition. Annu Rev Immunol. 2000 Apr;18(1):495–527.

143. Rabbitts TH. Chromosomal translocations in human cancer. Nature. 1994 Nov 10;372(6502):143–9.

144. Korsmeyer SJ. Chromosomal Translocations in Lymphoid Malignancies Reveal Novel Proto-Oncogenes. Annu Rev Immunol. 1992 Apr;10(1):785–807.

145. Khan FA, Ali SO. Physiological Roles of DNA Double-Strand Breaks. J Nucleic Acids. 2017 Oct 18;2017:1–20.

146. Haber JE. Mating-type genes and MAT switching in *Saccharomyces cerevisiae*. Genetics. 2012 May;191(1):33–64.

147. Barsoum E, Martinez P, Aström SU. Alpha3, a transposable element that promotes host sexual reproduction. Genes Dev. 2010 Jan 1;24(1):33–44.

148. Forney JD, Blackburn EH. Developmentally controlled telomere addition in wild-type and mutant paramecia. Mol Cell Biol. 1988 Jan;8(1):251–8.

149. Aylon Y, Kupiec M. DSB repair: the yeast paradigm. DNA Repair (Amst). 2004 Aug;3(8–9):797–815.

150. Bertuch AA, Lundblad V. The Ku heterodimer performs separable activities at double-strand breaks and chromosome termini. Mol Cell Biol. 2003 Nov 15;23(22):8202–15.

151. Martin SG, Laroche T, Suka N, Grunstein M, Gasser SM. Relocalization of telomeric Ku

and SIR proteins in response to DNA strand breaks in Yeast. Cell. 1999 May 28;97(5):621–33.

152. Boulton SJ, Jackson SP. Components of the Ku-dependent non-homologous end-joining pathway are involved in telomeric length maintenance and telomeric silencing. EMBO J. 1998 Mar 16;17(6):1819–28.

153. Nick McElhinny SA, Snowden CM, McCarville J, Ramsden DA. Ku recruits the XRCC4-ligase IV complex to DNA ends. Mol Cell Biol. 2000 May 1;20(9):2996–3003.

154. Teo S-H, Jackson SP. Lif1p targets the DNA ligase Lig4p to sites of DNA double-strand breaks. Curr Biol. 2000 Feb 1;10(3):165–8.

155. Kegel A, Sjöstrand JOO, Åström SU. Nej1p, a cell type-specific regulator of nonhomologous end joining in yeast. Curr Biol. 2001 Oct;11(20):1611–7.

156. Pastwa E, Błasiak J. Non-homologous DNA end joining. Acta Biochim Pol. 2003;50(4):891–908.

157. Chen L, Trujillo K, Ramos W, Sung P, Tomkinson AE. Promotion of Dnl4-catalyzed DNA end-Joining by the Rad50/Mre11/Xrs2 and Hdf1/Hdf2 Complexes. Mol Cell. 2001 Nov 21;8(5):1105–15.

158. Trujillo KM, Roh DH, Chen L, Van Komen S, Tomkinson A, Sung P. Yeast Xrs2 binds DNA and helps target rad50 and mre11 to DNA ends. J Biol Chem. 2003 Dec 5;278(49):48957–64.

159. Paull TT, Gellert M. A mechanistic basis for Mre11-directed DNA joining at microhomologies. Proc Natl Acad Sci U S A. 2000 Jun 6;97(12):6409–14.

160. Anderson DE, Trujillo KM, Sung P, Erickson HP. Structure of the Rad50 x Mre11 DNA

repair complex from *Saccharomyces cerevisiae* by electron microscopy. J Biol Chem. 2001 Oct 5;276(40):37027–33.

161. Aylon Y, Kupiec M. DSB repair: the yeast paradigm. DNA Repair (Amst). 2004 Aug 1;3(8–9):797–815.

162. Hays SL, Firmenich AA, Massey P, Banerjee R, Berg P. Studies of the Interaction between Rad52 Protein and the Yeast Single-Stranded DNA Binding Protein RPA. Mol Cell Biol. 2015;18(7):4400–6.

163. Krejci L, Damborsky J, Thomsen B, Duno M, Bendixen C. Molecular dissection of interactions between Rad51 and members of the recombination-repair group. Mol Cell Biol. 2001 Feb 1;21(3):966–76.

164. Lisby M, Rothstein R, Mortensen UH. Rad52 forms DNA repair and recombination centers during S phase. Proc Natl Acad Sci U S A. 2001 Jul 17;98(15):8276–82.

165. Miyazaki T, Bressan DA, Shinohara M, Haber JE, Shinohara A. *In vivo* assembly and disassembly of Rad51 and Rad52 complexes during double-strand break repair. EMBO J. 2004 Feb 25;23(4):939–49.

166. Mehta A, Haber JE. Sources of DNA double-strand breaks and models of recombinational DNA repair. Cold Spring Harb Perspect Biol. 2014 Aug 7;6(9):a016428.

167. Haber JE. The Many Interfaces of Mre11. Cell. 1998 Nov 25;95(5):583–6.

168. Ivanov EL, Sugawara N, White CI, Fabre F, Haber JE. Mutations in *XRS2* and *RAD50* delay but do not prevent mating-type switching in Saccharomyces cerevisiae. Mol Cell Biol. 1994 May 1;14(5):3414–25.

169. Sung P. Function of yeast Rad52 protein as a mediator between replication protein A and

the Rad51 recombinase. J Biol Chem. 1997 Nov 7;272(45):28194–7.

170. Wang X, Haber JE. Role of *Saccharomyces* single-stranded DNA-binding protein RPA in the strand invasion step of double-strand break repair. PLoS Biol. 2004 Jan 20;2(1):e21.

171. Sugawara N, Wang X, Haber JE. In vivo roles of Rad52, Rad54, and Rad55 proteins in Rad51-mediated recombination. Mol Cell. 2003;12(1):209–19.

172. Wilson MA, Kwon Y, Xu Y, Chung W-H, Chi P, Niu H, et al. Pif1 helicase and Polδ promote recombination-coupled DNA synthesis via bubble migration. Nature. 2013 Oct 17;502(7471):393–6.

173. Kramara J, Osia B, Malkova A. Break-Induced Replication: The where, the why, and the how. Trends Genet. 2018;34(7):518–31.

174. Malkova A, Ira G. Break-induced replication: functions and molecular mechanism. Curr Opin Genet Dev. 2013 Jun;23(3):271–9.

175. Bhargava R, Onyango DO, Stark JM. Regulation of single-strand annealing and its role in genome maintenance. Trends Genet. 2016;32(9):566–75.

176. Ozenberger BA, Roeder GS. A unique pathway of double-strand break repair operates in tandemly repeated genes. Mol Cell Biol. 1991 Mar;11(3):1222–31.

177. Malkova A, Ivanov EL, Haber JE. Double-strand break repair in the absence of *RAD51* in yeast: a possible role for break-induced DNA replication. Proc Natl Acad Sci U S A. 1996 Jul 9;93(14):7131–6.

178. Prado F, Cortés-Ledesma F, Huertas P, Aguilera A. Mitotic recombination in *Saccharomyces cerevisiae*. Curr Genet. 2003 Jan;42(4):185–98.

179. Zhang X, Paull TT. The Mre11/Rad50/Xrs2 complex and non-homologous end-joining of

incompatible ends in *S. cerevisiae*. DNA Repair (Amst). 2005 Nov 21;4(11):1281–94.

180. Lee K, Lee SE. *Saccharomyces cerevisiae* Sae2- and Tel1-dependent single-strand DNA formation at DNA break promotes microhomology-mediated end joining. Genetics. 2007 Aug;176(4):2003–14.

181. McVey M, Lee SE. MMEJ repair of double-strand breaks (director's cut): deleted sequences and alternative endings. Trends Genet. 2008 Nov;24(11):529–38.

182. Ma J-L, Kim EM, Haber JE, Lee SE. Yeast Mre11 and Rad1 Proteins Define a Ku-Independent Mechanism To Repair Double-Strand Breaks Lacking Overlapping End Sequences. Mol Cell Biol. 2003 Dec 1;23(23):8820–8.

183. Villarreal DD, Lee K, Deem A, Shim EY, Malkova A, Lee SE. Microhomology directs diverse DNA break repair pathways and chromosomal translocations. PLoS Genet. 2012 Nov 8;8(11):e1003026.

184. Bentley J, Diggle CP, Harnden P, Knowles MA, Kiltie AE. DNA double strand break repair in human bladder cancer is error prone and involves microhomology-associated end-joining. Nucleic Acids Res. 2004 Sep 23;32(17):5249–59.

185. Mattarucchi E, Guerini V, Rambaldi A, Campiotti L, Venco A, Pasquali F, et al. Microhomologies and interspersed repeat elements at genomic breakpoints in chronic myeloid leukemia. Genes, Chromosom Cancer. 2008 Jul;47(7):625–32.

186. Wilkie AO, Lamb J, Harris PC, Finney RD, Higgs DR. A truncated human chromosome 16 associated with alpha thalassaemia is stabilized by addition of telomeric repeat (TTAGGG)n. Nature. 1990 Aug 30;346(6287):868–71.

187. Pennaneach V, Putnam CD, Kolodner RD. Chromosome healing by *de novo* telomere

addition in *Saccharomyces cerevisiae*. Mol Microbiol. 2006 Mar;59(5):1357–68.

188. Prescott DM. The DNA of ciliated protozoa. Microbiol Rev. 1994 Jun;58(2):233–67.

189. Putnam CD, Pennaneach V, Kolodner RD. Chromosome healing through terminal deletions generated by de novo telomere additions in *Saccharomyces cerevisiae*. Proc Natl Acad Sci U S A. 2004 Sep 7;101(36):13262–7.

190. Chen C, Kolodner RD. Gross chromosomal rearrangements in *Saccharomyces cerevisiae* replication and recombination defective mutants. Nat Genet. 1999 Sep;23(1):81–5.

191. Ribeyre C, Shore D. Regulation of telomere addition at DNA double-strand breaks. Chromosoma. 2013 Jun 17;122(3):159–73.

192. Myung K, Chen C, Kolodner RD. Multiple pathways cooperate in the suppression of genome instability in *Saccharomyces cerevisiae*. Nature. 2001 Jun;411(6841):1073–6.

193. Kolodner RD, Putnam CD, Myung K. Maintenance of genome stability in Saccharomyces cerevisiae. Science. 2002 Jul 26;297(5581):552–7.

194. Putnam CD, Kolodner RD. Pathways and Mechanisms that Prevent Genome Instability in Saccharomyces cerevisiae. Genetics. 2017;206(3):1187–225.

195. Kramer KM, Haber JE. New telomeres in yeast are initiated with a highly selected subset of TG1-3 repeats. Genes Dev. 1993 Dec 1;7(12a):2345–56.

196. Mangahas JL, Alexander MK, Sandell LL, Zakian VA. Repair of Chromosome Ends after Telomere Loss in *Saccharomyces*. Koshland D, editor. Mol Biol Cell. 2001 Dec;12(12):4078–89.

197. Obodo UC, Epum EA, Platts MH, Seloff J, Dahlson NA, Velkovsky SM, et al. Endogenous Hot Spots of *De Novo* Telomere Addition in the Yeast Genome Contain Proximal

Enhancers That Bind Cdc13 . Mol Cell Biol. 2016;36(12):1750–63.

198. Schulz VP, Zakian VA. The saccharomyces PIF1 DNA helicase inhibits telomere elongation and *de novo* telomere formation. Cell. 1994 Jan 14;76(1):145–55.

199. Mangahas JL, Alexander MK, Sandell LL, Zakian VA. Repair of chromosome ends after telomere loss in *Saccharomyces*. Mol Biol Cell. 2001 Dec;12(12):4078–89.

200. Makovets S, Blackburn EH. DNA damage signalling prevents deleterious telomere addition at DNA breaks. Nat Cell Biol. 2009 Nov;11(11):1383–6.

201. Strecker J, Stinus S, Caballero MP, Szilard RK, Chang M, Durocher D. A sharp Pif1-dependent threshold separates DNA double-strand breaks from critically short telomeres. Elife. 2017;6.

202. Zhang W, Durocher D. De novo telomere formation is suppressed by the Mec1-dependent inhibition of Cdc13 accumulation at DNA breaks. Genes Dev. 2010;24(5):502–15.

203. Mitchell MT, Smith JS, Mason M, Harper S, Speicher DW, Johnson FB, et al. Cdc13 N-terminal dimerization, DNA binding, and telomere length regulation. Mol Cell Biol. 2010 Nov 15;30(22):5325–34.

204. Sun J, Yang Y, Wan K, Mao N, Yu T-Y, Lin Y-C, et al. Structural bases of dimerization of yeast telomere protein Cdc13 and its interaction with the catalytic subunit of DNA polymerase α. Cell Res. 2011 Feb 28;21(2):258–74.

205. Bianchi A, Negrini S, Shore D. Delivery of yeast telomerase to a DNA break depends on the recruitment functions of Cdc13 and Est1. Mol Cell. 2004 Oct 8;16(1):139–46.

206. Bianchi A, Negrini S, Shore D. Delivery of Yeast Telomerase to a DNA Break Depends on

the Recruitment Functions of Cdc13 and Est1. Mol Cell. 2004 Oct 8;16(1):139–46.

207. Piazza A, Serero A, Boulé J-B, Legoix-Né P, Lopes J, Nicolas A. Stimulation of gross chromosomal rearrangements by the human CEB1 and CEB25 minisatellites in *Saccharomyces cerevisiae* depends on G-quadruplexes or Cdc13. PLoS Genet. 2012;8(11):e1003033.

208. Osterhage JL, Friedman KL. Chromosome end maintenance by telomerase. J Biol Chem. 2009 Jun 12;284(24):16061–5.

209. Blackburn EH. Structure and function of telomeres. Nature. 1991 Apr 18;350(6319):569–73.

210. Hardy CF, Sussel L, Shore D. A RAP1-interacting protein involved in transcriptional silencing and telomere length regulation. Genes Dev. 1992 May 1;6(5):801–14.

211. Wotton D, Shore D. A novel Rap1p-interacting factor, Rif2p, cooperates with Rif1p to regulate telomere length in *Saccharomyces cerevisiae*. Genes Dev. 1997 Mar 15;11(6):748–60.

212. Hoeijmakers JHJ. Genome maintenance mechanisms for preventing cancer. Nature. 2001 May 17;411(6835):366–74.

213. Ray A, Runge KW. The C terminus of the major yeast telomere binding protein Rap1p enhances telomere formation. Mol Cell Biol. 1998 Mar 1;18(3):1284–95.

214. Grossi S, Bianchi A, Damay P, Shore D. Telomere formation by rap1p binding site arrays reveals end-specific length regulation requirements and active telomeric recombination. Mol Cell Biol. 2001 Dec 1;21(23):8117–28.

215. Lustig AJ, Kurtz S, Shore D. Involvement of the silencer and UAS binding protein RAP1 in

regulation of telomere length. Science. 1990 Oct 26;250(4980):549–53.

216. Lydeard JR, Jain S, Yamaguchi M, Haber JE. Break-induced replication and telomerase-independent telomere maintenance require Pol32. Nature. 2007 Aug 1;448(7155):820–3.

217. Lydeard JR, Lipkin-Moore Z, Jain S, Eapen V V., Haber JE. Sgs1 and Exo1 redundantly inhibit break-induced replication and de Novo telomere addition at broken chromosome ends. PLoS Genet. 2010;6(5):25.

218. Conrad MN, Wright JH, Wolf AJ, Zakian VA. RAP1 protein interacts with yeast telomeres *in vivo*: Overproduction alters telomere structure and decreases chromosome stability. Cell. 1990 Nov 16;63(4):739–50.

219. Lin J-J, Zakian VA. The *Saccharomyces* CDC13 protein is a single-strand TG1–3 telomeric DNA-binding protein in vitro that affects telomere behavior in vivo. Proc Natl Acad Sci. 1996 Nov 26;93(24):13760–5.

220. Bourns BD, Alexander MK, Smith AM, Zakian VA. Sir proteins, Rif proteins, and Cdc13p bind *Saccharomyces* telomeres in vivo. Mol Cell Biol. 1998 Sep 1;18(9):5600–8.

221. Tsukamoto Y, Taggart AK., Zakian VA. The role of the Mre11-Rad50-Xrs2 complex in telomerase- mediated lengthening of *Saccharomyces cerevisiae* telomeres. Curr Biol. 2001 Sep 4;11(17):1328–35.

222. Anderson EM, Halsey WA, Wuttke DS. Delineation of the high-affinity single-stranded telomeric DNA-binding domain of *Saccharomyces cerevisiae* Cdc13. Nucleic Acids Res. 2002 Oct 1;30(19):4305–13.

223. Fouladi B, Sabatier L, Miller D, Pottier G, Murnane JP. The relationship between spontaneous telomere loss and chromosome instability in a human tumor cell line.

Neoplasia. 2000 Jan 1;2(6):540–54.

224. Kostiner DR, Nguyen H, Cox VA, Cotter PD. Stabilization of a terminal inversion duplication of 8p by telomere capture from 18q. Cytogenet Genome Res. 2002;98(1):9–12.

225. Fortin F, Beaulieu Bergeron M, Fetni R, Lemieux N. Frequency of Chromosome Healing and Interstitial Telomeres in 40 Cases of Constitutional Abnormalities. Cytogenet Genome Res. 2009;125(3):176–85.

226. Bonaglia MC, Giorda R, Beri S, De Agostini C, Novara F, Fichera M, et al. Molecular Mechanisms Generating and Stabilizing Terminal 22q13 Deletions in 44 Subjects with Phelan/McDermid Syndrome. Spinner NB, editor. PLoS Genet. 2011 Jul 14;7(7):e1002173.

227. Ribeyre C, Shore D. Anticheckpoint pathways at telomeres in yeast. Nat Struct Mol Biol. 2012 Mar 12;19(3):307–13.

228. Hirano Y, Sugimoto K. Cdc13 Telomere Capping Decreases Mec1 Association but Does Not Affect Tel1 Association with DNA Ends. Bloom K, editor. Mol Biol Cell. 2007 Jun;18(6):2026–36.

229. Bairley RCB, Guillaume G, Vega LR, Friedman KL. A mutation in the catalytic subunit of yeast telomerase alters primer-template alignment while promoting processivity and protein-DNA binding. J Cell Sci. 2011 Dec 15;124(Pt 24):4241–52.

230. Aimee M. Eldridge, Wayne A. Halsey and, Wuttke* DS. Identification of the Determinants for the Specific Recognition of Single-Strand Telomeric DNA by Cdc13†. 2005;

231. Rhee HS, Pugh BF. Comprehensive Genome-wide Protein-DNA Interactions Detected at Single-Nucleotide Resolution. Cell. 2011 Dec 9;147(6):1408–19.

232. Murray AW, Claus TE, Szostak JW. Characterization of two telomeric DNA processing reactions in *Saccharomyces cerevisiae*. Mol Cell Biol. 1988 Nov;8(11):4642–50.

233. Ngo H-P, Lydall D. Survival and growth of yeast without telomere capping by Cdc13 in the Absence of Sgs1, Exo1, and Rad9. PLoS Genet. 2010 Aug 19;6(8):e1001072.

234. Greetham M, Skordalakes E, Lydall D, Connolly BA. The telomere binding protein Cdc13 and the single-stranded DNA binding protein RPA protect telomeric DNA from resection by exonucleases. J Mol Biol. 2015 Sep 25;427(19):3023–30.

235. Scherer S, Davis RW. Replacement of chromosome segments with altered DNA sequences constructed *in vitro*. Proc Natl Acad Sci U S A. 1979 Oct 1;76(10):4951–5.

236. Phillips JA, Chan A, Paeschke K, Zakian VA. The Pif1 Helicase, a Negative Regulator of Telomerase, Acts Preferentially at Long Telomeres. PLoS Genet. 2015 Apr 1;11(4).

237. Ji H, Adkins CJ, Cartwright BR, Friedman KL. Yeast Est2p affects telomere length by influencing association of Rap1p with telomeric chromatin. Mol Cell Biol. 2008 Apr 1;28(7):2380–90.

238. Formosa T, Nittis T. Dna2 mutants reveal interactions with Dna polymerase alpha and Ctf4, a Pol alpha accessory factor, and show that full Dna2 helicase activity is not essential for growth. Genetics. 1999 Apr;151(4):1459–70.

239. Brill SJ, Stillman B. Replication factor-A from *Saccharomyces cerevisiae* is encoded by three essential genes coordinately expressed at S phase. Genes Dev. 1991 Sep 1;5(9):1589–600.

240. Wang X, Haber JE. Role of *Saccharomyces* single-stranded DNA-binding protein RPA in the strand invasion step of double-strand break repair. PLoS Biol. 2004 Jan;2(1):E21.

241. Sugiyama T, Kowalczykowski SC. Rad52 protein associates with replication protein A (RPA)-single-stranded DNA to accelerate Rad51-mediated displacement of RPA and presynaptic complex formation. J Biol Chem. 2002 Aug 30;277(35):31663–72.

242. New JH, Sugiyama T, Zaitseva E, Kowalczykowski SC. Rad52 protein stimulates DNA strand exchange by Rad51 and replication protein A. Nature. 1998 Jan 22;391(6665):407–10.

243. Sung P, Krejci L, Van Komen S, Sehorn MG. Rad51 recombinase and recombination mediators. J Biol Chem. 2003 Oct 31;278(44):42729–32.

244. Mortensen UH, Bendixen C, Sunjevaric I, Rothstein R. DNA strand annealing is promoted by the yeast Rad52 protein. Proc Natl Acad Sci U S A. 1996 Oct 1;93(20):10729–34.

245. Sugiyama T, New JH, Kowalczykowski SC. DNA annealing by RAD52 protein is stimulated by specific interaction with the complex of replication protein A and single-stranded DNA. Proc Natl Acad Sci U S A. 1998 May 26;95(11):6049–54.

246. Verma P, Greenberg RA. Noncanonical views of homology-directed DNA repair. Genes Dev. 2016;30(10):1138–54.

247. Singer M, Gottschling D. TLC1: template RNA component of Saccharomyces cerevisiae telomerase. Science. 1994 Oct 21;266(5184):404–9.

248. Oza P, Jaspersen SL, Miele A, Dekker J, Peterson CL. Mechanisms that regulate localization of a DNA double-strand break to the nuclear periphery. Genes Dev. 2009;23(8):912–27.

249. Teste M-A, François JM, Parrou J-L. Characterization of a new multigene family encoding isomaltases in the yeast *Saccharomyces cerevisiae*, the IMA family. J Biol Chem. 2010 Aug 27;285(35):26815–24.

250. Bai Y, Symington LS. A Rad52 homolog is required for RAD51-independent mitotic recombination in *Saccharomyces cerevisiae*. Genes Dev. 1996 Aug 15;10(16):2025–37.

251. Sugawara N, Ira G, Haber JE. DNA Length Dependence of the single-strand annealing pathway and the role of *Saccharomyces cerevisiae* RAD59 in double-strand break repair. Mol Cell Biol. 2000 Jul 15;20(14):5300–9.

252. Jablonovich Z, Liefshitz B, Steinlauf R, Kupiec M. Characterization of the role played by the RAD59 gene of *Saccharomyces cerevisiae* in ectopic recombination. Curr Genet. 1999 Aug;36(1–2):13–20.

253. Signon L, Malkova A, Naylor ML, Klein H, Haber JE. Genetic requirements for RAD51- and RAD54-independent break-induced replication repair of a chromosomal double-strand break. Mol Cell Biol. 2001 Mar;21(6):2048–56.

254. Gerik KJ, Li X, Pautz A, Burgers PMJ. Characterization of the two small subunits of *Saccharomyces cerevisiae* DNA polymerase δ. J Biol Chem. 1998 Jul 31;273(31):19747–55.

255. Sung P, Stratton SA. Yeast Rad51 recombinase mediates polar DNA strand exchange in the absence of ATP hydrolysis. J Biol Chem. 1996 Nov 8;271(45):27983–6.

256. Lee SE, Pellicioli A, Vaze MB, Sugawara N, Malkova A, Foiani M, et al. Yeast Rad52 and Rad51 recombination proteins define a second pathway of DNA damage assessment in response to a single double-strand break. Mol Cell Biol. 2003 Dec;23(23):8913–23.

257. Seong C, Colavito S, Kwon Y, Sung P, Krejci L. Regulation of Rad51 recombinase presynaptic filament assembly via interactions with the Rad52 mediator and the Srs2 anti-recombinase. J Biol Chem. 2009 Sep 4;284(36):24363–71.

258. Krejci L, Song B, Bussen W, Rothstein R, Mortensen UH, Sung P. Interaction with Rad51 is indispensable for recombination mediator function of Rad52. J Biol Chem. 2002 Oct 18;277(42):40132–41.

259. Ouenzar F, Lalonde M, Laprade H, Morin G, Gallardo F, Tremblay-Belzile S, et al. Cell cycle-dependent spatial segregation of telomerase from sites of DNA damage. J Cell Biol. 2017;216(8):2355–71.

260. Firmenich AA, Elias-Arnanz M, Berg P. A novel allele of *Saccharomyces cerevisiae* RFA1 that is deficient in recombination and repair and suppressible by RAD52. Mol Cell Biol. 2015;15(3):1620–31.

261. Lee SE, Pellicioli A, Malkova A, Foiani M, Haber JE. The *Saccharomyces* recombination protein Tid1p is required for adaptation from G2/M arrest induced by a double-strand break. Curr Biol. 2001 Jul;11(13):1053–7.

262. Lee SE, Moore JK, Holmes A, Umezu K, Kolodner RD, Haber JE. *Saccharomyces* Ku70, Mre11/Rad50, and RPA Proteins Regulate Adaptation to G2/M Arrest after DNA Damage. Cell. 1998 Aug;94(3):399–409.

263. Gibb B, Ye LF, Kwon Y, Niu H, Sung P, Greene EC. Protein dynamics during presynaptic complex assembly on individual ssDNA molecules. Nat Struct Mol Biol. 2014 Oct;21(10):893.

264. Gibb B, Ye LF, Gergoudis SC, Kwon Y, Niu H, Sung P, et al. Concentration-dependent

exchange of replication protein A on single-stranded DNA revealed by single-molecule imaging. Spies M, editor. PLoS One. 2014 Feb 3;9(2):e87922.

265. Deng SK, Gibb B, de Almeida MJ, Greene EC, Symington LS. RPA antagonizes microhomology-mediated repair of DNA double-strand breaks. Nat Struct Mol Biol. 2014 Apr 9;21(4):405–12.

266. Sugiyama T, Kantake N. Dynamic Regulatory Interactions of Rad51, Rad52, and Replication Protein-A in Recombination Intermediates. J Mol Biol. 2009 Jul 3;390(1):45–55.

267. Villarreal DD, Lee K, Deem A, Shim EY, Malkova A, Lee SE. Microhomology Directs Diverse DNA Break Repair Pathways and Chromosomal Translocations. PLoS Genet. 2012 Nov 8;8(11):e1003026.

268. Wu Y, Kantake N, Sugiyama T, Kowalczykowski SC. Rad51 protein controls Rad52-mediated DNA annealing. J Biol Chem. 2008 May 23;283(21):14883–92.

269. Malkova A, Signon L, Schaefer CB, Naylor ML, Theis JF, Newlon CS, et al. RAD51-independent break-induced replication to repair a broken chromosome depends on a distant enhancer site. Genes Dev. 2001 May 1;15(9):1055–60.

270. Sikorski RS, Hieter P. A system of shuttle vectors and yeast host strains designed for efficient manipulation of DNA in *Saccharomyces cerevisiae*. Genetics. 1989 May;122(1):19–27.

271. Anand R, Memisoglu G, Haber J. Cas9-mediated gene editing in *Saccharomyces cerevisiae*. Protoc Exch. 2017 Apr 13;

272. Radford A. Methods in Yeast Genetics — A Laboratory Course Manual. Biochem Educ.

1991 Apr 1;19(2):101–2.

273. Tsukuda T, Trujillo KM, Martini E, Osley MA. Analysis of chromatin remodeling during formation of a DNA double-strand break at the yeast mating type locus. Methods. 2009 May;48(1):40–5.

274. Diede SJ, Gottschling DE. Exonuclease activity is required for sequence addition and Cdc13p loading at a *de novo* telomere. Curr Biol. 2001 Sep 4;11(17):1336–40.

275. Strecker J, Stinus S, Caballero MP, Szilard RK, Chang M, Durocher D. A sharp Pif1-dependent threshold separates DNA double-strand breaks from critically short telomeres. Elife. 2017 Aug 3;6.

276. Symington LS. Mechanism and regulation of DNA end resection in eukaryotes. Crit Rev Biochem Mol Biol. 2016;51(3):195–212.

277. Symington LS. Role of RAD52 Epistasis Group genes in homologous recombination and double-strand break repair. Microbiol Mol Biol Rev. 2002 Dec 1;66(4):630–70.

278. Ouenzar F, Lalonde M, Laprade H, Morin G, Gallardo F, Tremblay-Belzile S, et al. Cell cycle-dependent spatial segregation of telomerase from sites of DNA damage. J Cell Biol. 2017;216(8):2355–71.

279. Antoniacci LM, Kenna MA, Uetz P, Fields S, Skibbens R V. The Spindle Pole Body Assembly Component Mps3p/Nep98p Functions in Sister Chromatid Cohesion. J Biol Chem. 2004 Nov 19;279(47):49542–50.

280. Chen XJ. Mechanism of homologous recombination and implications for aging-related deletions in mitochondrial DNA. Microbiol Mol Biol Rev. 2013 Sep 1;77(3):476–96.

281. Yu AM, McVey M. Synthesis-dependent microhomology-mediated end joining accounts

for multiple types of repair junctions. Nucleic Acids Res. 2010 Sep;38(17):5706–17.